CHALMERS
UNIVERSITY OF TECHNOLOGY

PHD THESIS

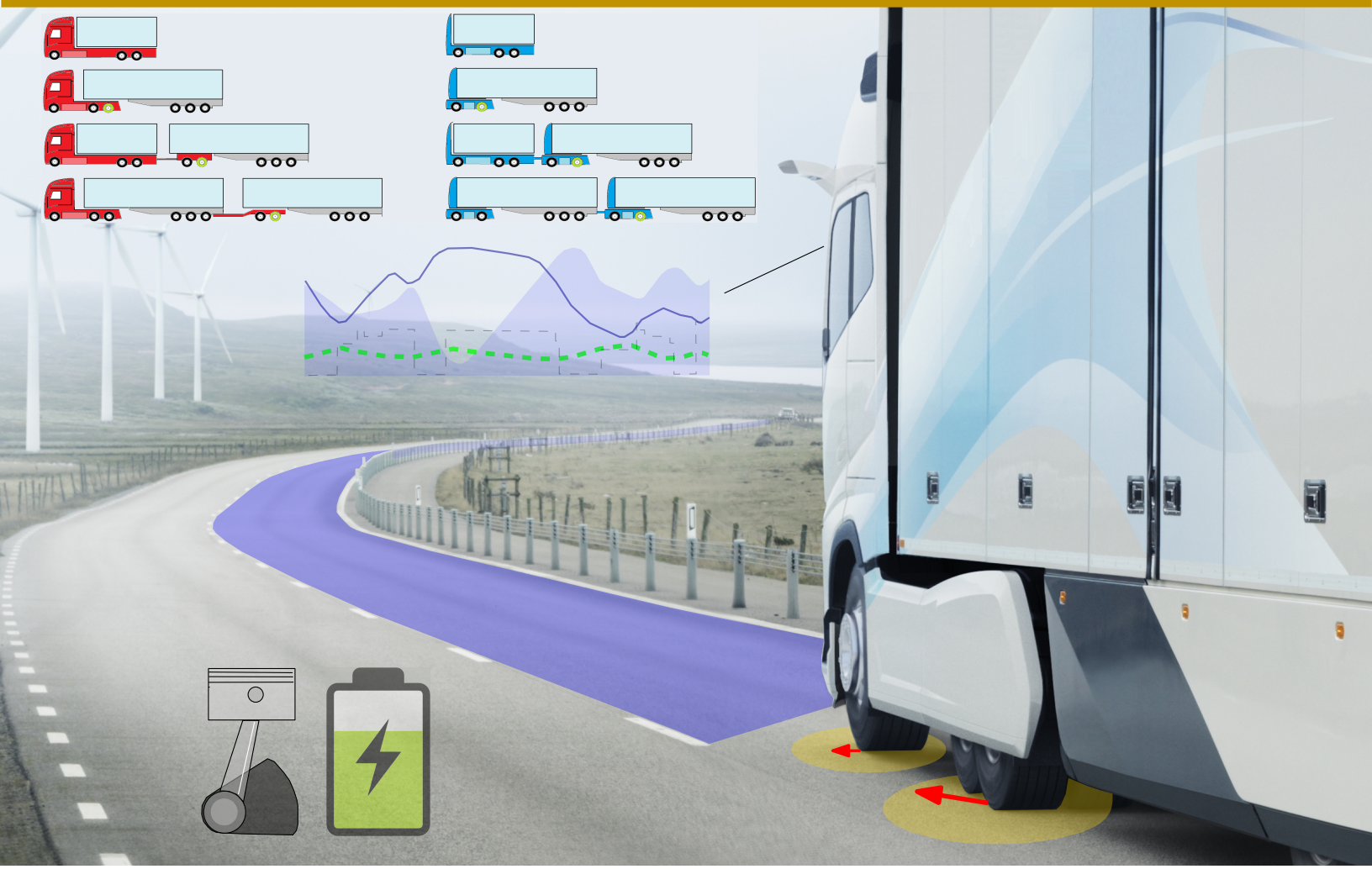

Transportation Mission-Based Optimization of Heavy Combination Road Vehicles and Distributed Propulsion

Including Predictive Energy and Motion Control

TOHEED GHANDRIZ

DEPARTMENT OF MECHANICS AND MARITIME SCIENCES
CHALMERS UNIVERSITY OF TECHNOLOGY
Gothenburg, Sweden 2020
www.chalmers.se

Thesis for the degree of doctor of philosophy
in
Machine and Vehicle Systems

Transportation Mission-Based Optimization of Heavy Combination Road Vehicles and Distributed Propulsion

Including Predictive Energy and Motion Control

TOHEED GHANDRIZ

Department of Mechanics and Maritime Sciences
CHALMERS UNIVERSITY OF TECHNOLOGY
Göteborg, Sweden 2020

Transportation Mission-Based Optimization of Heavy Combination Road Vehicles and Distributed Propulsion
Including Predictive Energy and Motion Control

TOHEED GHANDRIZ
ISBN 978-91-7905-415-1

Doctoral thesis at Chalmers University of Technology
Series number: 4882
ISSN 0346-718X

Department of Mechanics and Maritime Sciences
Chalmers University of Technology
SE–412 96 Göteborg
Sweden
Telephone: +46 (0)31–772 1000

Cover:
A Volvo truck (altered from the Volvo original image according to the approval). The vehicle looks ahead and plans optimal motion and energy usage, which is possible for any vehicle combination with distributed propulsion.

Chalmers Reproservice
Göteborg, Sweden 2020

To my parents
&
my beloved Fatemeh

"Simplicity does not precede complexity, but follows it."

Alan Perlis

Transportation Mission-Based Optimization of Heavy Combination Road Vehicles and Distributed Propulsion

Including Predictive Energy and Motion Control

Toheed Ghandriz
Department of Mechanics and Maritime Sciences
Chalmers University of Technology

Abstract

This thesis proposes methodologies to improve heavy vehicle design by reducing the total cost of ownership and by increasing energy efficiency and safety.

Environmental issues, consumers expectations and the growing demand for freight transport have created a competitive environment in providing better transportation solutions. In this thesis, it is proposed that freight vehicles can be designed in a more cost- and energy-efficient manner if they are customized for narrow ranges of operational domains and transportation use-cases. For this purpose, optimization-based methods were applied to minimize the total cost of ownership and to deliver customized vehicles with tailored propulsion components that best fit the given transportation missions and operational environment. Optimization-based design of the vehicle components was found to be effective due to the simultaneous consideration of the optimization of the transportation mission infrastructure, including charging stations, loading-unloading, routing and fleet composition and size, especially in case of electrified propulsion. Implementing integrated vehicle hardware-transportation optimization could reduce the total cost of ownership by up to 35% in the case of battery electric heavy vehicles.

Furthermore, in this thesis, the impacts of two future technological advancements, i.e., heavy vehicle electrification and automation, on road freight transport were discussed. It was shown that automation helps the adoption of battery electric heavy vehicles in freight transport. Moreover, the optimizations and simulations produced a large quantity of data that can help users to select the best vehicle in terms of the size, propulsion system, and driving system for a given transportation assignment.

The results of the optimizations revealed that battery electric and hybrid heavy combination vehicles exhibit the lowest total cost of ownership in certain transportation scenarios. In these vehicles, propulsion can be distributed over different axles of different units, thus the front units may be pushed by the rear units. Therefore, online optimal energy management strategies were proposed in this

thesis to optimally control the vehicle motion and propulsion in terms of the minimum energy usage and lateral stability. These involved detailed multitrailer vehicle modeling and the design and solution of nonlinear optimal control problems.

Keywords: transportation mission, propulsion system tailoring, optimization, heterogeneous heavy vehicle fleet, electrified propulsion, electromobility, automated driving systems, automation, optimal energy management, total cost of ownership, fleet sizing, long combination vehicles, single-track and two-track vehicle models, vehicle stability, motion control, longer heavier vehicles, optimal control, predictive energy management and vehicle stability.

Acknowledgments

First and foremost, I express my sincere gratitude to my supervisor Professor Bengt Jacobson for his encouragement and guidance through challenging problems. Bengt, your curiosity and patience during long discussions and supporting me with feedback greatly helped me to the end of this journey.

I would also like to extend my deepest gratitude to my cosupervisors Leo Laine and Peter Nilsson for the help and support you provided in understanding and solving practical problems. Leo, thank you for your great ideas about the existing problems, and Peter, thank you for sharing your knowledge and the support in performing experiments. Additionally, I would like to thank my former cosupervisor Manjurul Islam for fruitful discussions, support and feedback.

I had the privilege and honer to work with many wonderful people during my doctoral study. I would especially like to thank my papers' coauthors Jonas Hellgren for excellent support and guidance through practical problems and for opening my eyes to real-world vehicle-electrification complications, Nikolce Murgovski for helping me to better understand the challenges of nonlinear optimal control, and Niklas Fröjd for his support and acquiring experimental data and tire models.

Next, at Volvo GTT, I would like to thank Anders Eriksson, Rickard Andersson, Anders Svensson, Sofi Sjögren, Lena larsson, Inge Johansson, Stefan Edlund, Per Larsson, Peter Lindroth, and Pernilla Sustovic for giving me opportunity to work on practical problems. At REVERE lab, I would like to thank Fredrik von Corswant for his excellent support in performing experiments. I would also like to thank Selpi Selpi for follow-up PhD meetings and her efforts in making this journey pleasant.

Moreover, I am extremely grateful to all my present and past colleagues in the division of VEAS for providing a friendly environment with interesting and funny discussions and activities. I am really thankful to Simone Sebben for excellent management of the division; my friends and colleagues in vehicle dynamics group: Adithya, Alireza, Anton, Dragan, Fredrik, Ingemar, Juliette, Kristoffer, Luigi, Mathias, Mats, Pär, Sachin, Tushar and Weitao; and my friends in other groups especially Alexey, Jelena, Randi and Sina; and also Sonja for all your help and

kindness in administration and making the working environment even better. All of you made my PhD life much more fun and interesting.

I would also like to extend my sincere thanks to my former supervisors, before starting my PhD study, Claus Führer and Hilding Elmqvist. I would not start this wonderful journey without your support.

I am also grateful to my wonderful friends outside Chalmers. I am happy to have you all as friends. I especially thank Amir, Mohammad and Iman.

I would like to thank my family members for their love and support, my mom, and my siblings Babak, Maliheh, Shiva and Shima; my parents in law Bashir and Akram and siblings Nasibeh, Hamid and Elham. I am blessed to have you by my side.

My special thanks goes to my beloved wife Fatemeh. You are the reason for my happiness. Your support, love and patience are endless for me and words cannot express my love, gratitude and appreciation.

Finally, I gratefully acknowledge the financial support that this thesis received from the Swedish national research program FFI.

Toheed Ghandriz
Göteborg, November 2020

Thesis

This thesis comprises a summary and is based on the following appended papers:

Paper A
T. Ghandriz, J. Hellgren, M. Islam, L. Laine, and B. Jacobson, "Optimization based design of heterogeneous truck fleet and electric propulsion," in *2016 IEEE 19th International Conference on Intelligent Transportation Systems (ITSC)*. IEEE, 2016, pp. 328–335, doi: 10.1109/ITSC.2016.7795575

Paper B
T. Ghandriz, J. Hellgren, M. Islam, L. Laine, and B. Jacobson, "Sensitivity analysis of optimal energy management in plug-in hybrid heavy vehicles," in *2017 IEEE 2nd International Conference on Intelligent Transportation Engineering (ITSC)*. IEEE, 2017, pp. 320–327, doi: 10.1109/ICITE.2017.8056932

Paper C
T. Ghandriz, B. Jacobson, L. Laine, and J. Hellgren, "Impact of automated driving systems on road freight transport and electrified propulsion of heavy vehicles," *Transportation Research Part C: Emerging Technologies*, vol. 115, no. 102610, 2020. doi: 10.1016/j.trc.2020.102610

Paper D (appended in a shortened version)
T. Ghandriz, B. Jacobson, L. Laine, and J. Hellgren, "Optimization data on total cost of ownership for conventional and battery electric heavy vehicles driven by humans and by automated driving systems," *Data in brief*, no. 105566, 2020. doi: 10.1016/j.dib.2020.105566

Paper E
T. Ghandriz, B. Jacobson, M. Islam, J. Hellgren, and L. Laine, "Transportation-mission-based Optimization of Heterogeneous Heavy-vehicle Fleet Including Electrified Propulsion, Powertrain Tailoring, and Fleet Sizing,". Submitted for journal publication.

Paper F
T. Ghandriz, B. Jacobson, N. Murgovski, P. Nilsson, and L. Laine, "Real-time Predictive Energy Management of Hybrid Electric Heavy Vehicles by Sequential Programming,". Submitted for publication in IEEE Transactions on Vehicular Technology.

Paper G
T. Ghandriz, B. Jacobson, P. Nilsson, L. Laine, and N. Fröjd "Computationally Efficient Nonlinear One- and Two-Track Models for Multitrailer Road Vehicles,". *IEEE Access*, vol. 8, pp. 203854 - 203875, 2020, doi: 10.1109/ACCESS.2020.3037035

Paper H
T. Ghandriz, B. Jacobson, P. Nilsson, and L. Laine, "Trajectory-Following and Off-Tracking Minimization of Long Combination Vehicles: A Comparison Between Nonlinear and Linear Model Predictive Control". Submitted for journal publication.

Other publications by the author, not included in the thesis:

i
T. Ghandriz, and B. Jacobson "Predictive energy management of distributed propulsion over axles of long combination vehicles under lateral stability constraint,". Manuscript.

ii
T. Ghandriz, "Multitrailer vehicle simulation: Generation and Integration of Differential Equations," *Zenodo*, 2020. [Online]. Available: https://doi.org/10.5281/zenodo.4248263

iii
T. Ghandriz, and B. Jacobson, "A Vehicle Longitudinal Dynamical Model for Propulsion System Tailoring,". *Chalmers University of Technology*, Technical report, no. 2020:03.

iv
T. Ghandriz, "Transportation Mission Based Optimization of Heavy Vehicle Fleets including Propulsion Tailoring,". *Chalmers University of Technology*, Licentiate report, no. 2018:17.

v
T. Ghandriz, C. Führer, and H. Elmqvist, "Structural topology optimization of multibody systems," *Multibody System Dynamics*, vol. 39, pp. 135–147, 2017. doi: 10.1007/s11044-016-9542-7

vi
H. Elmqvist, A. Goteman, V. Roxling, and T. Ghandriz, "Generic Modelica Framework for MultiBody Contacts and Discrete Element Method," in *Proceedings of the 11th International Modelica Conference, Versailles, France, September 21-23, 2015* vol. 118, pp. 417–440. doi: 10.3384/ecp15118427

vii
T. Ghandriz, and C. Führer, "Topology Optimization of Dynamic Structures and Multibody Systems Based on Reduced Model Adjoint Sensitivity Analysis," in *Proceedings of the 28th Nordic Seminar on Computational Mechanics, 22 – 23 October, Tallinn, Estonia, 2015* pp. 55–58.

viii
T. Ghandriz, and H. Elmqvist, "Structural Topology Optimization of Multibody Systems having contacts between flexible bodies," in *Proceedings of the NAFEMS European Conference, Coupled MBS-FE Applications: From Classical Design to System Engineering, 20 - 21 October 2015, Turin, Italy* pp. 67-70.

ix
T. Ghandriz, C. Führer, and H. Elmqvist, "Structural Topology Optimization of Multibody Systems," in *Proceedings of Multibody Dynamics, ECCOMAS Thematic Conference, June 2015, Barcelona* pp. 828-838,

and patent applications:

x
T. Ghandriz, B. Jacobson, P. Nilsson, and L. Laine, "Predictive Energy and Motion Management for Multitrailer Heavy-Duty Vehicles," European patent application no. PCT/EP2020/082707, 2020.

xi
T. Ghandriz, B. Jacobson, P. Nilsson, and L. Laine, "Methods for Reducing High-Speed Off-Tracking in Multitrailer Heavy-Duty Vehicles," European patent application no. PCT/EP2020/082708, 2020.

In all the appended papers T. Ghandriz developed and was responsible for the conceptualization, methodology, software, validation, formal analysis, investigation, data curation, writing the original draft, review and editing, and visualization. The coauthors contributed in experimental data acquisition, review, editing, and supervision.

Acronyms

ADS	Automated Driving Systems
ADS–DV	Automated Driving Systems-Dedicated Vehicle
AGV	Automated Guided Vehicle
BEHV	Battery Electric Heavy Vehicle
CHV	Conventional Heavy Vehicle
COG	Center of Gravity
DAE	Differential Algebraic Equations
DAS	Driving Automation System
DP	Dynamic Programming
ECMS	Equivalent Consumption Minimization Strategy
EM	Electric Motor
EMS	Energy Management Strategy
ICE	Internal Combustion Engine
LCV	Long Combination Vehicle
LHV	Longer Heavier Vehicle
LP	Linear Program
LTI	Linear Time-Invariant
LTV	Linear Time-Varying
LU	Loading–Unloading
MINLP	Mixed Integer Nonlinear Programs
MPC	Model Predictive Control
NLP	Nonlinear Programs
NMPC	Nonlinear Model Predictive Control
NOCP	Nonlinear Optimal Control Problem
OCP	Optimal Control Problem
ODE	Ordinary Differential Equations
PMP	Pontryagin's Minimum Principle
PSO	Particle Swarm Optimization
QP	Quadratic Program

RHC	Receding Horizon Control
RTI	Real-Time Iteration
SLP	Sequential Linear Programming
SOC	State Of Charge
STL	Single-Track Linear
TCO	Total Cost of Ownership
TMMS	Transportation Mission Management System

Table of Contents

Chapter 1

Introduction

1.1 Motivations

New road transportation solutions can find their way to the market and be successfully accepted by consumers if they are economically competitive, energy efficient, and safe on roads.

Enhancement of road freight transport economy

In 2018, road freight transport accounted for 75.3% of the total EU inland tonne-kilometers of freight transport. The rest of the freight transport was performed using rail (18.7%) and inland waterways (6.0%) [34]. The selection of the transportation mode depends on factors such as cost, availability of infrastructure, accessibility, and speed.

The demand for road freight transport is growing [32] and a consequent increase in emissions and environmental damage is expected. The growing demand for road freight transport, pressure from regulators to fulfill environmental standards, technological advancements, and increasing consumer expectations create a competing environment for industrial players, original equipment manufacturers and logistics planners. These factors are often in contradiction to reducing vehicle costs. The primary drivers, however, for the adoption of a new road transport solution are the improved economy and profitability. The transport volume growth and the implementation of new technologies are two important sources of the future revenue increase in the truck industry [2]. Therefore, the competitiveness of new transport solutions depends on the development and implementation of new technologies, including driving automation systems (DASs) of different levels [122] and alternative propulsion systems and fuels, with lower prices.

Concerning the electrification of the propulsion system, environmental, technical, logistic, and financial factors, along with energy supply and infrastructure,

are essential, [132, 112, 128], whereas profitability is the primary reason for major transportation companies to adopt electrification.

Reducing emissions and improving energy efficiency

Heavy vehicles contributed 25% of road transport production of CO_2 in Europe in 2016 [32], and despite recent improvements in fuel efficiency, emissions from road freight transport are rising due to increasing traffic, emphasizing the importance of employing new transport solutions to meet environmental standards. In addition, according to Regulation (EU) 2018/842, CO_2 emissions of new heavy-duty vehicles must be reduced by 15% before the year 2025 and by 30% before 2030, compared to the emissions produced in 2019.

Increasing safety

In 2016, the World Health Organization reported approximately 1.35 million road traffic fatalities worldwide [146]. Such fatalities have shown an increasing trend. Heavy vehicles were involved in approximately 10% of road accident fatalities in 2016 [80, 33] in Europe. In recent years, advances in commercial vehicle safety has contributed to a decrease in fatalities related to these vehicles by approximately 40% between 2007 and 2016 in Europe [33]. In addition, DASs [122] have the potential to further decrease road accidents [3, 5, 17, 69] by performing complete or part of dynamic driving tasks. However, there are few publications related to driving automation and the active safety of heavy vehicles, despite differences in the dynamic behavior of these vehicles and passenger cars caused by differences in dimensions, center of gravity (COG), and articulation [135].

Moreover, among road freight transport solutions, long combination vehicles (LCVs) or longer heavier vehicles (LHVs), i.e., vehicles that have two or more articulated (towed) units, can help to satisfy the growing demand for road freight transport [118]. These vehicles occupy less space on the road for the same amount of transported freight. Moreover, LHVs of four vehicle units demonstrated reduced total cost of ownership (TCO) and fuel consumption by approximately 30% and 17%, respectively, on average compared to tractors and semi-trailers according to Papers C and D.

Despite the economic and environmental benefits of deploying LHVs, only a few countries allow LHVs on public roads, especially LHVs of four units, as their dynamic behavior must be improved and better controlled to ensure safe performance on the road [18, 48, 86]. This is especially important when the propulsion is distributed between axles of different vehicle units with the purpose of electrification and emissions reduction.

1.2 Main research questions

In freight transport, there are numerous contributing factors impacting transport efficiency and cost. Recognizing and understanding all these factors to include them in a mathematical model and optimization process to obtain the best solutions might not appear to be realistic. However, the development of such optimization models is possible if there is adequate information about potential future use-cases and the operational environment in which the vehicles are going to be employed. Moreover, considering closed-boundary use-cases opens up possibilities to find more cost- and energy-efficient customized vehicle-transport solutions.

Through implementation of mathematical modeling and optimization processes, this thesis addresses the following main questions.

- How can the road freight transportation efficiency and profitability be enhanced by tailoring the propulsion system of fleet freight vehicles when electrically propelled axles are allowed on any unit?
- How is the vehicle propulsion optimization coupled with the vehicle operational environment and infrastructure, and how do they affect each other?
- What are the answers to the above questions when automated driving systems are used?
- How can the motion and the powertrain of the designed vehicles be controlled in an optimal manner, considering the minimum energy usage and vehicle stability as components of the driving automation systems?

1.3 Background

1.3.1 Transportation mission

Road vehicle manufacturers often design heavy vehicles for a wide range of transportation missions and operational environments. Consumers purchase vehicles based on the intended use-case. If the use-case, for which the purchased vehicle is going to be employed is not clearly known, the vehicle optimality in terms of the operational and investment costs might be compromised. Moreover, if the consumers know the exact use-case of the vehicle, the designed vehicle might not be best-suited to perform the intended task of the consumer.

A simple example of choosing the correct vehicle for a specific transportation mission, regardless of the vehicle propulsion system, involves the selection of the appropriate vehicle size. The absolute investment and operational cost often increase with the size of the vehicle. To have a profitable business, the investment cost must be returned by the increased vehicle utilization and the time on the

road. Therefore, short-distance transportation assignments with long standing-still times result in low utilization, which makes large vehicles unsuitable for these kinds of assignments.

Vehicle size is only one aspect of the vehicle that influences the investment and operational cost. Other aspects, such as the propulsion system, driver, loading-unloading (LU), and driving cycle, also influence the TCO and must be considered when selecting the appropriate vehicle for a given transpiration mission all together.

Vehicle customization, however, is not a new objective of commercial-vehicle manufacturers. For example, the global truck application or the global transport application has already been developed to provide descriptions of vehicle utilization and the operational environment [30, 115] for vehicle customization and tailoring the vehicle hardware components. Such a tool can be incorporated with a more detailed description of the transportation mission characterized by nodes, demands, and available routes, to design even better customized vehicles, as performed in this thesis.

1.3.2 Automation

Major developments in automated driving systems (ADS) are expected in the near future and will reshape road transportation [142, 41]. ADS contribute to better user experience, efficiency, safety, mobility, productivity, energy, environment, and economy [3, 5, 14, 17, 54, 87, 95, 141, 142, 134, 74]. The user objectives and motivations differ for passenger cars and freight transport [141, 106], e.g., improving the user experience and reducing environmental damage for passenger cars and increasing the productivity and profitability for freight transport. In freight transport, the increased profitability caused by ADS is due to the reduction in labor costs and facilitated logistics and increased utilization and efficiency [142]. For instance, the driver cost disappears in high or full driving automation, whereas the cost of the transportation mission management system (TMMS) and the cost of sensors needed for road perception and response add up to the TCO. Moreover, in passenger cars, the reduction in fuel consumption achieved via ADS can reach 10% [96], whereas it is expected to be higher in freight transport, considering that heavy vehicles can form platoons, i.e., 8% and 15% for 10 m and 4 m gaps, respectively [136].

In the literature, different terms are used to refer to a “driving automation system” (DAS) and its features. This thesis follows the taxonomy defined in SAE standard J3016 [122]. According to this standard, a DAS refers to any system or feature that performs the entire or part of a dynamic driving task. Such systems can be categorized into five levels. A level–1 DAS (driver assistance) controls either lateral or longitudinal motion. A level–2 DAS (partial driving automation)

controls both lateral and longitudinal motion. A level–3 DAS (conditional driving automation) is capable of performing the entire dynamic driving task, but the driver should be ready to take control upon system request. In levels 1–3 of a DAS, a human driver must be present in the cabin. However, in level–4 (high driving automation) and level–5 (full driving automation), the presence of a human driver in the cabin is not needed: the DAS is capable of performing the entire dynamic driving task. In this case, a level–4 or level–5 DAS can stop the vehicle on the side of the road in the case of a failure. According to SAE standard J3016 [122], ADS refer to levels 3–5, and level–4 or level–5 DAS is referred to as an ADS–dedicated vehicle (ADS–DV). At levels 4 and 5, a remote dispatcher performs the dynamic driving task remotely, whenever necessary, and verifies the operational readiness of the vehicle. Levels 4 and 5 differ in their operational design domains. The operational design domain refers to the conditions under which a given DAS is designed to operate. A level–4 DAS is limited to a specific operational design domain, whereas a level–5 DAS is designed to operate on all roads and conditions that are navigable by a human driver.

1.3.3 Electrification

Battery electric and plug-in hybrid heavy vehicles produce less emissions than conventional vehicles, provided that the electric energy comes from renewable sources. However, the profitability of these vehicles is a concern in transportation. Factors that affect the profitability of these vehicles include operating range, payload, weight and volume of goods, charging infrastructure, utilization level, purchase cost, battery life, energy consumption, average speed, available routes, incentives, and logistics, according to [147], [132], [20], [40], [133], [85], [12], [101], [59], [112], [130] and [131].

For example, in addition to TCO, an important deciding factor for the adoption of battery electric heavy vehicles (BEHVs) in freight transport is their operating range, which is limited by battery capacity. Large batteries increase the vehicle TCO, which emphasizes the importance of BEHV customization based on the known transportation mission and other factors mentioned above. Hybrid vehicles that use battery or fuel cells as the sources of power were designed to increase the operating range; however, they also benefit from vehicle customization.

In regards to the impacts of high or full driving automation, i.e., increased utilization level, enhanced mission planning and logistics, improved energy management, and reduced energy consumption, and the requirement of BEHVs profitability, it can be concluded that ADSs increase BEHVs profitability and productivity, as is shown in this thesis.

1.3.4 Total cost of ownership

TCO is a measure for comparative analysis of competitive technologies. For instance, the profitability of vehicles with different powertrains can be compared using TCO [20, 40, 85, 130, 147, 84, 53, 131, 133, 112, 141, 111, 83]. The TCO of a vehicle includes the operational costs and the depreciation of the purchase price. Operational costs include the costs of fuel/energy, maintenance, taxes, and insurance, as well as the operational costs related to automation, e.g., remote dispatchers and TMMS, in the case of commercial ADS–DVs. Purchase price includes vehicle hardware component costs and the cost of additional sensors and investment in remote dispatchers, in the case of ADS–DVs, and the cost of charging infrastructure and LU.

For ADS–DVs, TCO analysis is rare in literature. Wadud Z. [141] performed a TCO analysis of conventional private and commercial vehicles and studied the potential adoption of ADS–DVs on public roads. The author stated that as the driver share of TCO increases, automation become more beneficial, e.g., in small commercial vehicles.

Moreover, as regards road vehicle competitive powertrain technologies, the literature about TCO all involves human drivers.

In the road freight transport sector, the literature confirms that the following factors help the competitiveness of the electric trucks against conventional counterparts: high utilization, low speed, frequent stops, tax incentives, long planning time horizon, i.e., vehicle life time beyond 10 years [20, 40], vehicle efficiency associated with the driving cycle, diesel fuel price, battery price and replacement, charging infrastructure, purchase price [85], vehicle customization, subsidies and exemption from city tolls, intermediate and quick charging, multishift operations, improvements in routing and scheduling [130], the period of ownership, the residual value and the second life of the battery [84, 83].

1.3.5 Infrastructure

Infrastructure in this thesis refers to LU devices that are available in LU points, as well as the charging stations and available routes. LU can be performed either with the help of the personnel and driver or automatically. Infrastructure is important because it has a direct impact on vehicle utilization and driver cost, and, thus, the TCO. LU and charging time reduce the vehicle time on-road and the utilization, while the driver cost is not reduced. On the other hand, there is a trade-off between the increased operational cost imposed by the LU and charging time and the investment cost spent on the LU devices and charging station power to reduce those operational costs. Therefore, depending on the transportation mission, the optimum infrastructure varies. For example, for quick LU of containers, having

an additional semitrailer, i.e., swapping a loaded semitrailer with an unloaded one or vice-versa, can reduce TCO, whereas other means of LU might yield a lower TCO if the container is not full.

Moreover, in freight transport, the driver often assists loading-unloading (LU) of the freight. Full automation of freight transport, therefore, also involves automation of LU. Automated guided vehicle (AGV) systems optimize the material flow and reduce personnel [41]. AGVs can be used for automated LU because they can operate automatically by themselves 24/7 due to the repetitive nature of the operations. The use of AGV systems in industry is widespread, as they are very useful in multishift operations and reducing TCO [138, 89].

Furthermore, in this thesis, charging stations are utilized at the LU point or consumer locations (if their existence is allowed by the optimizer). This approach saves costs and time compared to the use of publicly scarce charging stations [81] if LU and charging occur at the same place and time [131].

1.3.6 Predictive energy management

LHVs with distributed propulsion might yield the lowest TCO for a wide range of transportation assignments. In addition, advanced control strategies such as model predictive control (MPC) can be used for safe and energy-efficient operations. However, these control strategies do not need to be included in TCO minimization processes because they have a negligible effect (less than 2%) on the TCO, and all vehicles benefit to a similar extent by using these strategies. Therefore, the strategies do not affect comparative studies among different powertrains that are equipped with these strategies. However, inclusion of the advanced control strategies in LHVs is important for safe operation, which at the same time enhances the energy efficiency.

Optimal control, in particular MPC, is a suitable approach to solve control problems of multi-input multi-output systems involving many constraints. Moreover, any objective can be included as long as it can be described by a function of states, inputs and time (or distance). These properties make MPC a suitable method for minimizing vehicle energy consumption. In addition, an estimation of the future evolution of the system based on road topography and surrounding environment data is effective in reducing the energy consumption [125, 97, 42, 56, 126, 66, 67, 100, 137, 94, 21].

The literature reports different approaches for solving optimal control problems related to vehicle energy management using a point mass description of vehicle dynamics. The effectiveness of an approach in real-time applications depends on the problem definition and the number of states and control actions. As such, methods based on Pontryagin's minimum principle (PMP), dynamic programming (DP) according to Paper B and [126] , and direct methods, e.g., sequential

quadratic programming (SQP) [67, 100], are popular. PMP-base methods use PMP to derive analytic expressions to find the optimal solution. The equivalent consumption minimization strategy (ECMS) is a well-known example of PMP in hybrid electric vehicle energy management. In this problem, a dual variable replaces the actual problem state variable, and the prime problem is translated into a boundary-value problem that can be solved using shooting techniques. However, PMP techniques are computationally inefficient in the case of frequently activated state constraints.

DP is a useful method for solving optimal control problems involving integer decisions, i.e., mixed-integer optimal control problems. DP is based on Bellman's principle of optimality [8]. However, the inefficient implementation of DP in the presence of many state and control variables makes DP suitable mainly for off-line applications or applications with a low number of states and input decisions. For problems that involve two or more continuous states, direct methods are suitable, e.g., SQP, where, the state of charge (SOC) and speed profile can be simultaneously optimized. Integer states, i.e., engine on/off and gear profiles can also be added, for example, by combining convex optimization and DP [67, 100] or by combining DP and PMP [137]. Further explanation of the above approaches can be found in later chapters of this thesis. Overviews of different methods are provided in [94] and [21].

1.3.7 Vehicle motion modeling

Models of vehicle motion are needed to evaluate the performance of combination vehicles and their safe and energy-efficient optimal control. The longitudinal and lateral dynamic motion of a vehicle can be described by a mathematical model, with the purpose of developing early conceptual designs, as an alternative to performing real-world experiments [91, 4, 19, 78, 28, 38], or as a state prediction model within a controller, e.g., for motion control [36, 37, 35] and/or for powertrain control [67, 100].

The fidelity and complexity of mathematical models differ depending on the application of the vehicle model. In every application, there is a trade-off between model accuracy and computational efficiency, and the modeling often entails simplifications and linearization. For optimization and control design in real-time applications, proper simplification and/or linearization of the model is necessary to capture important dynamic behavior while maintaining computational efficiency [25, 52, 120, 92, 139, 123, 99, 61, 145, 63, 129, 104]. In vehicle control applications, a simple model, e.g., a point mass or a single-track linear (STL) model, is often used for state prediction. Then, a more complicated vehicle model is used for control allocation in the second control layer, e.g., for powertrain control [67] or motion control [148].

In the literature, STL models are widely used as linear models to describe the motion of articulated vehicles and LHVs [92, 62, 13, 76]. These models approximate vehicle motion in certain driving scenarios and in certain applications with an acceptable accuracy. These scenarios include active steering and feedback motion control in nonoptimal control applications and steady state maneuvers at constant speed with small steering and articulation angles. STL models are derived by assuming small articulation, steering and tire slip angles and a linear tire model, by decoupling the longitudinal and lateral equations and by neglecting longitudinal acceleration. However, early system linearization, as in the case of STL models, where the nature of the maneuver has not been taken into account, are not suitable for applications of optimal control with long prediction horizons and combined steering, braking and propulsion control. Moreover, depending on the maneuver, the essential dynamics can be lost, including the accuracy in the estimation of articulation angles and lateral acceleration on curved roads, the relation between longitudinal and lateral dynamics, and phenomena from non-Ackermann geometry. Comparisons between STL models and high-fidelity models can be found in [62, 13].

1.3.8 Vehicle lateral stability

Understanding the lateral stability of combination vehicles is important for improving the safety within vehicle predictive motion control.

Free-response lateral stability

If longitudinal and lateral dynamics are decoupled, then the lateral equation of motion can be linearized given a constant longitudinal speed. In this case, the system dynamics can be expressed in state-space form, whereas the system matrix depends on the vehicle parameters such as mass distribution, wheelbases, and position of articulation points [92]. In most cases, and for normal mass distributions, the articulated vehicles are designed such that the eigenvalues of the continuous-system matrix are all negative, indicating that the linear system is mathematically stable. Asymptotic stability of the nonlinear system, however, requires a careful proof using the Lyapunov theorem [73].

Vehicle-driver closed-loop stability

The articulated vehicle stability often refers to vehicle-driver closed-loop stability. Instability is defined as an unbounded articulation angle and/or loss of control by deviating from the desired path [92], e.g., jack-knifing or trailer swing, as shown in Fig. 1.1. In these cases, the vehicle might be mathematically stable in free response to disturbances.

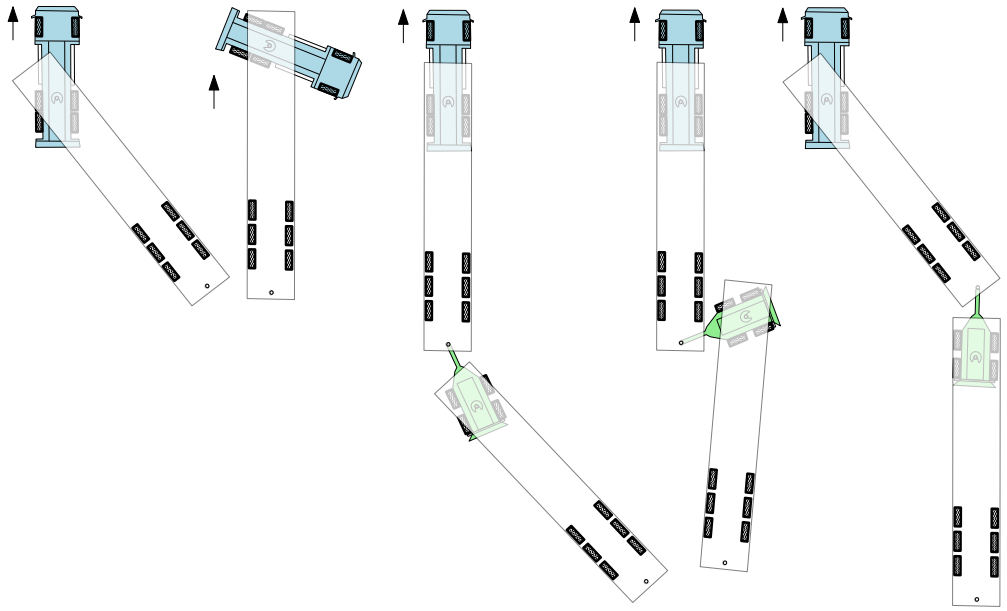

Figure 1.1: Examples of losing yaw stability, i.e., jack-knifing and trailer (or dolly) swing.

According to ISO 14791 [64], rearward amplification and dynamic off-tracking are measures for determining the lateral stability of articulated vehicles, which are related to the system forced response. The rearward amplification refers to the ratio between the maximum vehicle response of the last unit and the maximum response of the first unit during a certain maneuver. The response can be characterized by the lateral acceleration and/or yaw rate. The dynamic off-tracking (also known as overshoot in a high-speed maneuver) refers to the maximum deviation of the path of the last unit, e.g., the center point of the rear edge or the axle, from the path of the first unit, e.g., the center point of the front edge or the axle, during a certain maneuver.

1.3.9 Motion planning and motion control

In this thesis, safety critical situations are basically avoided by the predictive energy management controller including lateral stability constraints. However, the control strategies are also designed to include path tracking in the cost function rather than as constraints to reduce lateral off-tracking. Reduction in lateral off-tracking was not included in the energy management controller in this thesis, but it was included as a separate controller that can intervene whenever necessary, used parallel to energy management, or when the energy management controller is off.

Motion planning is a part of the dynamic driving task in level-3 and higher

levels of DAS and refers to computing a collision-free and dynamically feasible motion trajectory [108]. Motion control is thus a low-level control layer responsible for generating control actions that are executed by actuators to track the trajectory generated by the motion planner. In the case of articulated vehicles and LHVs, vehicle stability must be assured by both control layers such that the motion planner generates a feasible path for the motion controller to track the path and maintain stability. In this case, the two layers can be merged into a single control layer using a single vehicle model [140].

Direct implementation of motion planning and the control algorithms developed for passenger cars [51] is not possible for articulated heavy vehicles, especially for LHVs, due to differences in the height of the COG and weight, as well as the presence of articulated units. Because of these differences, the path generated by the motion planner of a passenger car might be infeasible for LHVs and may cause instability.

For heavy and articulated vehicles, the literature on motion planning is not rich. Simple vehicle models with zero slip were used, for example, in [46] for path planning of a truck and trailer using splines and in [90] for path planning of a two-trailer vehicle using a lattice-based approach. A more complicated vehicle model was used in [102, 103] for a four-unit LHV, i.e., an A-double, where the longitudinal and lateral dynamics were decoupled using a STL model. A first-order model of the powertrain was used to control the acceleration. MPC found its applications in motion planning, e.g., linear time-varying MPC (LTV-MPC) was used in [88] for motion planning of a single-unit heavy vehicle, where model linearization was performed around the operating point using a single-track vehicle model with constant speed and linear tires. A nonlinear MPC (NMPC) with real time iteration (RTI) approach [27, 49] was used in [140] for real-time trajectory planning and control of an A-double, where the relation between the longitudinal and lateral dynamics was neglected by the authors and it was assumed that all the vehicle units were at the same longitudinal position. In that work, mainly the steering input of the first axle was controlled, and the objectives included driver comfort, tracking performance, and maintaining a safe distance from other road users.

The literature on the motion control of LHVs focuses mainly on active steering. Active steering of LHVs refers to controlling the steered axles (usually trailers axles) to reduce off-tracking. A vehicle model that is often used in active steering is STL [77, 76, 119, 55, 61, 119, 116].

STL models limit the control design to specific scenarios, and a different design must be used if the driving scenario is changed. For example, path-following at low speeds and lateral stability at high speeds are contradictory design goals that were discussed in [55, 61]. These contradictory design goals were addressed in [70], where longitudinal velocity was used as a scheduling parameter in a gain-scheduled

controller.

MPC is not popular in the active steering literature. An LTV-MPC was used in [9] with a nonlinear single-track model. The LTV-MPC was built via piecewise linear approximation of the model for different values of trailer angle. The objective was to reduce the off-tracking of a tractor-semitrailer. In the vehicle model, the longitudinal and lateral dynamics were decoupled, and a linear tire model was used.

In addition to active steering, the literature reports on the use of differential braking to reduce off-tracking of LHVs [39, 93]. However, this approach was implemented via heuristics and repetitive simulations rather than by performing robust optimization.

1.4 Main contributions

This thesis contributes to three overlapping categories related to the design and control of articulated heavy vehicles and LHVs.

1.4.1 Mission, infrastructure and propulsion tailoring

As was stated in licentiate thesis [44], through implementation of optimization processes, this thesis contributes to enhancing road freight transportation efficiency and profitability by optimizing missions, fleet propulsion systems and infrastructure. Profitability is a key factor for transportation companies to move towards new solutions; therefore, the total cost of fleet ownership (TCO) was considered as an optimization objective in most of the cases in this thesis, and related comparisons are made. The optimization design variables varied with the problems studied. The variables were related to the transportation mission and vehicle hardware, in particular, the propulsion system. Within the propulsion system, the thesis especially considered adding electric propulsion on some units in LHVs. Transportation mission-related design variables included route, fleet composition, fleet size, number of trips, speed, and infrastructure, such as LU scheme and charging station (for electric vehicles) at each node of the transportation network. Correspondingly, vehicle-related design variables included vehicle size, type of propulsion system, i.e., a choice between combustion-powered, battery electric and hybrid powertrains, internal combustion engine (ICE) size, type of electric motors, number of powered axles, recharging power, and size and type of the batteries.

Electrified propulsion proved to be one of the main solutions for green transportation. As the literature and real-word experience of transportation companies suggest, the profitability of battery electric vehicles can be improved by customiz-

ing the vehicle hardware. Indeed, this thesis identified an interconnection between different cost indicators, and considering all these indicators in an integrated optimization process could make a fleet of BEHVs competitive with their conventional counterparts in a wide range of transportation missions.

Furthermore, the highest potential revenue offered by new technologies in the near future comes from deploying ADS–DVs. In this thesis, it was also shown that these kind of heavy vehicles might benefit substantially from simultaneous optimization of the vehicle hardware-infrastructure. It was revealed to what extent ADS facilitate BEHVs in different transportation scenarios, and corresponding sensitivity analyses were performed.

1.4.2 Vehicle modeling and optimal motion control

In this thesis, a systematic approach was proposed for efficient modeling of two- and one-track multitrailer vehicles with an arbitrary number of units and different fidelity. The obtained models are nonlinear; however, methods for linearization depending on the nature of problem were provided. The performance of the generated models in predicting the dynamic behavior of the LHVs was validated against experimental data. The models described the coupled longitudinal and lateral dynamics and could be used for measuring the vehicle performance characteristics and to facilitate coupled steering, braking and propulsion control in any driving scenario and in optimal control applications.

It was demonstrated that a good choice of a linearization method depends on the nature of the problem and the maneuver, whereas the accuracy of STL models should not be taken for granted in all applications. This approach is particularly important in motion planning and motion control involving long prediction horizons where MPC is used. Through comparison of nonlinear and linear MPC, i.e., comparison between SQP and LTV-MPC, for trajectory-following and off-tracking minimization of an A-double LHV, it was shown that STL models suffer from inaccurate prediction of vehicle dynamic behavior in long prediction horizons.

1.4.3 Predictive energy management under lateral stability constraints

As electrifying the vehicle units was shown to be cost- and energy-effective, this thesis proposed real-time predictive energy management strategies for minimizing the energy consumption of hybrid electric vehicles, including DP, and sequential programming, e.g., SQP and sequential linear programming (SLP). The energy management strategies considered road topography, road speed limits, and integer decisions for engine on/off and gear selection. Moreover, the distribution

of braking and propulsion among different axles of different vehicle units could cause instability; therefore, the problem of predictive energy management of hybrid vehicles with distributed propulsion was studied in this thesis. The problem of real-time optimal EMS of hybrid vehicles was extended to include a detailed model of vehicle lateral dynamics, the vehicle stability constraints and safe driving. Such a problem definition was essential for guaranteeing safe control of distributed propulsion in LHVs. The proposed nonlinear optimal control problem (NOCP) included 12 states and five inputs for the subject LHV, which was an A-double. The lateral dynamic model was highly nonlinear. A strategy was proposed to address the lateral dynamic stability constraints inside the EMS NOCP, which made the real-time implementation of the algorithm possible.

More detailed contributions of this thesis can be found in section 1.6.

1.5 Limitations

The limitations of this thesis are listed in the following; some were already mentioned in the licentiate thesis [44].

- In regards to freight transportation with many contributing factors, an accurate description must be obtained via clear communication between transportation companies, logistic industries and vehicle manufacturers. Thus, close cooperation between these stakeholders should be implemented during strategic levels of decision making. This thesis assumed that such cooperation results in a deterministic description of the transportation assignments. Therefore, possible uncertainties in the description of the transport mission were neglected. Therefore, the designed vehicles are optimum only for the assigned mission. The vehicles can be designed for a wide range of missions if they are required to meet strong performance characteristics, which yields increased TCO.

- The operational environment and the operating cycles used for TCO optimizations included prescribed reference speed profiles based on the representative road data, and no unexpected change in surrounding environment, e.g., caused by wind and traffic disturbances, were considered. Therefore, TCO calculation does not include the increased energy consumption and trip time caused by these disturbances.

- In the case of fleet vehicle-infrastructure design and fleet sizing via TCO minimization, efficient vehicle longitudinal dynamic and powertrain models were used. Because the optimization processes needed to be solved for many different scenarios, the vehicle model simulations had to be computationally

efficient; thus, the lateral dynamics were neglected during TCO minimization. This may result in an underestimation of the energy consumption which is negligible in TCO calculation for driving in highways.

- The source of power in the designed vehicles included diesel ICEs and batteries, and both in parallel hybrid vehicles, whereas alternative power sources, such as fuel cells and series hybrid, were not included.

- The control strategies for evaluating energy consumption of different powertrain configurations during TCO minimization followed rule-based strategies rather than optimal strategies. As shown in Paper B, the contribution of the optimal energy management strategies in TCO reduction could be negligible in smooth traffic and was relatively similar for different vehicle powertrain configurations.

- The vehicle models used for motion control in this thesis were derived based on assumptions to assure efficient simulation while capturing the important dynamics. The vehicle models were limited to the yaw-plane motion, moment- and friction-free articulation joints, and a small wheel inertia. Moreover, the longitudinal speed could not be zero, and longitudinal tire slips were not directly calculated: it was assumed that there was a slip controller that finds the appropriate slip based on the given tire force.

- The results are based on simulations. No experimental verification was performed for the proposed control algorithms. However, the developed vehicle mathematical models were verified using experimental data.

- This thesis assumes that the information about the surrounding environments, as well as the required feedback signals, is available.

1.6 Outline

The first four chapters of this thesis provide a summary of the appended papers. Parts of Chapter 5, however, include topics that were not presented in those papers.

There are two main parts studied in details in this thesis: 1) transportation mission-based optimization of heavy vehicle fleets, including propulsion tailoring, and 2) applications of optimal control in minimum-energy transportation, including lateral stability and motion control.

The relation between the appended papers and the other publications not included in this thesis is depicted in Fig. 1.2.

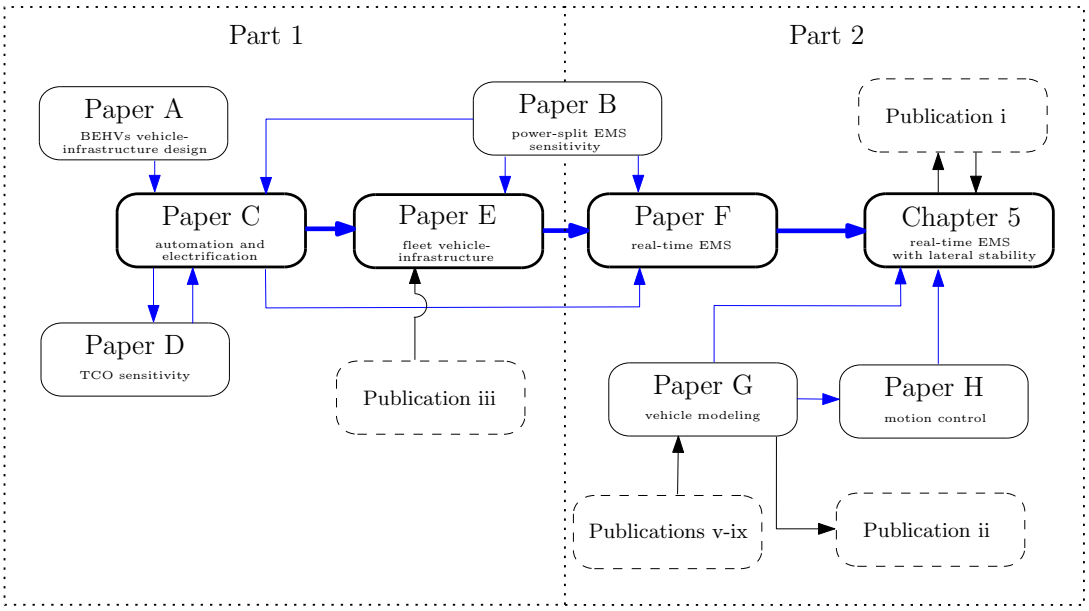

Figure 1.2: The relation between the appended papers, relevant publications, and Chapter 5 of this thesis. Some parts of Chapter 5 are not presented in any of the appended papers.

The content of each of the appended papers and their contributions are described in the following:

Paper A, BEHVs vehicle-infrastructure design

In Paper A, the vehicle-infrastructure design problem was discussed. The problem was defined as minimizing TCO by determining the number of vehicles of type i to employ on route j, for $i = 1, \ldots, n_v$ and $j = 1, \ldots, n_r$, where n_v and n_r denote the total number of vehicle types and available routes. The case-study problem solved in Paper A included only electrified propulsion and three routes. The vehicle-related design parameters included the vehicle size, type and number of electric motors and the type and number of battery packs. The transportation task-related design parameters included selection of the route and the recharging power at each node. The design parameters were selected from a discrete set, and the reference speed was set according to the legal speed limit of the road. The simplicity of the transportation task comprising only two nodes made it possible to solve the problem by enumeration, i.e., simulating all the possible cases and picking the best one. Therefore, it was possible to avoid the use of optimization methods. The solution of the case study problem in Paper A was not a heterogeneous fleet but a single battery electric rigid truck operating on a single route.

Paper B, power-split EMS sensitivity

In Paper A, the study was limited to BEHVs owing to the user request. However, a more general definition of vehicle-transport design must include a greater number of design parameters. Therefore, propulsion systems, such as combustion-powered and hybrid, were included in Paper B. In the case of hybrid propulsion, the EMS is important for energy-cost evaluation along with the selection of the propulsion components. In that paper, EMS referred to a strategy of splitting the total requested power between ICE and electric motors. A poor EMS could result in over-sizing the batteries and ICE. Thus, the selection of the propulsion components is coupled with the EMS. However, considering this coupling in the vehicle-infrastructure optimization process, particularly in the conceptual design stages, causes a time resource problem since the simulation time of a sophisticated optimal EMS for the entire trip could be long. To investigate the possibility of implementing simpler EMS approaches than the optimal EMS during the vehicle-infrastructure optimization process, a sensitivity analysis was conducted to determine the effect of different propulsion system components on the value gained by implementing the optimal EMS in Paper B. The "value" reflected the reduction in the operational costs (or the objective cost), such as the cost of fuel, electric energy, battery wear, and the cost of changing the ICE state from off to on, compared to the costs obtained by a simpler EMS. The simpler EMS was a rule-based EMS or an instantaneous EMS, where the upcoming prediction horizon was not considered. Dynamic programming was used as a solution method for optimal EMS. The value gained by the optimal EMS was calculated with respect to the variations in vehicle total mass, ICE size, battery size, electric motors maximum power, smoothness of the traffic, and the inclusion and exclusion of the battery degradation cost in the cost function.

Paper C, automation and electrification

Paper C discussed the influence of ADS on the vehicle propulsion system, specially in BEHVs. Moreover, the impact of the ADS on the optimum propulsion systems and infrastructure both in the BEHVs and the conventional heavy vehicles (CHVs) was studied, and transportation missions with different characteristics were considered, i.e., transportation missions with different driving ranges (distances between LU points or charging stations), road hillinesses, average reference speed and vehicle size. The study, however, did not include hybrid vehicles.

The vehicle-infrastructure design variables included the size of ICE, type and number of electric motors, type and size of battery packs, charging power and LU scheme. To make the vehicle utilization independent of the filled capacity, missions were defined such that vehicles always travel fully loaded up to their gross mass. Moreover, a sensitivity analysis was performed for sample missions to study the

effects of parameter variations on the TCO of the optimal vehicle-infrastructure.

Paper D, TCO sensitivity

In Paper D, sensitivity analyses were performed for many different transportation scenarios to demonstrate the dependence of the TCO and its cost indicators to various parameters, including vehicle utilization, battery price, ICE efficiency, vehicle life time, discount rate, price of diesel fuel, price of electric energy, and price of ADS-specific hardware. The sensitivity analyses revealed the competitiveness between different transportation solutions, i.e., BEHVs with human drivers, ADS–DV BEHVs, CHVs with human drivers and ADS–DV CHVs, and the variation with respect to different parameters.

Paper E, fleet vehicle-infrastructure

In Paper E, the vehicle-infrastructure problem presented in Paper C, where missions comprised exclusively two LU nodes, was extended to consider a transportation network comprising more LU nodes. Moreover, the transportation network included different routes between LU nodes. In addition, the design of a mixed fleet was considered, where the vehicles could differ in size, propulsion system and components of the propulsion system. The charging infrastructure and the LU scheme at each of the nodes were also decided. The inclusion of all these design variables resulted in a complex problem that was solved with the proposed methodology, which assumed a limited number of available routes.

As the results of papers C and E suggested, the hybrid and electric heavy vehicles were cost-efficient in various transportation scenarios. The propulsion needed to be distributed between different units and axles of LHVs, both for logistic reasons and to reduce the TCO. Optimal control of energy usage, however, was not considered in the TCO minimization. The rest of the papers of this thesis studied optimal energy management, the effects of distributed propulsion on energy management, and optimal motion control.

Paper F, real time EMS

In Paper F, the problem of predictive energy management of hybrid electric vehicles was studied in a three-layer control hierarchy. The first layer generated the desired optimal longitudinal speed and the state of charge trajectories, whereas the second and third layers were responsible for following the desired trajectories. Quadratic and linear sequential programming were used as solution methods to solve the nonlinear optimal control problem in the first control layer, and the related comparisons were made. The SQP was studied with/without an updating cost function. The SLP was more efficient than the SQP. In both cases, the gear

integer decisions were handled by solving an instantaneous optimization problem over the prediction horizon sequentially. The main contribution of this paper is the implementation of an efficient SLP algorithm for solving the NOCP considering the road topography and speed limits ahead.

In Paper F, the vehicle was assumed to be a point mass, and the lateral dynamics were neglected.

Paper G, vehicle modeling

In Paper G, equations of motion of multitrailer vehicles with arbitrary number of vehicle units were derived symbolically using Lagrangian dynamics. The vehicles could have either one or two tracks, with different levels of complexity and fidelity, whereas in the appended code, the user had the option to include different force elements, the lateral load transfer, and linear or nonlinear tire models. The obtained equations were a nonlinear system of implicit differential equations in minimum order, i.e., the number of unknowns equaled the number of equations that described the coupled longitudinal and lateral dynamics in the yaw-plane. Moreover, the Paper compared the ability of the proposed model to predict the vehicle dynamic behavior with the experimental data. In addition, the performance of the vehicles with different fidelity was also compared. The modeled vehicles included a nonlinear model of a two-track 11-axle LHV, and similar vehicles but with different numbers of axles and tracks, i.e., a nonlinear single-track 6-axle vehicle model and a linear single-track 6-axle vehicle model. The main conclusion was that the nonlinear single-track 6-axle vehicle model, which was more efficient than the two-track 11-axle counterpart, predicted the vehicle dynamic motion with an acceptable level of compliance with the experimental data. The models could be used for evaluating the vehicle lateral performance and for the vehicle state prediction in optimal control applications, e.g., for combined optimal control of steering, braking and propulsion. Such an application of the vehicle model was studied in Paper H.

Paper H, motion control

The combined optimal steering, braking and propulsion control was tested for motion control of an A-double in Paper H. The trajectory-following and off-tracking minimization problem was solved with the nonlinear and linear optimal control approaches. The Paper described the differences among LTV-MPC, SQP and RTI and showed that the LTV-MPC gives a similar solution as the SQP if the model is linearized around a reference guess trajectory that considers the nature of the maneuver in the prediction horizon. This was an important conclusion showing that the system linearization can be done off-line and only once, e.g., at the beginning

or during the trip, if information about the future road and maneuver is available. This was a foundation for the inclusion of the lateral stability constraints in the long-horizon predictive energy management of distributed propulsion, which is studied in this thesis.

The rest of this thesis is organized as follows: Chapter 2 presents most of the methods that were used to solve the problems defined in the thesis; Chapter 3 defines the problem of vehicle-infrastructure design and provides a summary of the results; Chapter 4 outlines a summary of the optimal motion control of LHVs, i.e., optimal control of combined steering, braking and propulsion; Chapter 5 introduces and solves the predictive energy management problem, including the lateral stability constraints. This chapter is then followed by concluding remarks, appendices and references. Finally, the appended papers follow in the printed version of this thesis.

Chapter 2

Methods

2.1 Optimization problems

The general form of an optimization problem is

$$\begin{aligned} &\text{find} && x \in \mathbb{R}^N && \\ &\text{to minimize} && f(x) && \text{(2.1a)} \\ &\text{subject to} && g(x) = 0, && \text{(2.1b)} \\ & && h(x) \leq 0, && \text{(2.1c)} \end{aligned}$$

where x is a decision variable (also referred to as design variable), $f : \mathbb{R}^N \to \mathbb{R}$ is a cost function, $g : \mathbb{R}^N \to \mathbb{R}^m$ represent a set of equality constraints, and $h : \mathbb{R}^N \to \mathbb{R}^q$ denote a set of inequality constraints. Depending on the properties of the decision variables, cost function, and constraints, approaches to solving optimization problem (2.1) differ. This thesis concerns different problems with the following characteristics:

1. decision variables are bound to be discrete along with the nonsmooth cost function and constraints, used mostly for TCO minimization;

2. combined discrete and continuous decision variables along with nonlinear and smooth cost function and constraints, known as mixed integer nonlinear programs (MINLP), used for EMS;

3. continuous decision variables along with a nonlinear and smooth cost function and constraints, known as nonlinear programs (NLP), used for motion control.

2.2 Derivative-free optimization[1]

This section focuses on solving the problems with properties stated in (1) above. The other forms are discussed in later sections.

Derivative-free and stochastic optimization methods are suitable for solving problems of form (1), as they rely only on the value of the cost function rather than its derivative [117, 143]. Starting from a guess population of solutions, stochastic methods can be used to find near-global solutions iteratively. A particular interest of this thesis is particle swarm optimization (PSO) [72, 143]. PSO has been shown to be one of the best methods for finding a near-global solution with the least number of function evaluations for a nonsmooth cost function and constraints [117], as long as the number of decision variables remains less than 30. This is the case with the problems studied in this thesis.

In PSO, as the name suggests, a swarm of particles move towards the optima with a relative speed and distance from each other and the best particle found in the previous iteration. Algorithm 1 describes the steps of solving optimization problem (2.1) using the PSO method, where the decision variables are bound to be integers.

Algorithm 1 might not find the global optima or even a feasible solution unless the initialization is feasible and the algorithm is repeated multiple times. For more details, refer to [143]. Notably, the PSO presented in algorithm 1 is not restricted to integer nonlinear nonsmooth programs but can be updated to solve any MINLP. In this thesis, PSO was used to solve different problems in papers A, B, C, and E.

[1] Derivative-free optimization, in particular PSO, was used in Papers C, D, and E for TCO minimization and in Paper G for tuning the vehicle parameters. Most parts of this section were already presented in Paper D.

Algorithm 1 PSO

Input: bounds of the design variables $x_{\min}$ and $x_{\max}$ and their speeds of change $v_{\min}$ and $v_{\max}$ and tuning parameters used for updating the speeds: $\beta = 0.99$, $w_{\min} = 0.4$, and $\Delta t = 1$;

Initialization: Assign a large value to the initial cost functions, and for some random values $r_{\mathrm{x},ik} \in [0,1]$ and $r_{\mathrm{v},ik} \in [0,1]$, initialize the positions x_{ik} and the speeds v_{ik} of n particles, for $i = 1,\dots,n$ and $k = 1,\dots,N$, as well as the speed updating weighting factor w; where, n is the number of particles in the swarm and N is the number of dimensions in the search space;

$x_{ik} = \lfloor x_{\min,ik} + r_{\mathrm{x},ik}(x_{\max,ik} - x_{\min,ik}) \rceil$, where $\lfloor . \rceil$ returns the closest integer,

$v_{ik} = r_{\mathrm{v},ik}(x_{\max,ik} - x_{\min,ik}) - 0.5(x_{\max,ik} - x_{\min,ik})$,

$f(x_i^{\mathrm{b}}) = 10^{16}$, where x_i^{b} is the best position of particle i,

$f(x^{\mathrm{gb}}) = 10^{16}$, where x^{gb} is the global best position of the particles;

1: **while** *not converged* **do**

2: Evaluate the cost function $f(x_i)$, $i = 1,\dots,n$;

3: Update the best position of each particle and the best global position:

$x_i^{\mathrm{b}} \leftarrow x_i$, if $\{f(x_i) < f(x_i^{\mathrm{b}}),\ g(x_i) = 0,\ h(x_i) \le 0\}$, $i = 1,\dots,n$,

$x^{\mathrm{gb}} \leftarrow x_i$, if $\{f(x_i) < f(x^{\mathrm{gb}}),\ g(x_i) = 0,\ h(x_i) \le 0\}$, $i = 1,\dots,n$,

4: Update velocities and positions using random variables $q \in [0,1]$ and $p \in [0,1]$, for $i = 1,\dots,n$ and $k = 1,\dots,N$:

$v_{ik} \leftarrow w\ v_{ik} + 2\ q\ (x_{ik}^{\mathrm{b}} - x_{ik})/\Delta t + 2\ r\ (x^{\mathrm{gb}} - x_{ik})/\Delta t$,

$v_{\min} \le v_{ik} \le v_{\max}$,

$x_{ik} \leftarrow \lfloor x_{ik} + \Delta t v_{ik} \rceil$

$w \leftarrow \max(\beta\ w, w_{\min})$;

5: **end while**

6: **return** x^{gb}.

2.3 Nonlinear optimal control

A NOCP aims to find control law trajectories for a dynamic system such that a cost functional is minimized. In this thesis, the problems are nonlinear since the cost function, e.g., fuel consumption, battery degradation, and electric energy, as well as the constraints, e.g., propulsion system and battery losses, vehicle model, and stability constraints, are nonlinear functions.

The trajectories are often defined over time. In this thesis, however, it is more convenient to describe the trajectories over space, as in the sequel, problem constraints are defined as functions of space rather than time. The nonlinear

optimal control problem in continuous form is thus defined as

$$
\begin{aligned}
&\text{find} && u(s),\\
&\text{to minimize} && C_{\mathrm{t}}(x(s_{\mathrm{f}}), s_{\mathrm{f}}) + \int_{s_0}^{s_{\mathrm{f}}} L\big(x(s), u(s), s\big) ds, && \text{(2.2a)}\\
&\text{subject to} && g\big(x(s), \frac{dx(s)}{ds}, u(s), s\big) = 0, && \text{(2.2b)}\\
& && h\big(x(s), \frac{dx(s)}{ds}, u(s), s\big) \leq 0, && \text{(2.2c)}\\
& && x(0) = \hat{x},
\end{aligned}
$$

where C_{t} is the terminal cost, L denotes the stage cost, g denotes the dynamic system of which the inputs and states are denoted by $u(s)$ and $x(s)$, respectively, h denotes inequality constraints, the initial state is $\hat{x}$, and s_0 and s_{f} represent the start and final distance.

Different approaches to solving NOCPs exist. As discussed in Chapter 1, in this thesis, direct methods, in particular sequential programming and DP, were preferred. The following sections describe these methods.

2.3.1 Sequential programming[2]

Sequential programming is a direct method for solving NOCPs. When implementing the direct methods, the OCP (2.2) must be discretized and then optimized [49]. The space is discretized to N steps assuming a zero-order-holder that keeps the controls constant within the discretization step. Then, the state derivatives are approximated by, e.g., explicit Euler, multistep methods, or Runge-Kutta method, [15, 31], whereas the chosen method should be suitable for implicit ODEs such as (2.2b). The OCP in discretized form reads

$$
\begin{aligned}
&\text{find} && x^{(k+1)}, u^k,\ k = 0, \ldots, N-1\\
&\text{to minimize} && C_{\mathrm{t}}\big(x^N, N\big) + \sum_{k=0}^{N-1} L\big(x^k, u^k, k\big) && \text{(2.3a)}\\
&\text{subject to} && \text{for } \ k = 0, \ldots, N-1,\\
& && g(x^{(k+1)}, x^k, u^k, k) = 0, && \text{(2.3b)}\\
& && h(x^{(k+1)}, x^k, u^k, k) \leq 0, && \text{(2.3c)}\\
& && x^0 = \hat{x},
\end{aligned}
$$

[2]Sequential programming was used in Papers F and H for optimal energy and motion control. Most parts of this section were already presented in those papers.

where the same notation as in (2.2) is used.

OCP (2.3) is a nonlinear program in the form of (2.1). It can be approximated as a quadratic program (QP) or a linear program (LP). In the case of QP, the cost function is convex and constraints are linear. In the case of LP, both the cost function and constraints are linear. The linearization (or the convex quadratic approximation) can be performed around a reference guess trajectory, which can be the same as the desired path, if it is available.

Define

$$\begin{aligned} y^k &= [x^{(k+1)}, x^k, u^k]^T \\ y_0^k &= [x_0^{(k+1)}, x_0^k, u_0^k]^T. \end{aligned} \tag{2.4}$$

The linear constraints can be derived using the first-order Taylor expansion around the guess states and inputs y_0^k, $k = 0, \ldots, N-1$, according to

$$F(y_0^k) + J_{\mathrm{F}}(y^k)|_{y_0^k}(y^k - y_0^k) = 0, \tag{2.5}$$

$$h(y_0^k) + J_{\mathrm{h}}(y^k)|_{y_0^k}(y^k - y_0^k) \leq 0, \tag{2.6}$$

where J denotes the Jacobian matrix, e.g., $J_{\mathrm{F}}(\cdot)$ is the Jacobian matrix of F, i.e., $J_{\mathrm{F}ij}(y) = \frac{\partial F_i}{\partial y_j}$, $i = 1, \ldots, m$, $j = 1, \ldots, n$, where m is the number of single functions in F and n is the number of function arguments, i.e., the size of vector y.

Define the global state vector $\boldsymbol{x}$ and input vector $\boldsymbol{u}$ as

$$\begin{aligned} \boldsymbol{x} &= [x^0, x^1, x^2, \ldots, x^N] \\ \boldsymbol{u} &= [u^0, u^1, u^2, \ldots, u^{(N-1)}]. \end{aligned}$$

If the cost function is not convex, then it should be approximated by a convex function. Assume that the cost function is quadratic and convex and measures the deviation from a given desired path $\boldsymbol{x}_{\mathrm{des}}$ and $\boldsymbol{u}_{\mathrm{des}}$. The quadratic program (QP, or the LTV-OCP) approximating the NOCP can then be written as

$\mathrm{QP}_{\mathrm{NOCP}}(\hat{x}, \boldsymbol{x}_0, \boldsymbol{u}_0, \boldsymbol{x}_{\mathrm{des}}, \boldsymbol{u}_{\mathrm{des}}) =$

find	$x^{(k+1)}, u^k,\ k = 0, \ldots, N-1$
to minimize	$C_{\mathrm{t}}\big(x^N, x_{\mathrm{des}}\big) +$
	$\displaystyle\sum_{k=0}^{N-1} \begin{bmatrix} x^k - x_{\mathrm{des}}^k \\ u^k - u_{\mathrm{des}}^k \end{bmatrix}^T W_k \begin{bmatrix} x^k - x_{\mathrm{des}}^k \\ u^k - u_{\mathrm{des}}^k \end{bmatrix}$ (2.7a)
subject to	for $k = 0, \ldots, N-1$
	$F(y_0^k) + J_F(y^k)|_{y_0^k}(y^k - y_0^k) = 0,$ (2.7b)

$$
\begin{aligned}
& h(y_0^k) + J_h(y^k)|_{y_0^k}(y^k - y_0^k) \leq 0, && \text{(2.7c)}\\
& y^k = [x^{(k+1)}, x^k, u^k]^T \\
& y_0^k = [x_0^{(k+1)}, x_0^k, u_0^k]^T \\
& x^0 = \hat{x},
\end{aligned}
$$

where $\boldsymbol{x}_0$ and $\boldsymbol{u}_0$ denote the initial linearization guess state and input trajectories.

The problem defined in (2.7) is an LTV-OCP. The solution of $\mathrm{QP}_{\mathrm{NOCP}}(\hat{x}, \boldsymbol{x}_0, \boldsymbol{u}_0, \boldsymbol{x}_{\mathrm{des}}, \boldsymbol{u}_{\mathrm{des}})$ can be used to define new linearization trajectories $\boldsymbol{x}_1$ and $\boldsymbol{u}_1$. The subscript NOCP indicates that the QP is an approximation of a NOCP. Therefore, a Newton iteration scheme can be constructed to solve the NOCP, i.e., the $\mathrm{QP}_{\mathrm{NOCP}}$ can be approximated again around the new trajectories to define a new LTV-OCP $\mathrm{QP}_{\mathrm{NOCP}}(\hat{x}, \boldsymbol{x}_1, \boldsymbol{u}_1, \boldsymbol{x}_{\mathrm{des}}, \boldsymbol{u}_{\mathrm{des}})$. Continued iteration results in an SQP that gives the solution of the NOCP upon convergence [10, 11, 49]. The steps of the SQP are summarized in Algorithm 2.

Algorithm 2 SQP

Input: $\hat{x}, \boldsymbol{x}_0, \boldsymbol{u}_0, \boldsymbol{x}_{\mathrm{des}}, \boldsymbol{u}_{\mathrm{des}}$;
Initialization : $j \leftarrow 0$;
1: **while** *not converged* **do**
2: Evaluate Jacobians $J_F(y^k)|_{y_j^k}$ and $J_h(y^k)|_{y_j^k}$, for $k = 0, \ldots, N-1$, and linearize the constraints (also perform a convex approximation of the cost function if needed);
3: Solve $\mathrm{QP}_{\mathrm{NOCP}}(\hat{x}, \boldsymbol{x}_j, \boldsymbol{u}_j, \boldsymbol{x}_{\mathrm{des}}, \boldsymbol{u}_{\mathrm{des}})$ to find $\boldsymbol{x}$ and $\boldsymbol{u}$ by calling a QP solver (e.g. [6, 50]);
4: Update the states-inputs guess $[\boldsymbol{x}_j, \boldsymbol{u}_j]$ to ensure a descent in the Newton direction using step size $\alpha \in]0, 1]$ [105]:
$[\boldsymbol{x}_{(j+1)}, \boldsymbol{u}_{(j+1)}] = [\boldsymbol{x}_j, \boldsymbol{u}_j] + \alpha\big([\boldsymbol{x}, \boldsymbol{u}] - [\boldsymbol{x}_j, \boldsymbol{u}_j]\big)$;
5: $j \leftarrow j + 1$;
6: **end while**
7: **return** $[\boldsymbol{x}, \boldsymbol{u}]$.

2.3.2 Nonlinear model predictive control

NOCP generates the optimal control trajectories for a dynamic system over a time (or space) interval based on the system state estimation at time (or space) zero. However, the accuracy of the control actions to control the plant dynamic system diminishes as the plant system gets further from the estimated initial state. This occurs because 1) the initial state estimate might be inaccurate; 2)

the prediction mathematical model does not perfectly replicate the plant real-world model; 3) external disturbances might be present; 4) the system dynamics is highly nonlinear. Therefore, the actual system states might not match the predicted ones.

The NMPC approach reduces the imperfection in the control law by solving the NOCP at time (or space) step i given the state estimate $\hat{x}^i$ over a time (or space) interval of N steps, known as the prediction horizon. From the obtained optimal control trajectory, only the first input is applied to the plant. The prediction horizon moves one step forward, the state estimate is update accordingly, and the process is repeated.

The SQP is computationally expensive for most real-time NMPC applications. The number of Newton iterations before convergence can be reduced if the SQP is warm-started. An approach for warm-starting the SQP proposed by RTI results in an efficiently solution to the NOCP. According to the RTI approach [27, 49], Algorithm 2 is iterated only once using a full Newton step, $\alpha = 1$. The solution is then used as a good-quality linearization guess for the NOCP linearization in the next prediction horizon.

2.3.3 Dynamic programming[3]

In this thesis, DP was used for optimal energy management of hybrid-electric vehicles, where a single state was allowed in the problem, i.e., the power split, and the battery degradation was included in the cost function in Paper B.

DP is a numerical method for solving the NOCP (2.3) and mixed integer OCPs based on Bellman's optimality principle [8]. In DP, states and control actions and the time (or space) horizon are all discretized in their admissible ranges. Let i, j and k denote discretization indices for states, x, control variable, u and distance, s, respectively. Also, let define J_0 as the cost-to-go from stage 0 of NOCP (2.3a), and assume that the system dynamic equation (2.3b) is explicit, i.e.,

$$J_0 = C_{\mathrm{t}}\big(x_N, N\big) + \sum_{k=0}^{N-1} L\big(x_k, u_k, k\big), \tag{2.8}$$

$$x_{k+1} = f(x_k, u_k, k), \tag{2.9}$$

Let J_l be the cost-to-go from stage l. According to Bellman's principle of optimality [8], the minimum cost-to-go J_l^* can then be found as

$$J_l^*(x_l, l) = \min_{u_l}\{L(x_l, u_l, l) + J_{l+1}^*(f(x_l, u_l, l), l+1)\} \tag{2.10}$$

[3]Dynamic programming was used in Paper B for optimal energy management, i.e., the optimal power split, in hybrid vehicles. Most parts of this section were already presented in that paper.

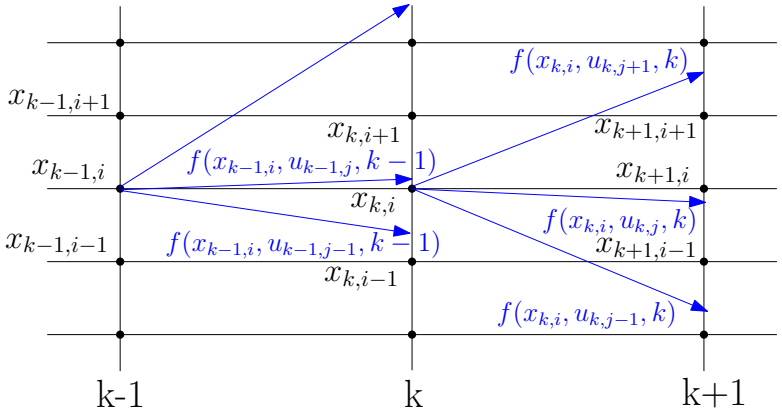

Figure 2.1: Illustration of DP and the grid of the state variable in different stages (from Paper B).

with

$$J_N^*(x_N, N) = C_\mathrm{t}\big(x_N, N\big) \tag{2.11}$$

where equation (2.9) is used for calculating x_{l+1} in J_{l+1}^*.

Therefore, the optimal states and input trajectories can be found by solving (2.10) backward in time (or space), if the final state is known. If the final state is not known, then (2.10) must be solved for a grid of all possible final states.

Note that interpolation is a component of cost-to-go approximation for each state as described in Section VI in Paper B.

The computational cost of DP is considerable, which makes it uninteresting for practical applications. The algorithm complexity increases exponentially when a new state or control input is added. There are thorough studies on reducing the DP computational cost [22, 16, 68] via parallel computing, coarse partitioning, and neural networks. Coarse partitioning is one technique that considerably reduces the computational cost of DP [22, 8, 22] and was applied in this thesis (Paper B).

2.4 Multitrailer vehicle motion modeling[4]

This section is based on the derivation of the vehicle model presented in Paper G. As mentioned in section 1.3.7, vehicle motion modeling was needed to evaluate the performance of combination vehicles and their safe and energy-efficient predictive control.

The dynamic equations of one- and two-track multitrailer vehicles can be explained using a system of differential algebraic equations (DAE). Derivation of a complete set of equations based on the available physics and knowledge of the

[4]Multitrailer vehicle motion modeling was thoroughly discussed in Paper G. This section includes new materials in addition to that paper.

system yields a high-fidelity system model. The chosen system fidelity and accuracy, however, depend on the available computation time and application for which the model is used. Models of different fidelity have been used in different parts of this thesis. In this section, a summary of these models is provided. The following assumptions are common among different models:

- the motion is limited to the yaw-plane;
- the articulation joints have no friction and are moment-free;
- the air resistance force acts only on the front ground level of the first unit;
- the vehicle longitudinal speed cannot be zero.

The derivation of the vehicle nonlinear dynamic equation, as well as equations for lateral and longitudinal load transfer, are presented in Paper G.

The nonlinear dynamic equation of the vehicle is a system of implicit ordinary differential equations (ODE) or a system of differential algebraic equations (DAE) of the form

$$F\big(x(t), \frac{dx(t)}{dt}, u(t), y(t), t\big) = 0, \tag{2.12}$$

in the time domain and

$$F\big(x(s), \frac{dx(s)}{ds}, u(s), y(s), s\big) = 0, \tag{2.13}$$

in the space domain, where t denotes the time, s denotes the distance traveled, and x, u, and y denote the state, input and algebraic variables, respectively. The independent variable of the dynamic system can be distance traveled s rather than time t since the road curvature and grade and legal speed limits are described in s.

The state vector x in the space domain is

$$\begin{aligned} x = [&X_1, Y_1, \phi_1, \theta_i \\ &v_{\mathrm{x}}, v_{\mathrm{y}}, \frac{d\phi_1}{ds}, \frac{d\theta_i}{ds}], \end{aligned} \tag{2.14}$$

where X_1 and Y_1 denote the global coordinates of the first units' center of gravity (COG), ϕ_1 denotes the angle of the first unit with respect to the global X-axis, v_{x} and v_{y} denote the velocity components of the first unit's COG in the first unit's local system of coordinates, and θ_i denotes the articulation angle between units i and $i+1$. The input vector is defined as

$$u = [F_{\mathrm{xw}ij}, F_{\mathrm{xw}i(j+n_{\mathrm{a}i})}, \delta_{ij}, \delta_{i(j+n_{\mathrm{a}i})}], \tag{2.15}$$

where $F_{\mathrm{xw}ij}$ denotes the i^{th} unit's j^{th} right-wheel longitudinal force caused by the propulsion or braking actuation, $F_{\mathrm{xw}i(j+n_{\mathrm{a}i})}$ is a similar force for a left wheel, $n_{\mathrm{a}i}$ denotes the number of axles in the i^{th} unit, δ_{ij} denotes denotes the i^{th} unit's j^{th} right-wheel steering angle, and $\delta_{i(j+n_{\mathrm{a}i})}$ denotes the steering angle of the left wheels. In the case of a single-track vehicle, the indices of the left wheels are neglected.

Lagrange dynamics [127, 92, 104] (and in Paper G) were used to derive most of the equations. MATLAB code for generating the equation of motion of a vehicle with an arbitrary number of units together with simulation examples have been provided in publication ii [43]. The code and equations are explained in Paper G, including an experimental validation.

Let ua and sa be binary matrices defining unit axles and steerable axles, respectively. For an A-double LHV, i.e., a four-unit LHV that is a tractor-semitrailer-dolly-semitrailer, as shown in Fig. 2.3,

$$\begin{aligned} ua = [&1,1,1;\\ &1,1,1;\\ &1,1,0;\\ &1,1,1], \end{aligned} \tag{2.16}$$

$$\begin{aligned} sa = [&1,0,0;\\ &0,0,0;\\ &1,0,0;\\ &0,0,0]. \end{aligned} \tag{2.17}$$

Each of the rows of the above matrices provides information about the vehicle units and their axles; moreover, the total number of rows corresponds to the total number of units n_{u}, e.g., $ua_{ij} = 1$ and $sa_{ij} = 1$ means that there is an axle j on unit i that is steerable. The number of columns of the above matrices defines the maximum number of axles in a unit n_{a}.

The Lagrange equation is given by

$$\frac{d}{dt}\frac{\partial T}{\partial \dot{q}_l} - \frac{\partial T}{\partial q_l} + \frac{\partial V}{\partial q_l} = Q_l, \quad l = 1, \ldots, n_g, \tag{2.18}$$

where T and V denote the system kinetic and potential energies, n_g is the total number of generalized coordinates of the system, and a dot ($\dot{}$) above a variable represents the time derivative. The generalized coordinates q is given by

$$q = [X_1, Y_1, \phi_1, \theta_i], \quad i = 1, \ldots, n_{\mathrm{u}} - 1 \tag{2.19}$$

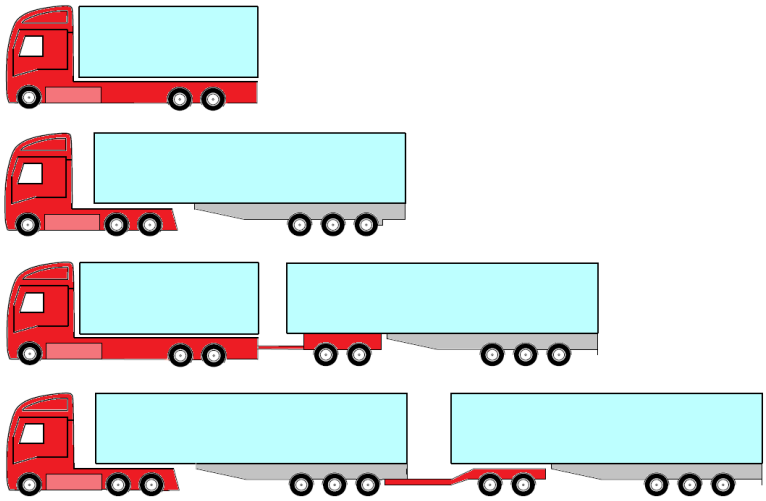

Figure 2.2: Examples of modeled vehicles.

where X_1, Y_1 denotes the position of the COG of the first unit in the global inertia coordinate system and ϕ_1 and θ_i denote the global yaw angle of the first unit and articulation angles, respectively. The generalized force Q_l is given by

$$Q_l = \sum_{k=1}^{n_\mathrm{f}} \left(F_{\mathrm{X}k} \frac{\partial P_{\mathrm{X}k}}{\partial q_l} + F_{\mathrm{Y}k} \frac{\partial P_{\mathrm{Y}k}}{\partial q_l} \right), \quad l = 1, \ldots, n_g, \tag{2.20}$$

where n_f denotes the total number of force elements, $F_{\mathrm{X}k}$ and $F_{\mathrm{Y}k}$ are their X and Y components, and $P_{\mathrm{X}k}$ and $P_{\mathrm{Y}k}$ are their X and Y positions in the global inertia frame.

The potential energy is zero since there is no flexible body in the system and the gravitational forces are considered as force elements acting on the system. The kinetic energy can be defined as

$$T = \frac{1}{2} \sum_{i=1}^{n_\mathrm{u}} \left(m_i (v_{\mathrm{X}i}^2 + v_{\mathrm{Y}i}^2) + J_i \dot{\phi}_i^2 \right), \tag{2.21}$$

where i is the vehicle unit index, m_i, J_i, and ϕ_i denote the vehicle unit mass, vehicle unit yaw moment of inertia, and vehicle unit yaw angle in global frame, respectively, and $v_{\mathrm{X}i}$ and $v_{\mathrm{Y}i}$ denote the global velocity components of the COG of unit i.

A detailed derivation is provided in Paper G. Examples of vehicles that are modeled are shown in Figs. 2.2 and 2.3.

For example, the nonlinear equations of a single-track single-unit vehicle with a linear tire model, including the gravitational, rolling and air resistance forces

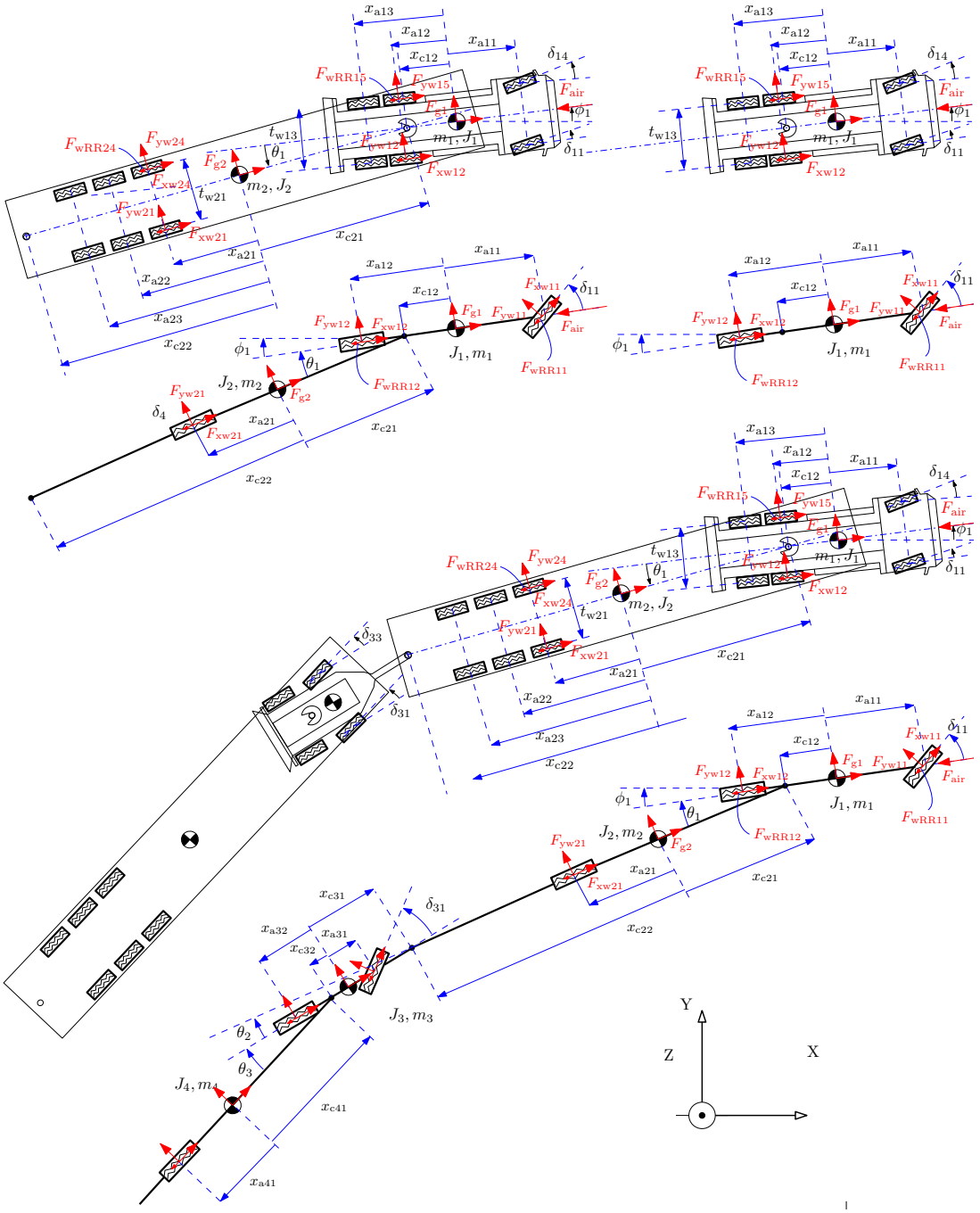

Figure 2.3: Examples of modeled vehicles. The figures illustrates the vehicles' dimensions, i.e., the coupling positions x_c relative to the unit COGs, the axle positions x_a, the articulation angles θ, steering angles δ, unit masses m, and unit moments of inertia J, as well as examples of the forces acting on the vehicle, i.e., the lateral forces F_{yw}, the axle longitudinal forces F_{xw} as a result of the propulsion/braking actuation, rolling resistance forces F_{wRR}, air resistance F_{air}, and the gravitational forces F_g.

but excluding the lateral and longitudinal load transfers, are

$$\begin{aligned} m_1(\dot{v}_\mathrm{x} - v_\mathrm{y}\dot{\phi}_1) =& F_\mathrm{air} + \cos(\delta_1)\ F_\mathrm{xw11} + F_\mathrm{xw12} + \\ & \cos(\phi_1)(F_\mathrm{11X} + F_\mathrm{12X} + F_\mathrm{g1X} + F_\mathrm{RR11X} + F_\mathrm{RR12X}) + \\ & + \sin(\phi_1)(F_\mathrm{11Y} + F_\mathrm{12Y} + F_\mathrm{g1Y} + F_\mathrm{RR11Y} + F_\mathrm{RR12Y}), \end{aligned} \tag{2.22a}$$

$$\begin{aligned} m_1(\dot{v}_\mathrm{y} + v_\mathrm{x}\dot{\phi}_1) =& \sin(\delta_1)\ F_\mathrm{xw11} + \\ & \cos(\phi_1)(F_\mathrm{11Y} + F_\mathrm{12Y} + F_\mathrm{g1Y} + F_\mathrm{RR11Y} + F_\mathrm{RR12Y}) - \\ & \sin(\phi_1)(F_\mathrm{11X} + F_\mathrm{12X} + F_\mathrm{g1X} + F_\mathrm{RR11X} + F_\mathrm{RR12X}), \end{aligned} \tag{2.22b}$$

$$\begin{aligned} J_1\ddot{\phi}_1 =& \sin(\delta_1)\ F_\mathrm{xw11}\ x_\mathrm{a11} + \\ & \cos(\phi_1)(F_\mathrm{11Y}x_\mathrm{a11} + F_\mathrm{12Y}x_\mathrm{a12} + F_\mathrm{RR11Y}x_\mathrm{a11} + F_\mathrm{RR12Y}x_\mathrm{a12}) - \\ & \sin(\phi_1)(F_\mathrm{11X}x_\mathrm{a11} - F_\mathrm{12X}x_\mathrm{a12} - F_\mathrm{RR11X}x_\mathrm{a11} - F_\mathrm{RR12X}x_\mathrm{a12}), \end{aligned} \tag{2.22c}$$

where the gravitational resistance forces are caused by the road pitch and banking angles, $F_\mathrm{air} = -(A_\mathrm{f}c_\mathrm{d}\rho_\mathrm{a}\ \cos(\phi_1)\ \mathrm{sign}(v_\mathrm{x})\ v_\mathrm{x}^2)/2$, and the other force components in the global system of coordinates are defined as

$$F_\mathrm{g1X} = g\ m_1\ \cos(\phi_1)\ \sin(\lambda_\mathrm{p1}) - g\ m_1\ \sin(\phi_1)\ \sin(\lambda_\mathrm{b1}), \tag{2.23a}$$

$$F_\mathrm{g1Y} = g\ m_1\ \cos(\phi_1)\ \sin(\lambda_\mathrm{b1}) + g\ m_1\ \sin(\phi_1)\ \sin(\lambda_\mathrm{p1}), \tag{2.23b}$$

$$\begin{aligned} F_\mathrm{11X} =& (C_{11}\ n_\mathrm{ta11}\ \sin(\delta_1 + \phi_1)\ (\cos(\delta_1 + \phi_1)\ (\cos(\phi_1)\ v_\mathrm{y} + \\ & \sin(\phi_1)\ v_\mathrm{x} + x_\mathrm{a11}\ \cos(\phi_1)\ \dot{\phi}_1) + \sin(\delta_1 + \phi_1)\ (\sin(\phi_1)\ v_\mathrm{y} - \cos(\phi_1)\ v_\mathrm{x} + \\ & x_\mathrm{a11}\ \sin(\phi_1)\ \dot{\phi}_1)))/|\sin(\delta_1 + \phi_1)\ (\cos(\phi_1)\ v_\mathrm{y} + \sin(\phi_1)\ v_\mathrm{x} + \\ & x_\mathrm{a11}\ \cos(\phi_1)\ \dot{\phi}_1) - \cos(\delta_1 + \phi_1)\ (\sin(\phi_1)\ v_\mathrm{y} - \cos(\phi_1)\ v_\mathrm{x} + x_\mathrm{a11}\ \sin(\phi_1)\ \dot{\phi}_1)|, \end{aligned} \tag{2.23c}$$

$$\begin{aligned} F_\mathrm{11Y} =& -(C_{11}\ n_\mathrm{ta11}\ \cos(\delta_1 + \phi_1)\ (\cos(\delta_1 + \phi_1)\ (\cos(\phi_1)\ v_\mathrm{y} + \\ & \sin(\phi_1)\ v_\mathrm{x} + x_\mathrm{a11}\ \cos(\phi_1)\ \dot{\phi}_1) + \sin(\delta_1 + \phi_1)\ (\sin(\phi_1)\ v_\mathrm{y} - \cos(\phi_1)\ v_\mathrm{x} + \\ & x_\mathrm{a11}\ \sin(\phi_1)\ \dot{\phi}_1)))/|\sin(\delta_1 + \phi_1)\ (\cos(\phi_1)\ v_\mathrm{y} + \sin(\phi_1)\ v_\mathrm{x} + \\ & x_\mathrm{a11}\ \cos(\phi_1)\ \dot{\phi}_1) - \cos(\delta_1 + \phi_1)\ (\sin(\phi_1)\ v_\mathrm{y} - \cos(\phi_1)\ v_\mathrm{x} + x_\mathrm{a11}\ \sin(\phi_1)\ \dot{\phi}_1)|, \end{aligned} \tag{2.23d}$$

$$F_\mathrm{RR11X} = -F_\mathrm{Z11}\ fr\ \mathrm{sign}(v_\mathrm{x})\ \cos(\delta_1 + \phi_1)\ \cos(\lambda_\mathrm{b1})\ \cos(\lambda_\mathrm{p1}), \tag{2.23e}$$

$$F_\mathrm{RR11Y} = -F_\mathrm{Z11}\ fr\ \mathrm{sign}(v_\mathrm{x})\ \sin(\delta_1 + \phi_1)\ \cos(\lambda_\mathrm{b1})\ \cos(\lambda_\mathrm{p1}), \tag{2.23f}$$

$$\begin{aligned} F_\mathrm{12X} =& (C_{12}\ n_\mathrm{ta12}\ \sin(\phi_1)\ (\cos(\phi_1)\ (\cos(\phi_1)\ v_\mathrm{y} + \sin(\phi_1)\ v_\mathrm{x} + \\ & x_\mathrm{a12}\ \cos(\phi_1)\ \dot{\phi}_1) + \sin(\phi_1)\ (\sin(\phi_1)\ v_\mathrm{y} - \cos(\phi_1)\ v_\mathrm{x} + \\ & x_\mathrm{a12}\ \sin(\phi_1)\ \dot{\phi}_1)))/|(\sin(\phi_1)\ (\cos(\phi_1)\ v_\mathrm{y} + \sin(\phi_1)\ v_\mathrm{x} + x_\mathrm{a12}\ \cos(\phi_1)\ \dot{\phi}_1) - \\ & \cos(\phi_1)\ (\sin(\phi_1)\ v_\mathrm{y} - \cos(\phi_1)\ v_\mathrm{x} + x_\mathrm{a12}\ \sin(\phi_1)\ \dot{\phi}_1))|, \end{aligned} \tag{2.23g}$$

$$F_{12\mathrm{Y}} = -(C_{12}\ n_{\mathrm{ta12}}\ \cos(\phi_1)\ (\cos(\phi_1)\ (\cos(\phi_1)\ v_{\mathrm{y}} + \sin(\phi_1)\ v_{\mathrm{x}} + x_{\mathrm{a12}}\ \cos(\phi_1)\ \dot{\phi}_1) + \sin(\phi_1)\ (\sin(\phi_1)\ v_{\mathrm{y}} - \cos(\phi_1)\ v_{\mathrm{x}} + x_{\mathrm{a12}}\ \sin(\phi_1)\ \dot{\phi}_1)))/|(\sin(\phi_1)\ (\cos(\phi_1)\ v_{\mathrm{y}} + \sin(\phi_1)\ v_{\mathrm{x}} + x_{\mathrm{a12}}\ \cos(\phi_1)\ \dot{\phi}_1) - \cos(\phi_1)\ (\sin(\phi_1)\ v_{\mathrm{y}} - \cos(\phi_1)\ v_{\mathrm{x}} + x_{\mathrm{a12}}\ \sin(\phi_1)\ \dot{\phi}_1))|, \tag{2.23h}$$

$$F_{\mathrm{RR12X}} = -F_{\mathrm{Z12}}\ fr\ \cos(\phi_1)\ \mathrm{sign}(v_{\mathrm{x}})\ \cos(\lambda_{\mathrm{b1}})\ \cos(\lambda_{\mathrm{p1}}), \tag{2.23i}$$

$$F_{\mathrm{RR12Y}} = -F_{\mathrm{Z12}}\ fr\ \sin(\phi_1)\ \mathrm{sign}(v_{\mathrm{x}})\ \cos(\lambda_{\mathrm{b1}})\ \cos(\lambda_{\mathrm{p1}}), \tag{2.23j}$$

where in addition to the parameters and variables defined in Fig. 2.3, C_{ij} denotes the cornering stiffness of a single tire, $F_{\mathrm{Z}ij}$ denotes the axle static vertical force of a flat ground, g, $\lambda_{\mathrm{p}i}$, $\lambda_{\mathrm{b}i}$, f_{r}, ρ_{a}, A_{f} and c_{d} denote the gravity acceleration, road grade, road banking angle, rolling resistance coefficient, air density, equivalent vehicle front area and air drag coefficient, respectively, $n_{\mathrm{ta}ij}$ denotes the number of tires per axle, and i and j denote unit and axle indices, respectively. See [43] for automatic generation of the equations.

2.4.1 Linearization

A common approach in vehicle dynamics for system linearization is to remove nonlinear terms and assume a linear tire model and small steering and articulation angles [62, 92, 104].

In this thesis, model linearization is often performed according to (2.7b), which results in an LTV system. An alternative approach is to neglect the longitudinal dynamic equation and linearize the rest of the model around an operating condition described by a constant speed and straight-line deriving, where all the states and their derivatives are zero, except v_{x}, which is nonzero. Such a linearization process results in a linear time-invariant (LTI) system, which is often used for system stability analysis [92] and building STL models. This linearization approach is an alternative systematic method for building STL models compared to, for example, [62, 92]. In the case of setting the gravitational and rolling resistance forces to zero, the linear system takes the form

$$\dot{x} = A\ x + B\ u, \tag{2.24}$$

where the states are $x = [\phi_1, \theta_i, v_{\mathrm{y}}, \dot{\phi}_1, \dot{\theta}_i]$, $i = 1, \ldots, n_{\mathrm{u}} - 1$ and the inputs are, for a single-track vehicle, $u = [\delta_{ij}]$, $i = 1, \ldots, n_{\mathrm{u}}$ and $j = 1, \ldots, n_{\mathrm{a}}$ and, for a two-track vehicle, $u = [\delta_{ij}, \delta_{ik}]$, $i = 1, \ldots, n_{\mathrm{u}}$, and $k = n_{\mathrm{a}} + 1, \ldots, 2n_{\mathrm{a}}$, for steerable axles, i.e., $sa_{ij} \neq 0$, where n_u and n_a stand for the numbers of vehicle units and axles, respectively.

For example, the LTI form of (2.22)-(2.23), which is related to the lateral motion of a single-unit single-track vehicle, is

$$A = \begin{bmatrix} 0 & 0 & 1 \\ 0 & \frac{-(C_{11}\ n_{\mathrm{ta11}}+C_{12}\ n_{\mathrm{ta12}})}{m_1\ |v_{\mathrm{x}}|} & \frac{-(m_1\ v_{\mathrm{x}}\ |v_{\mathrm{x}}|+C_{11}\ n_{\mathrm{ta11}}\ x_{\mathrm{a11}}+C_{12}\ n_{\mathrm{ta12}}\ x_{\mathrm{a12}})}{m_1\ |v_{\mathrm{x}}|} \\ 0 & \frac{-(C_{11}\ n_{\mathrm{ta11}}\ x_{\mathrm{a11}}+C_{12}\ n_{\mathrm{ta12}}\ x_{\mathrm{a12}})}{(J_1\ |v_{\mathrm{x}}|)} & \frac{-(C_{11}\ n_{\mathrm{ta11}}\ x_{\mathrm{a11}}^2+C_{12}\ n_{\mathrm{ta12}}\ x_{\mathrm{a12}}^2)}{J_1\ |v_{\mathrm{x}}|} \end{bmatrix}. \quad (2.25)$$

$$B = \begin{bmatrix} 0 \\ \frac{-(C_{11}\ n_{\mathrm{ta11}}\ v_{\mathrm{x}})}{|v_{\mathrm{x}}|} \\ -x_{\mathrm{a11}}\ (\frac{C_{11}\ n_{\mathrm{ta11}}\ v_{\mathrm{x}}}{|v_{\mathrm{x}}|}) \end{bmatrix}. \quad (2.26)$$

where $x = [\phi_1, v_{\mathrm{y}}, \dot{\phi}_1]$ and $u = [\delta_{11}]$.

2.4.2 Reducing the number of states in the longitudinal dynamics[5]

In the literature, the longitudinal and lateral dynamics are often decoupled. Lateral dynamics can be well approximated based on the longitudinal speed and neglecting the longitudinal acceleration when the combined slip is not present. In the literature, with the objective of evaluating energy consumption, the longitudinal dynamics are decoupled from the lateral dynamics for the sake of efficient computations for long trip distances. However, such decoupling causes inaccurate speed prediction on curvy roads, where the steering angle is not zero. The main reason for such an inaccuracy is neglecting the rotational inertia of the vehicle units and the tires' side slips in the longitudinal dynamics equation. For example, a tire side slip produces a force component opposite to the vehicle longitudinal motion which is neglected. This section discusses how to compromise between efficient computations and model accuracy regarding the longitudinal speed prediction.

In (2.22) and (2.23), the longitudinal dynamics are coupled with the lateral dynamics. Rearranging the terms and assuming that the road banking angle λ_{b1} is zero yields

$$\begin{aligned} m_1\dot{v}_{\mathrm{x}} =& m_1\ v_{\mathrm{y}}\dot{\phi}_1 + F_{\mathrm{air}} + \cos(\delta_1)\ F_{\mathrm{xw11}} + F_{\mathrm{xw12}} + g\ m_1\ \sin(\lambda_{\mathrm{p1}}) - \\ & F_{\mathrm{Z12}}\ fr\ \mathrm{sign}(v_{\mathrm{x}})\ \cos(\lambda_{\mathrm{p1}}) + \\ & \cos(\phi_1)(F_{\mathrm{11X}} + F_{\mathrm{12X}} + F_{\mathrm{RR11X}}) + \\ & \sin(\phi_1)(F_{\mathrm{11Y}} + F_{\mathrm{12Y}} + F_{\mathrm{RR11Y}}) \approx \\ & F_{\mathrm{air}} + F_{\mathrm{xw11}} + F_{\mathrm{xw12}} + g\ m_1\ \sin(\lambda_{\mathrm{p1}}) - \\ & (F_{\mathrm{Z11}} + F_{\mathrm{Z12}})\ fr\ \mathrm{sign}(v_{\mathrm{x}})\ \cos(\lambda_{\mathrm{p1}}) + \end{aligned}$$

[5]This section was not presented in any of the appended papers.

$$m_1\ v_{\mathrm{y}}\dot{\phi}_1 + \cos(\phi_1)(F_{11\mathrm{X}} + F_{12\mathrm{X}}) + \sin(\phi_1)(F_{11\mathrm{Y}} + F_{12\mathrm{Y}}) \tag{2.27}$$

The last three terms in (2.27) are zeros in case of a zero toe angle and the absence of steering (i.e., no differential braking/propulsion and zero steering angles). These terms account for the coupling between the lateral and longitudinal dynamics in the longitudinal dynamic equation (2.27). Let $F_{\mathrm{steer}}(x, u)$ be a function that contains these terms, i.e.,

$$F_{\mathrm{steer}}(\phi_1, v_{\mathrm{x}}, v_{\mathrm{y}}, \dot{\phi}_1) = m_1\ v_{\mathrm{y}}\dot{\phi}_1 + \cos(\phi_1)(F_{11\mathrm{X}} + F_{12\mathrm{X}}) + \sin(\phi_1)(F_{11\mathrm{Y}} + F_{12\mathrm{Y}}). \tag{2.28}$$

Therefore, the longitudinal dynamics equation is approximated as

$$m_1\dot{v}_{\mathrm{x}} \approx F_{\mathrm{air}} + F_{\mathrm{xw11}} + F_{\mathrm{xw12}} + g\ m_1\ \sin(\lambda_{\mathrm{p1}}) - (F_{\mathrm{Z11}} + F_{\mathrm{Z12}})\ fr\ \mathrm{sign}(v_{\mathrm{x}})\ \cos(\lambda_{\mathrm{p1}}) + F_{\mathrm{steer}}(\phi_1, v_{\mathrm{x}}, v_{\mathrm{y}}, \dot{\phi}_1). \tag{2.29}$$

All the terms except F_{steer} in (2.29) include a single state v_{x}, whereas $F_{\mathrm{steer}}(x, u)$ is a function of all the states and inputs. Further approximation can be performed if the term $F_{\mathrm{steer}}(x, u)$ is approximated by a fitting function that includes a smaller number of states. For example, such a fitting function can have the form

$$F_{\mathrm{steer}}^{\mathrm{approx}}(v_{\mathrm{x}}, \delta_{11}) = c\ v_{\mathrm{x}}\ \delta_{11}^2, \tag{2.30}$$

where c is a constant that must be found for a given vehicle. The term F_{steer} is particularly important for articulated vehicles. In Figs. 2.4-2.9, the simulation results are compared for three different cases for the single-track 6-axle and 4-unit vehicle (single-track A-double with lumped axles) shown in Fig. 2.3. The cases include 1) coupled lateral and longitudinal dynamics; 2) decoupled longitudinal and lateral dynamics, i.e., neglecting the term $F_{\mathrm{steer}}(x, u)$ in the longitudinal dynamics equation; and 3) mild coupling of the lateral and longitudinal dynamics, i.e., by including the term $F_{\mathrm{steer}}^{\mathrm{approx}}(v_{\mathrm{x}}, \delta_{11})$, where $c = 0.009 \sum_i \sum_j C_{ij}$. The wheels do not receive either propulsion or braking force via actuation.

The shown approximation of the steering effects in (2.30) performs relatively well for steering angles less than 0.12 rad. For larger steering angles, (2.30) overestimates the resistance forces and thus needs to be updated if large steering angles are dominant in a maneuver. Notably, (2.30) is used in this thesis to evaluate the energy consumption of long distance trips, which will be explained in the sequel.

2.5 Powertrain modeling[6]

In this section, dynamic equations of a parallel hybrid powertrain are derived, as are equations for evaluating fuel consumption, electric energy consumption, state

[6]Part of the contents of this section were already presented in Paper F.

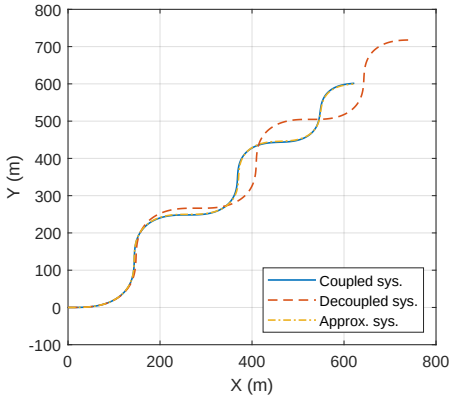

Figure 2.4: The trajectory of a single-track 6-axle and 4-unit vehicle simulated using coupled, decoupled and approximated lateral and longitudinal system dynamics in a sine-steer maneuver.

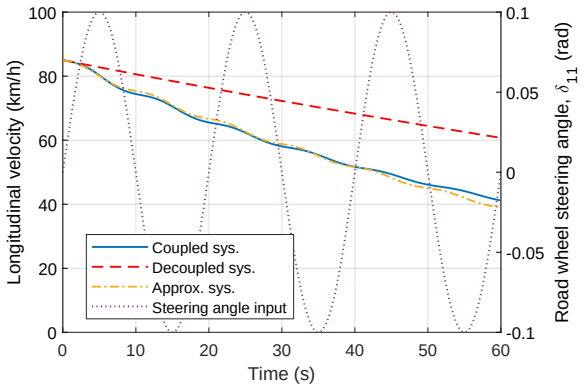

Figure 2.5: The longitudinal velocity of a single-track 6-axle and 4-unit vehicle simulated using coupled, decoupled and approximated lateral and longitudinal system dynamics in a sine-steer maneuver. The road wheel steering angle is also shown.

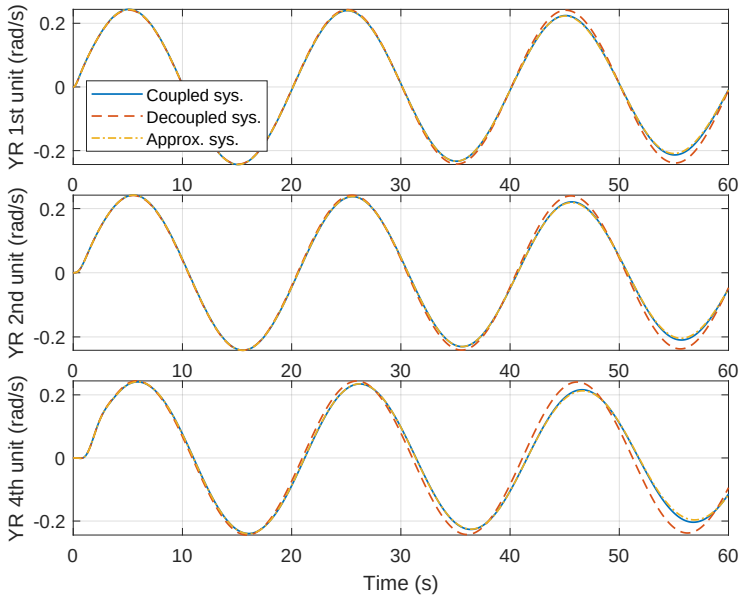

Figure 2.6: Illustration of the yaw rates (YR), i.e., $\dot{\phi}_1$, $\dot{\phi}_2$, and $\dot{\phi}_3$, of a single-track 6-axle and 4-unit vehicle simulated using coupled, decoupled and approximated lateral and longitudinal system dynamics in a sine-steer maneuver.

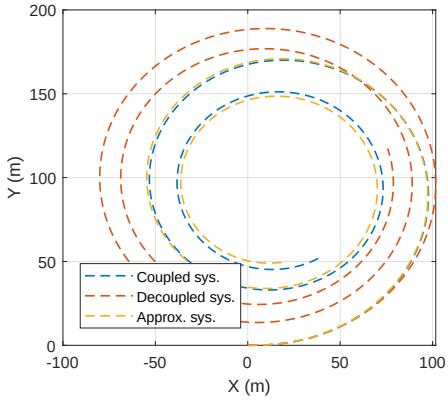

Figure 2.7: The trajectory of a single-track 6-axle and 4-unit vehicle simulated using coupled, decoupled and approximated lateral and longitudinal system dynamics in a constant-steer maneuver.

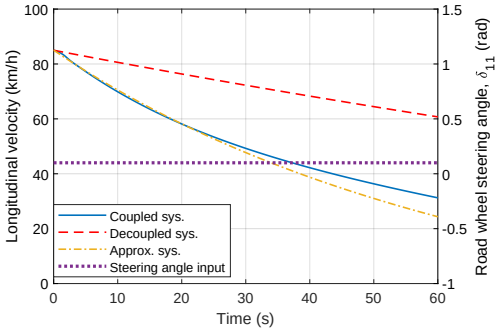

Figure 2.8: The longitudinal velocity of a single-track 6-axle and 4-unit vehicle simulated using coupled, decoupled and approximated lateral and longitudinal system dynamics in a constant-steer maneuver. The road wheel steering angle is also shown.

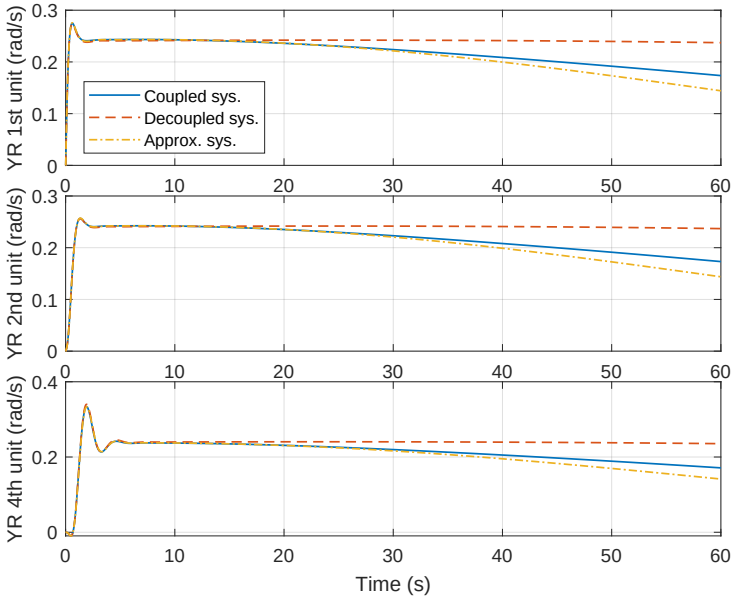

Figure 2.9: Illustration of the yaw rate (YR) of a single-track 6-axle and 4-unit vehicle simulated using coupled, decoupled and approximated lateral and longitudinal system dynamics in a constant-steer maneuver.

of charge of batteries, and energy dissipated in different parts of the powertrain. Notably, conventional and fully electric powertrains can easily be derived from the equations of the hybrid powertrain. Parts of this section can also be found in Paper F. The powertrain model derived in this section was used in the TCO evaluation and the NOCP problems of predictive energy and motion control of this thesis.

Following (2.29), the total force at wheels $F_{\mathrm{w}}(t)$, i.e., the sum of forces acting on wheels caused by propulsion/braking, at time t is given by

$$F_{\mathrm{w}}(t) = m\dot{v}_{\mathrm{x}}(t) + F_{\mathrm{g}}(s(t)) + F_{\mathrm{roll}}(s(t)) + F_{\mathrm{air}}(v_{\mathrm{x}}(t)) + F_{\mathrm{steer}}^{\mathrm{approx}}(s(t)). \tag{2.31}$$

where m is the vehicle total mass or equivalent total mass, $s(t)$ is the traveled distance at time t, and F_{g}, F_{roll}, and F_{air} represent the road grade, rolling resistance (modeled as a body force), and air resistance forces, respectively, as defined below.

$$F_g(s(t)) = -mg \sin\, \lambda_{\mathrm{p}}(s(t)) \tag{2.32}$$

$$F_{roll}(s(t)) = mgf_{\mathrm{r}} \cos\, \lambda_{\mathrm{p}}(s(t)) \tag{2.33}$$

$$F_{air}(v_{\mathrm{x}}(t)) = 0.5\rho_{\mathrm{a}} A_{\mathrm{f}} c_{\mathrm{d}} v_{\mathrm{x}}(t)^2 \tag{2.34}$$

where g, λ_{p}, f_{r}, ρ_{a}, A_{f} and c_{d} represent the gravitational constant, road grade (positive downhill), rolling resistance coefficient, air density, equivalent vehicle front area and air drag coefficient, respectively.

The term $F_{\mathrm{steer}}^{\mathrm{approx}}$ approximates all forces caused by steering and the articulation angles, i.e., side slips of the tires, as well as the rotational inertia given by (2.28). This term is zero in straight road driving and is negligible in single-unit vehicles. However, for articulated vehicles on curved roads, the term cannot be neglected for accurate state and energy consumption estimations, as was discussed in section 2.4.2, so it is approximated according to (2.30). Therefore, the longitudinal dynamic equation depends on a single state v_{x}.

The total power at the wheels $P_{\mathrm{w}}(t)$, shown in Fig. 2.10, required for vehicle acceleration and compensating resistance forces becomes

$$P_{\mathrm{w}}(t) = F_{\mathrm{w}}(t) v_{\mathrm{x}}(t), \tag{2.35}$$

The energy flow (i.e., power) between different powertrain subsystems is shown in Fig. 2.10. At an instance or a given interval of time, let P_{f}, P_{e}, P_{de}, P_{ew}, and P_{det} denote, respectively, the power of fuel, the power at ICE output, the power dissipated in ICE, the power at ICE transmission output and the power dissipated

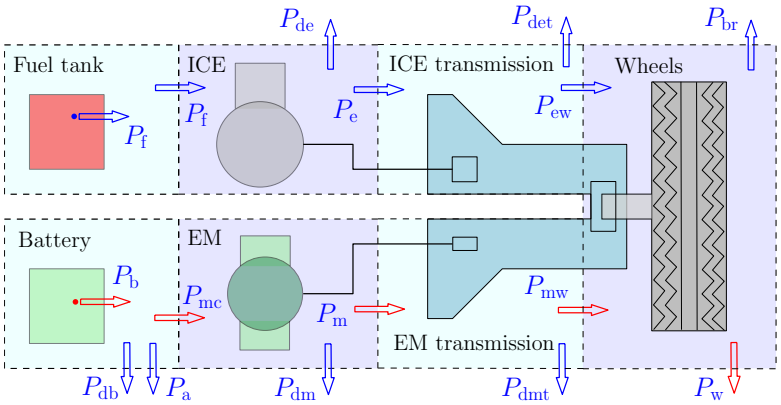

Figure 2.10: Energy flow (i.e., input/output power) in different powertrain subsystems. A blue arrow means that the power can be zero or positive, while a red arrow indicates that the power can also be negative. A dot before an arrow indicates a source of power. This figure is reused from Paper F.

in ICE transmission. On the electric propulsion side, let P_b, P_db, P_a, P_mc, P_dm, P_m, P_dmt and P_mw represent the powers provided by or stored in the battery, dissipated in the battery, used for auxiliaries, consumed or regenerated by EM, dissipated in EM, at EM output/input to/from transmission, dissipated in EM transmission and at output/input to/from wheels, respectively. Likewise, let P_br be the friction brake power. Then, by defining the energy flow as positive if it flows out of a subsystem, e.g., all dissipative terms are positive, the power balance equation for each subsystem can be written as follows. A power balance can be assumed since there is no energy storage or generation inside the powertrain, except that in the fuel tank and battery, i.e., no inertial flywheels or elastic shafts are modeled.

$$P_\mathrm{e} + P_\mathrm{de} - P_\mathrm{f} = 0 \tag{2.36a}$$
$$P_\mathrm{ew} + P_\mathrm{det} - P_\mathrm{e} = 0 \tag{2.36b}$$
$$P_\mathrm{w} + P_\mathrm{br} - P_\mathrm{ew} - P_\mathrm{mw} = 0 \tag{2.36c}$$
$$P_\mathrm{mw} + P_\mathrm{dmt} - P_\mathrm{m} = 0 \tag{2.36d}$$
$$P_\mathrm{m} + P_\mathrm{dm} - P_\mathrm{mc} = 0 \tag{2.36e}$$
$$P_\mathrm{mc} + P_\mathrm{db} + P_\mathrm{a} - P_\mathrm{b} = 0. \tag{2.36f}$$

In Eqs. (2.36), function arguments are omitted for increased readability. For example, the powertrain components dissipations are, in general, nonlinear functions of speed, component power, selected ICE gear, γ_e, and selected EM gear, γ_m. Furthermore, terms describing the inertia of rotating parts in the driveline and wheels and energy loss due to tire longitudinal slip are neglected; however,

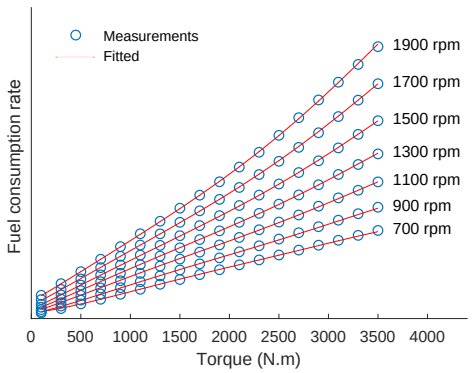

Figure 2.11: Fuel consumption rate obtained by experimental measurements together with a fitted surface of degree 5.

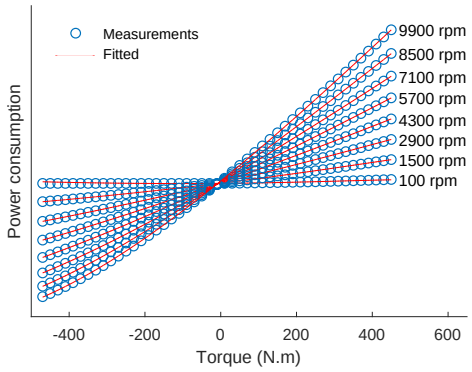

Figure 2.12: EM power consumption (i.e., P_{mc}) obtained by experimental measurements. The measurement data have been fitted by two surfaces of degree 5 for positive and negative torques.

the inertia of rotating parts of the powertrain can be taken into account by considering the equivalent additional mass in the term involving the acceleration [65]. Moreover, stopping and reversing are not modeled.

The power dissipation of the ICE and EM can be modeled by direct use of data from measured maps or by using high-degree nonlinear fitted curves. Measurements have been performed for varying torques and angular speeds. The torque and angular speed of ICE and EM can be calculated based on their power and vehicle speed, as follows.

$$\omega_{\mathrm{e}}(t) = \frac{r_{\mathrm{e}}(\gamma_{\mathrm{e}}(t))}{R_{\mathrm{w}}} v_{\mathrm{x}}(t), \quad T_{\mathrm{e}}(t) = \frac{1}{\omega_{\mathrm{e}}(t)} P_{\mathrm{e}}(t) \tag{2.37}$$

$$\omega_{\mathrm{m}}(t) = \frac{r_{\mathrm{m}}(\gamma_{m}(t))}{R_{\mathrm{w}}} v_{\mathrm{x}}(t), \quad T_{\mathrm{m}}(t) = \frac{1}{\omega_{\mathrm{m}}(t)} P_{\mathrm{m}}(t) \tag{2.38}$$

where R_{w}, r_{e}, T_{e}, ω_{e}, r_{m}, T_{m} and ω_{m} denote the wheel radius, gear ratio from wheel to engine, engine torque, engine speed, gear ratio from wheel to EM, EM torque and speed, respectively. Eqs. (2.37) and (2.38) cannot be applied to the neutral gear. Furthermore, power P, energy E, force F, torque T and velocity v_{x} are related according to

$$P(s) = \frac{dE(s)}{dt} = v_{\mathrm{x}}(s) \frac{dE(s)}{ds} = v_{\mathrm{x}}(s) F(s) = \omega(s) T(s). \tag{2.39}$$

A general polynomial surface fitting of degree n is given by the following expressions for ICE fuel energy rate $\dot{E}_f = P_{\mathrm{f}}$ and EM consumed power P_{mc}. Any

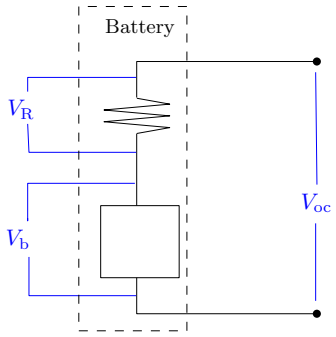

Figure 2.13: Battery schematic.

other surface fitting function could also be valid.

$$P_f(\omega_e(t), T_e(t)) = \sum_{i=0}^{n}\sum_{j=0}^{n} a_{ij}\omega_e(t)T_e(t)^j \tag{2.40}$$

$$P_{mc}(\omega_m(t), T_m(t)) = \begin{cases} \sum_{i=0}^{n}\sum_{j=0}^{n} h_{ij}^{+}\omega_m(t)T_m(t)^j, & T_m(t) > 0 \\ \sum_{i=0}^{n}\sum_{j=0}^{n} h_{ij}^{-}\omega_m(t)T_m(t)^j, & T_m(t) \leq 0 \end{cases} \tag{2.41}$$

where a_{ij}, h_{ij}^{+} and h_{ij}^{-} represent coefficients of the fitted functions. Fig. 2.11 shows measurements and a polynomial surface fitting of the engine fuel energy rate, where the degree of the fitted surface is 5, resulting in a very good approximation of measurements. Similarly, a fitted surface for P_{mc} is shown in Fig. 2.12. Two different fitted polynomial surfaces have been used, one for positive torques and one for negative torques, to ensure that torque and P_{mc} have the same sign, e.g., positive torque yields positive P_{mc}.

The battery is modeled with a constant open circuit voltage, V_{oc}, and resistance, R [59]. Therefore, the battery dissipated energy can be calculated as follows, assuming that the voltage drop due to battery resistance is negligible, i.e., $V_{oc} \approx V_b$; see Fig. 2.13.

$$P_{db}(P_{mc}(t), P_a(t)) = \frac{R}{V_b^2}(P_{mc} + P_a)^2. \tag{2.42}$$

Furthermore, transmission dissipation is assumed to be linear with respect to the power input being independent of gear selection; thus,

$$P_{det}(P_e(t)) = P_e(t) - \eta_{te}P_e(t), \quad P_e(t) \geq 0 \tag{2.43}$$

and

$$P_{\mathrm{dmt}}(P_{\mathrm{m}}(t)) = \begin{cases} P_{\mathrm{m}}(t) - \eta_{\mathrm{tm}} P_{\mathrm{m}}(t), & P_{\mathrm{m}}(t) > 0 \\ -(\dfrac{P_{\mathrm{m}}(t)}{\eta_{\mathrm{tm}}} - P_{\mathrm{m}}(t)), & P_{\mathrm{m}}(t) \leq 0 \end{cases} \tag{2.44}$$

where η_{te} and η_{tm} represent the transmission efficiency of the engine and EM, respectively. The negative sign in the second part of (2.44) is needed to keep P_{dmt} always positive.

In addition to the energy balance of the powertrain components, their capability limits in transforming energy should be considered. The limits of transforming energy in the engine and EM are enforced by limiting the maximum and minimum torque that can be produced. Fig. 2.14.a shows measurements of the maximum engine torque versus speed together with piecewise fitted curves. Similarly, Fig. 2.14.b illustrates the torque limits of EM. The polynomial curve fitting of degree n for each of the pieces is given by

$$T_{li}(\omega(t)) = \sum_{j=0}^{n} b_{ij} \omega(t)^j, \ i = 1, \ldots, 4 \tag{2.45}$$

where T_l represents the torque limit, either of the engine or EM, depending on the fitted curve and coefficients b_i.

Finally, the storage capacity and power of the battery should be limited. The state of charge (SOC) is used as a state and a measure for battery capacity, which is given by

$$SOC(t_{\mathrm{f}}) = SOC(t_0) - \frac{1}{E_{\mathrm{bmax}}} \int_{t_0}^{t_{\mathrm{f}}} P_{\mathrm{b}}(t) dt, \tag{2.46}$$

where E_{bmax} denotes the maximum energy capacity of the battery.

In predictive (optimal) energy management, fuel consumption is part of the cost function. As discussed in section 2.3, an NMPC or NOCP is easier to handle if the cost function is convex and does not need to be repeatedly approximated by convex functions. Sequential approximation of the cost function in predictive energy management can be avoided if the measured fuel consumption data are fitted with a convex function.

Depending on the chosen state variable, e.g., vehicle forward velocity or kinetic energy, the fitted functions differ. The kinetic energy E_{v} is given by

$$E_{\mathrm{v}}(s) = \frac{1}{2} m v(s)^2. \tag{2.47}$$

Considering $\frac{dv(s)}{ds} = \frac{\dot{v}(t)}{v_{\mathrm{x}}(t)}$ and

$$\frac{d(\cdot)}{dt} = \frac{d(\cdot)}{ds}\frac{ds}{dt} \approx v_{\mathrm{x}} \frac{d(\cdot)}{ds}, \tag{2.48}$$

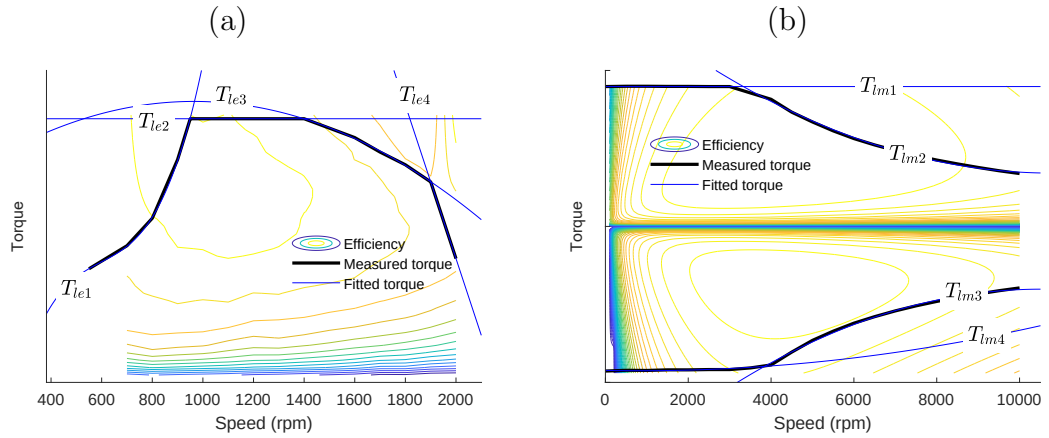

Figure 2.14: Torque limit versus speed obtained by experimental measurements and the fitted curves; a) Engine with quadratic fitted curves T_{le1}-T_{le4}; b) EM with fitted curves T_{lm1}-T_{lm4}.

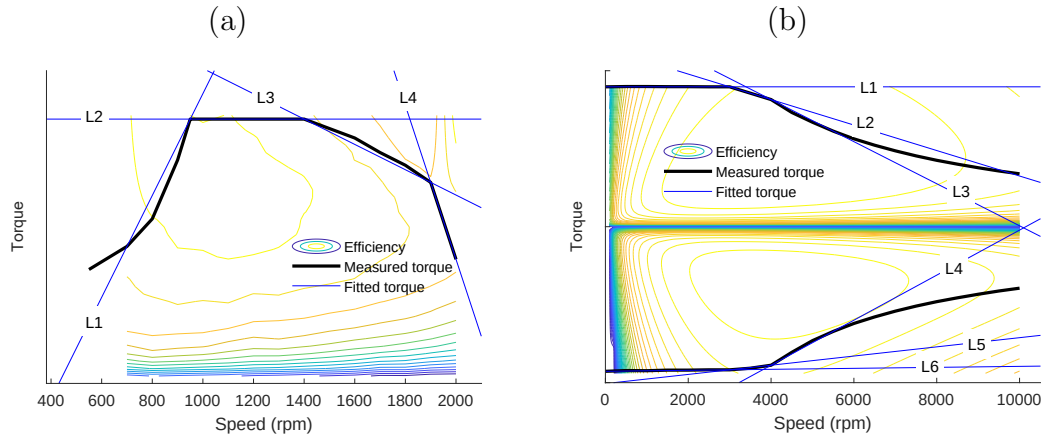

Figure 2.15: Torque limit versus speed obtained by experimental measurements and the affine fitted curves; a) Engine with affine fitted curves L1-L4; b) EM with affine fitted curves L1-L6.

the derivative of the kinetic energy with respect to the traveled distance is

$$\frac{dE_{\mathrm{v}}(s)}{ds} = mv(s)\frac{dv(s)}{ds} = m\dot{v}(t) \tag{2.49}$$

which makes (2.31) linear with respect to the kinetic energy.

Table 2.1 provides different polynomials that can be used to fit the measured fuel consumption rate data. The root mean square error between the fitted surface and the measured data is also given. If a change in the independent variable from time to space is performed using (2.48), then the fuel time rate is changed to the fuel space rate, and the fitted curve in (2.40) must be divided by the velocity.

Similarly, it is easier to handle the NMPC if the torque limits of the ICE and EMs are linear (affine) such that their sequential linearization can be avoided.

Table 2.1: Different polynomial surfaces for fitting the measured fuel consumption rate data. This table was not presented in the appended papers.

No.	Fuel time rate surface fitting	RMSE (g/s)	Description
1	$\sum_{i=0}^{5}\sum_{j=0}^{5} a_{ij}\omega_{\mathrm{e}}(t)T_{\mathrm{e}}(t)^j$	0.1034	nonlinear
2	$a_{10}\omega_{\mathrm{e}}+a_{20}\omega_{\mathrm{e}}^2+a_{11}\omega_{\mathrm{e}}T_{\mathrm{e}}+a_{30}\omega_{\mathrm{e}}^3+a_{21}\omega_{\mathrm{e}}^2T_{\mathrm{e}}+a_{12}\omega_{\mathrm{e}}T_{\mathrm{e}}^2$	0.3213	convex in space domain (after division by ω_{e}) if velocity is a state
3	$a_{00}+a_{10}\omega_{\mathrm{e}}+a_{20}\omega_{\mathrm{e}}^2+a_{11}\omega_{\mathrm{e}}T_{\mathrm{e}}+a_{30}\omega_{\mathrm{e}}^3+a_{21}\omega_{\mathrm{e}}^2T_{\mathrm{e}}+a_{12}\omega_{\mathrm{e}}T_{\mathrm{e}}^2$	0.3201	nonlinear
4	$a_{10}\omega_{\mathrm{e}}+a_{20}\omega_{\mathrm{e}}^2+a_{11}\omega_{\mathrm{e}}T_{\mathrm{e}}+a_{30}\omega_{\mathrm{e}}^3+a_{12}\omega_{\mathrm{e}}T_{\mathrm{e}}^2$	0.4880	convex in space domain (after division by ω_{e}) if velocity is a state
5	$a_{00}+a_{10}\omega_{\mathrm{e}}+a_{11}\omega_{\mathrm{e}}T_{\mathrm{e}}+a_{30}\omega_{\mathrm{e}}^3+a_{12}\omega_{\mathrm{e}}T_{\mathrm{e}}^2++a_{50}\omega_{\mathrm{e}}^5$	0.4873	nonlinear, suitable if kinetic energy is a state
6	$a_{10}\omega_{\mathrm{e}}+a_{11}\omega_{\mathrm{e}}T_{\mathrm{e}}+a_{30}\omega_{\mathrm{e}}^3+a_{12}\omega_{\mathrm{e}}T_{\mathrm{e}}^2++a_{50}\omega_{\mathrm{e}}^5$	0.4916	convex (after division by ω_{e}) if kinetic energy is a state

Surface no. 1 gives the best fit. Surface no. 2 is convex and gives a better fit than the other convex curves. In general, the convexity of a function with the term $\omega_{\mathrm{e}}T$ (after division by ω_{e} in surface no. 2) is not guaranteed. However, for the given fuel rate data, surface no. 2 results in a convex fitting function.

The affine fits of the torque limits are shown in Fig. 2.15.

The disadvantage of efficiency-based measurements of EM losses is that the losses at zero power and nonzero speed (zero torque and nonzero speed) are undefined or set to zero. This problem can be addressed using measured data other than efficiency or using a fitting function that is nonzero at zero torque and nonzero speed. The power consumed or regenerated by EM based on the known efficiency map can be calculated as

$$P_{\mathrm{mc}}(\omega_{\mathrm{m}},T_{\mathrm{m}})=\begin{cases}\dfrac{\omega_{\mathrm{m}}T_{\mathrm{m}}}{\eta_m(\omega_{\mathrm{m}},T_{\mathrm{m}})}, & T_{\mathrm{m}}>0\\ \omega_{\mathrm{m}}T_{\mathrm{m}}\eta_m(\omega_{\mathrm{m}},T_{\mathrm{m}}), & T_{\mathrm{m}}\leq 0.\end{cases} \tag{2.50}$$

Therefore, the EM power loss P_{dm} is

$$P_{\mathrm{dm}}(\omega_{\mathrm{m}},T_{\mathrm{m}})=P_{\mathrm{mc}}(\omega_{\mathrm{m}},T_{\mathrm{m}})-\omega_{\mathrm{m}}T_{\mathrm{m}}. \tag{2.51}$$

Fig. 2.16 shows the EM power loss as a function of ω_{m} and T_{m}, both for the measured data and the fitted curve. Based on the measurement of the efficiencies, the loss is zero at zero torque. The fitted curve, however, gives a more realistic loss that is nonzero for nonzero motor speed.

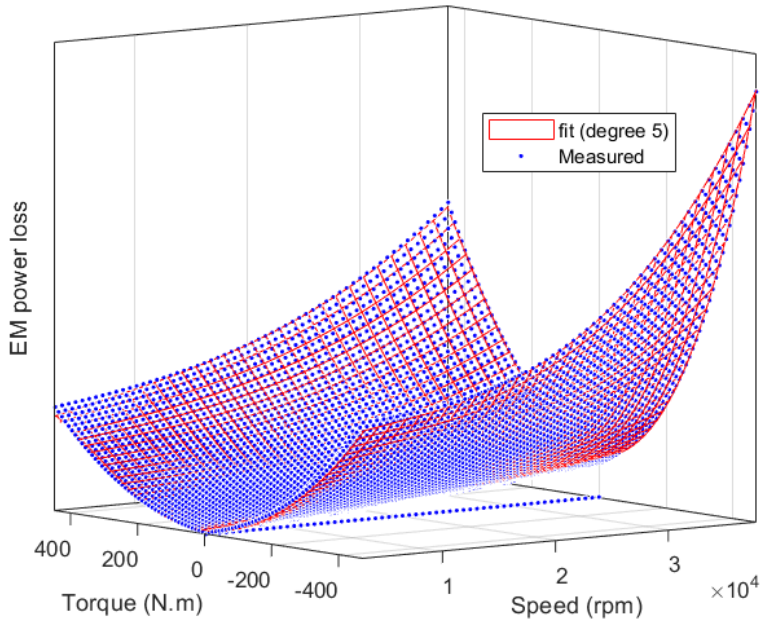

Figure 2.16: EM power loss.

2.6 Plug-in charging and battery health[7]

State of charge and trip time

When evaluating the total cost of ownership, the total trip time needs to be calculated, according to [45]. Given the vehicle speed $v_{\mathrm{x}}(s)$, the driving (travel) time or road t_{tor} can be calculated as

$$t_{\mathrm{tor}} = \int_{\mathrm{s_0}}^{s_{\mathrm{f}}} \frac{ds}{v_{\mathrm{x}}(s)}, \tag{2.52}$$

where s_0 and s_{f} denote the start and end distance.

Assume that the vehicle visits several LU nodes with charging stations where the batteries are charged. Following (2.46), the SOC between charging stations can be calculated as follows:

$$SOC(s) = SOC(s_i) + \int_{\mathrm{s}_i}^{s} \frac{-P_{\mathrm{b}}(S)}{E_{\mathrm{bmax}}}\, dS, \qquad s_i < s \leq s_{i+1}, \forall i \in \boldsymbol{I}_n, \tag{2.53}$$

where s_i denotes the distance of node i from the depot, i.e., the starting position, $\boldsymbol{I}_n$ is the index set of all LU nodes in the mission, and $SOC(s_i)$ denotes the state

[7]The content of this section is based on publication iii [45], which was not presented in any of the appended papers.

of charge of the battery packs immediately after leaving node i, defined as

$$SOC(s_i) = SOC(s_i^-) + \int_0^{t_{\mathrm{ch},i}} \frac{P_{\mathrm{ch},i}(\tau)}{E_{\mathrm{bmax}}}\, d\tau, \tag{2.54}$$

where $SOC(s_i^-)$ denotes state of charge at arrival to node i, $P_{\mathrm{ch},i}$ denotes the recharging power from the charging station at node i, and $t_{\mathrm{ch},i}$ denotes the charging time. The charging power is assumed to be constant, and the charging time is assumed to be linear with respect to SOC [98]; thus,

$$SOC(s_i) = SOC(s_i^-) + \frac{t_{\mathrm{ch},i}\, P_{\mathrm{ch},i}}{E_{\mathrm{bmax}}}. \tag{2.55}$$

For a plug-in hybrid vehicle, the recharging time $t_{\mathrm{ch},i}$ can be the same as the LU time and can be calculated as

$$t_{\mathrm{ch},i} = \min\big(\max(t_{\mathrm{lu},i}, t_{\mathrm{s},i}), \frac{[SOC_{\max} - SOC(s_i^-)]\, E_{\mathrm{bmax}}}{P_{\mathrm{ch},i}}\big), \tag{2.56}$$

where t_{lu} and t_s denote the loading-unloading time and a fixed minimum service time, respectively. According to (2.56), the charging time ends if $SOC_{\max}$ is reached.

An electric vehicle, however, must ensure that it can reach the next charging station; therefore, its recharging time might be longer than the loading-unloading and service times at a node. Let $\Delta SOC(s_{i+1}^-) = SOC(s_{i+1}^-) - SOC(s_i)$ be the charge required to reach node $(i+1)$ from node i. This value can be calculated in advance by simulating the vehicle motion on the road for the whole trip, without considering any limits on SOC.

To reach node $(i+1)$, $\forall i \in \boldsymbol{I}_n$, the following must hold:

$$SOC(s_{i+1}^-) \geq SOC_{\min}, \tag{2.57}$$

therefore,

$$[\Delta SOC(s_{i+1}^-) + SOC(s_i)] \geq SOC_{\min}, \tag{2.58}$$

and using (2.55) in (2.58):

$$[\Delta SOC(s_{i+1}^-) + SOC(s_i^-) + \frac{t_{\mathrm{ch},i}\, P_{\mathrm{ch},i}}{E_{\mathrm{bmax}}}] \geq SOC_{\min}, \tag{2.59}$$

therefore,

$$t_{\mathrm{ch},i} \geq \frac{[SOC_{\min} - \Delta SOC(s_{i+1}^-) - SOC(s_i^-)]E_{\mathrm{bmax}}}{P_{\mathrm{ch},i}}, \tag{2.60}$$

and

$$t_{\mathrm{ch},i} = \begin{cases} \min\Big(& \max\big(t_{\mathrm{lu},i}, t_{\mathrm{s},i}, \dfrac{[SOC_{\min} - \Delta SOC(s_{i+1}^{-}) - SOC(s_i^{-})]E_{\mathrm{bmax}}}{P_{\mathrm{ch},i}}\big), \\ & \dfrac{[SOC_{\max} - SOC(s_i^{-})]\,E_{\mathrm{bmax}}}{P_{\mathrm{ch},i}}\Big), \quad P_{\mathrm{ch},i} > 0 \\ 0, & \text{otherwise.} \end{cases} \tag{2.61}$$

Finally, the total trip time t_{tr} is defined as

$$t_{\mathrm{tr}} = t_{\mathrm{tor}} + \sum_{i \in \boldsymbol{I}_n} \max(t_{\mathrm{lu},i}, t_{\mathrm{s},i}, t_{\mathrm{ch},i}). \tag{2.62}$$

Battery state of health

Battery degradation and, consequently, battery replacement during the vehicle service life are important factors in TCO calculations of BEHVs and hybrid vehicles. In this thesis, a state of health model developed for lithium-iron-phosphate batteries [144, 60] was used. The state of health of a battery, S_{h}, is defined as follows:

$$S_{\mathrm{h}}(t) = 1 - \frac{1}{2\,N_{\mathrm{cycle}}\,E_{\mathrm{bmax}}} \int_0^t (|P_{\mathrm{b}}(\tau)| + |P_{\mathrm{ch}}(\tau)|) d\tau \tag{2.63}$$

where N_{cycle} denotes the number of charge-discharge cycles before the end of life of the battery. Essentially, N_{cycle} is a function of the c-rate and various parameters. In this thesis, however, it was assumed to be constant and to vary only with the battery type. Moreover, the battery end of life occurrs when the battery capacity reaches 80% of the initial capacity. A review of the literature on battery degradation and behavior is provided in [113].

2.7 Operating cycles[8]

The operating cycle refers to all the information about the surrounding environment and road that affects the driving situation [114]. An operating cycle is an essential part of a transportation mission (section 1.3.1), where the demands of pick-up and delivery of goods are excluded. In this thesis, depending on the studied context, different descriptions of the operating cycles were used. They were characterized by road X-Y-Z coordinates relative to a fixed origin, i.e., the

[8]Parts of this section is based on publication iii [45], which is not presented in any of the appended papers.

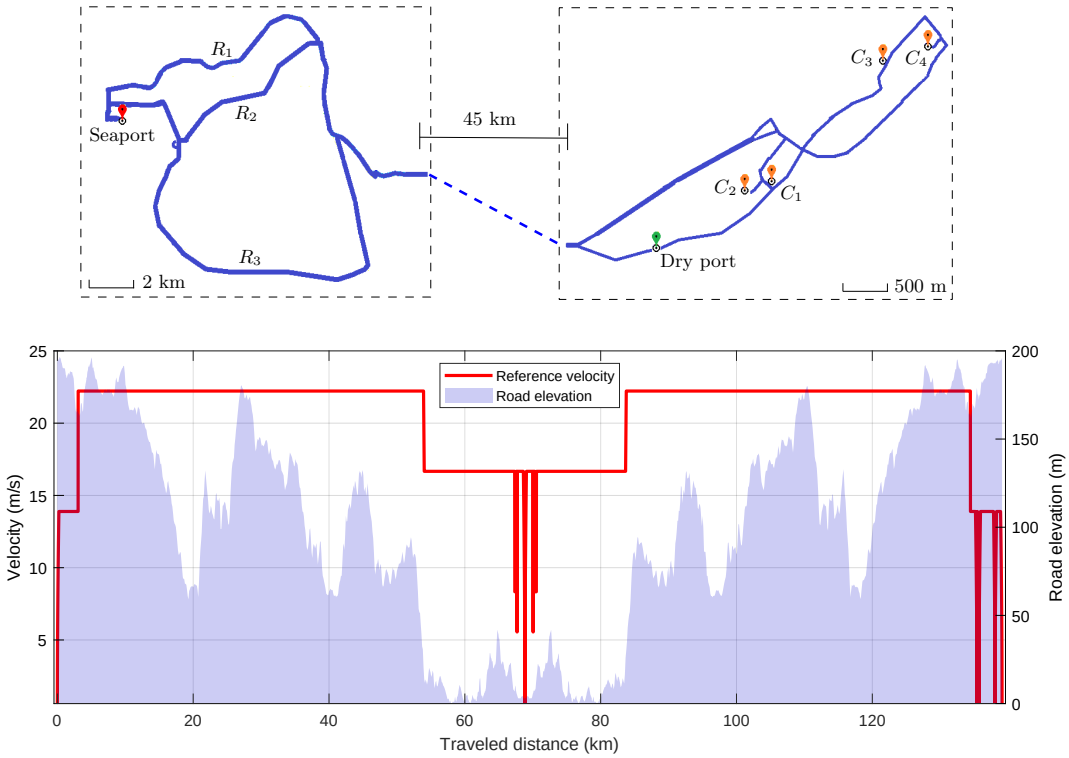

Figure 2.17: Top: map; bottom: the elevation and speed limit of a round-trip route in the map passing all nodes.

topographic data, the position of the LU nodes, and the road speed limit or a representative reference speed on the road.

In the context of propulsion tailoring, the operating cycle has been viewed static and deterministic, meaning that the surrounding environment was assumed to be fixed and known in advance without uncertainty. This assumption was needed due to the fact that vehicle design cannot change during operation. A representative reference speed has been defined to describe the driving situation and traffic. The reference speed varies depending on the road section, for example, on highways, rural areas, close to a red light and along a curve, and the daily reference speed was overridden while negotiating a curve such that the lateral acceleration remained below 1.5 m/s^2. An example is shown in Fig. 2.17.

In the context of predictive energy management, however, real-time variation in traffic can be considered by enforcing a real-time hard constraint on the road speed limit based on traffic flow, or a constraint on vehicle traveled time as a function of distance traveled based on the leading vehicle, i.e., the subject vehicle and the leading vehicle cannot be a in the same position (with a safety offset) at the same time. Therefore, the velocity of the leading vehicle can influence the optimal energy management of the vehicle.

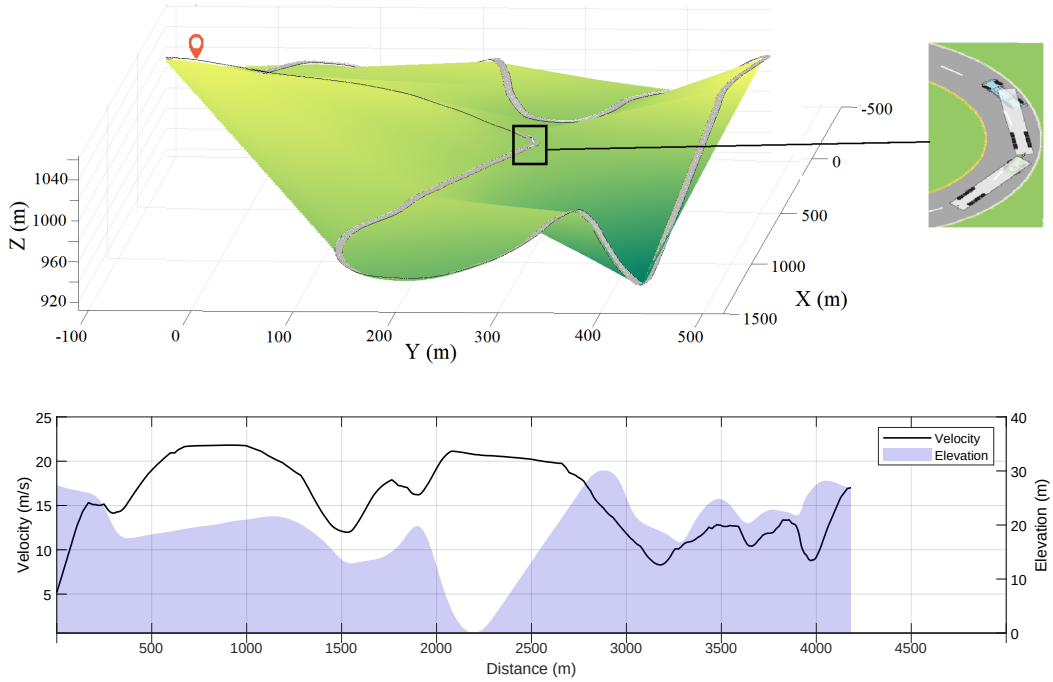

Figure 2.18: Top: road in X-Y-Z coordinates (the Z-coordinate is scaled by a factor of 5 for the sake of visibility); bottom: the elevation and a reference speed profile. The shown road is the country road track on proving ground Hällered.

Real-world topographic data were used for most of the studies in this thesis. The topographic data, i.e., the road longitude, latitude, and altitude, were obtained either from publicly available map data or by performing measurements using an OxTS RT3000 GNSS inertial system [1]. The conversion from longitude l_{o}, latitude l_{a}, and altitude l_{t} was performed as follows:

$$\begin{aligned} X &= (l_{\mathrm{t}} + R_{\mathrm{e}})\cos(l_{\mathrm{a}}\frac{\pi}{180})\sin(l_{\mathrm{o}}\frac{\pi}{180}), \\ Y &= (l_{\mathrm{t}} + R_{\mathrm{e}})\sin(l_{\mathrm{a}}\frac{\pi}{180}), \\ Z &= l_{\mathrm{t}}, \end{aligned} \tag{2.64}$$

where $R_{\mathrm{e}} = 6371000$ m is the earth's radius from the center to sea level. An example of a road in X-Y-Z coordinates is shown in Fig. 2.18.

Chapter 3

Transportation Mission-Based Optimization including Propulsion Tailoring

The main objective of this chapter is to design vehicles that perform transportation assignments with the lowest TCO. The set of design variables differs depending on the transportation assignment. They include different vehicle powertrain components, propulsion systems, vehicle loading capacities (Fig. 3.1), routes (a small set of available routes), and infrastructure, i.e., charging stations power and locations, and LU schemes. The different propulsion systems include conventional, battery electric, and hybrid propulsion. Therefore, by performing TCO minimization on different transportation missions, those missions where the zero-emission BEHVs are more profitable than the CHVs are identified, and the competitiveness between different transportation solutions is presented. This chapter is a short summery of papers A, C, D, and E.

3.1 TCO definition[1]

The annual TCO C of a single vehicle is defined as

$$C = c_{\text{opr}} + c_{\text{dep}}, \tag{3.1}$$

$$c_{\text{opr}} = c_{\text{elec}} + c_{\text{fuel}} + c_{\text{driver}} + c_{\text{maint}} + c_{\text{tax}} + c_{\text{insu}} + c_{\text{tmms}}, \tag{3.2}$$

$$c_{\text{dep}} = (p - \frac{R_{\text{v}}}{(1+r)^{n_{\text{y}}}} + p_{\text{batt,tot}} - \frac{R_{\text{b}}}{(1+r)^{n_{\text{y}}}}) \frac{r}{1-(1+r)^{-n_{\text{y}}}}, \tag{3.3}$$

where c_{opr} indicates the yearly operational cost, c_{dep} denotes the depreciation cost, and c_{elec}, c_{fuel}, c_{driver}, c_{maint}, c_{tax}, c_{insu}, and c_{tmms} denote the annual costs of

[1]The content of this section is based on Papers C and E.

Figure 3.1: Different vehicle sizes included in the vehicle-infrastructure design. From top to bottom, they are rigid truck, tractor-semitrailer, Nordic combination, and A-double (Courtesy of Volvo Trucks).

electric energy, diesel fuel, driver, vehicle maintenance, taxes, and insurance and the operational cost related to the TMMS (in case of ADS-DVs), respectively. In (3.3), r denotes the discount rate (or interest); n_{y} denotes the economic life time (or planning horizon) in years; R_{v} denotes the vehicle-infrastructure rest (or resale) value, i.e., the price of a product at the end of its service life; R_{b} is the battery rest value; $p_{\mathrm{batt,tot}}$ denotes the purchase price of the all batteries including the replaced ones; and p denotes the purchase price of products at the start of the service life, i.e., the price of chassis p_{chass}, excluding the powertrain, EMs p_{em}, transmission p_{trans}, battery packs p_{batt}, ICE p_{ice}, LU components p_{lu}, recharging infrastructure p_{rech}, ADS p_{ads}, and the TMMS p_{tmms}, given by

$$p = p_{\mathrm{chass}} + p_{\mathrm{em}} + p_{\mathrm{trans}} + p_{\mathrm{ice}} + p_{\mathrm{lu}} + p_{\mathrm{rech}} + p_{\mathrm{ads}} + p_{\mathrm{tmms}}, \tag{3.4}$$

where c_{tmms}, p_{ads}, and p_{tmms} are set to zero if the vehicle has a human driver. In addition, some terms of the TCO defined above might be zero depending on the type of propulsion.

The battery's operational life is separated from that of the other vehicle components since the last replaced battery might be in a good health condition. Moreover, the maintenance cost of BEHVs was assumed to be 50% of that of CHVs [40, 85]. In this thesis, the battery end of life occurred when the battery capacity reached 80% of the initial capacity, and the rest value was set to zero, neglecting a possible second life application [84]. Furthermore, an additional payload was considered for BEHVs according to EU directive 2015/719, without considering any other incentives.

3.2 Fleet and infrastructure optimization[2]

In this section, a methodology is proposed to design a fleet of heavy vehicles that together perform a set of transportation assignments with the lowest TCO. Therefore, the optimum fleet varies depending on the defined assignments and the road network. In the case of having a single vehicle and a single route, the problem of propulsion design has a simple structure, as discussed in section 2.2, i.e., a single optimization problem where the decision variables are bound to be discrete along with a nonsmooth cost function and constraints. Such an optimization problem can be defined as

find	*size of the vehicle and the propulsion components*	
to minimize	*TCO per unit freight transported*	(3.5)
subject to	*vehicle model constraints*	

[2]This section is a short summary of Papers A and E, together with additional material.

performance constraints
transportation task constraints.

In optimization problem (3.5), the propulsion components include the type and size of the ICE, type, size and number of EMs, type, size and number of battery packs, and the location of the propelled axles. Alternative power sources, for example, fuel cells, could also be included; however, they were not studied in this thesis.

Vehicle-model constraints relate to the system dynamic, recharging, and powertrain models, including all the equations and inequalities described in sections 2.5-2.7. Performance constraints guarantee proper functionality and safety of the vehicles on roads [29, 121, 71, 75]. In this Chapter, performance constraints are related to the longitudinal motion of the vehicle, i.e., startability, gradeability, acceleration, and down-grade holding capabilities. The maximum grade on which a laden vehicle can start forward motion and travel 10 m in less than 10 s is referred to as startability. Gradeability is the maximum grade on which a laden vehicle can maintain forward motion at a certain speed, e.g., at 80 km/h. On a road with zero grade, acceleration capability is defined as the time taken by a laden vehicle to start motion form rest and travel 100 m. Down-grade holding capability refers to the maximum downhill road grade on which a laden vehicle can maintain constant forward speed using auxiliary brakes, i.e., the ICE and/or EMs.

Finally, transportation task constraints ensure performance of the transportation mission. These constraints relate to the working time, pick-up, delivery, recharging power, and rules prescribed for LU operations. In this thesis, problems of kind (3.5) are solved using PSO.

A more complex problem than the one in (3.5) is to design a fleet of vehicles of different types working together on a transportation network comprising several pick-up and delivery nodes and different route connections. The problem becomes even more complex if the design of the infrastructure is included. For a given set of transportation assignments on a transportation network, the general problem of designing a vehicle fleet and infrastructure is defined as follows:

find	*missions, routes within missions, types and numbers of vehicles in each mission, number of trips performed by each vehicle in each mission, charging power of each vehicle at each node, loading–unloading scheme of each vehicle at each node*	
to minimize	*vehicle fleet and infrastructure TCO*	(3.6)
subject to	*vehicle-model constraints*	

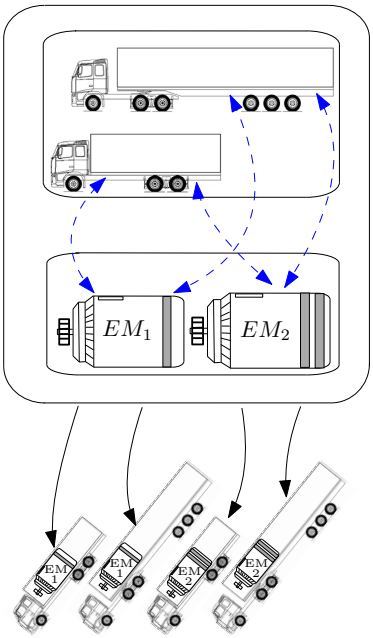

Figure 3.2: A small set of vehicle-design parameters used to build the vehicle types.

performance constraints
transportation task constraints

A vehicle type is described by its size and propulsion system, i.e., the set of all possible vehicles built from the design variables of problem (3.5), hereinafter referred to as "design parameters". A simple example of a set of vehicle types, including only two vehicle design parameters, i.e., the vehicle size and type of electric motor, is shown in Fig. 3.2. Fig. 3.3 provides an example of vehicle design parameters.

A "mission" is a part of a transportation network that includes at least two nodes. A vehicle visits all the nodes of a mission. A mission also includes a single or multiple cyclic routes that connect the nodes. A mission is thus defined by its routes and nodes together with the demands on the pick-up and delivery of goods. A vehicle operates repetitively in a single mission during the entirety of its service life.

Vehicle design and infrastructure design are coupled problems. For example, the number of vehicles and the infrastructure design influence the optimum vehicle propulsion design. For example, for a single vehicle, optimization might indicate that installation of many battery packs results in lower cost compared to installing a fast-charging power source. However, if the recharging infrastructure is shared between multiple vehicles, the installation of a fast-charging alternative may be more feasible. Such an example is shown in Fig. 3.4.

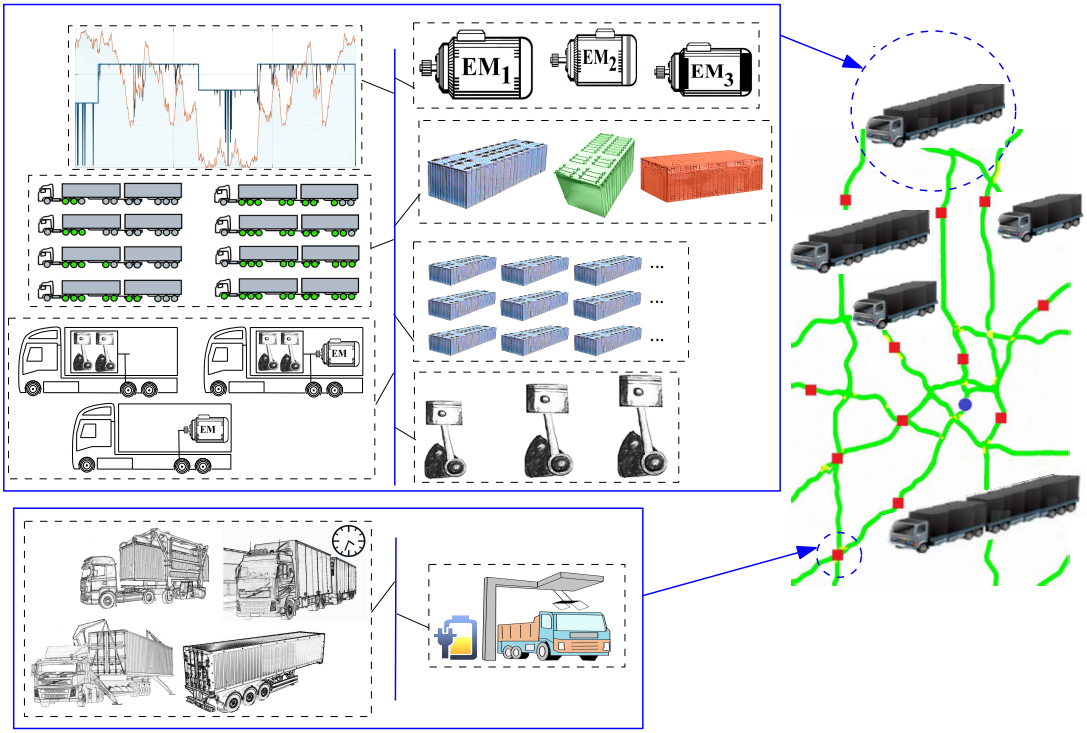

Figure 3.3: Illustration of the vehicle-infrastructure design parameters and the transportation network. The vehicle design parameters include the types and number of EMs, types and number of battery packs, number of propelled axles, and selection of conventional, battery electric or hybrid powertrains. The route for performing the given mission of the vehicle can also be part of the vehicle design parameters. The infrastructure design parameters include the LU scheme and location and the charging power of the charging station (reused from publication iv [44]).

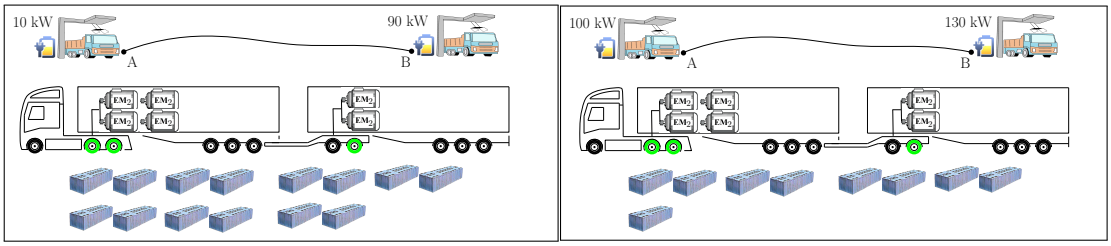

Figure 3.4: Influence of the number of vehicles in the fleet on the design of the vehicle and charging infrastructure; left: one vehicle in the fleet; right: two vehicles in the fleet.

In vehicle routing problems, the route search space is large and the number of possible vehicle types is small because vehicles usually differ only in their sizes. In the vehicle routing literature, the vehicle hardware setup (e.g., powertrain) is known [24, 7, 58, 79], and the fleet size and optimum routes are found. Therefore, the possibility of a reduction in TCO and emissions via coupled hardware design and fleet optimization has not been considered. The literature on heterogeneous

vehicle routing problems accounts for differently sized and powered vehicles [47, 81, 26, 124, 20, 57], but the number of vehicle types is very small (less than six) and not many route–vehicle aspects are investigated. The same holds for fleet-size and mixed-vehicle routing problems [82, 79, 79, 58]. In this thesis, however, the vehicle design search space is large and the route search space is small. This property, together with the nonlinear cost function and constraints to accurately evaluate the performance of each vehicle, made inclusion of many route–vehicle aspects possible within the vehicle-infrastructure design optimization problem.

Furthermore, the same property, i.e., inclusion of a transportation network that has a small route search space, made the proposed methodology for solving problem (3.6) applicable by means of reasonable computational resources that could find near global optimal solutions (or even a global solution, as for the given problem, 60% of the runs of the algorithm yielded the same solution).

In this thesis, it was proposed to divide the large optimization problem (3.6) into smaller subproblems of the form (3.5). The solution of the subproblems could then be used in an allocation optimization problem to decide the final optimized mixed fleet and the infrastructure. An example of solutions related to the transportation network, shown in Fig. 2.17, is shown in Fig. 3.5, where the optimal fleet comprises BEHVs. Factors such as low-density goods that allowed big batteries without reducing the vehicle loading capacity, charging during service time, i.e., during performing LU and the waiting time on the seaport, night charging, optimal charging stations, and high utilization, all enhanced the competitiveness of BEHVs compared to CHVs and hybrid vehicles for the given set of transportation assignments. More details about the solution method, vehicle specifications, and the competitiveness of different propulsion hardware are provided in Paper E.

3.3 Automation and electrification[3]

One contribution of this thesis is a demonstration of the competitiveness of different transportation solutions and identification of those transportation scenarios where BEHVs, including the corresponding infrastructure, exhibit the lowest TCO. In addition, ADS-DVs, as shown in Figs. 3.6 and 3.7, will play an important role in road freight transportation in the near future; therefore, their influence on propulsion design and competitiveness between vehicles with different sources of power, i.e., BEHVs and CHVs, were studied in this thesis. For this purpose, optimization problems of the form (3.5) were solved, including the infrastructure design and excluding the vehicle size from the design variables, for different transportation scenarios. The transportation scenarios differed in terms

[3]This section is a summary of Papers C and D, together with additional material.

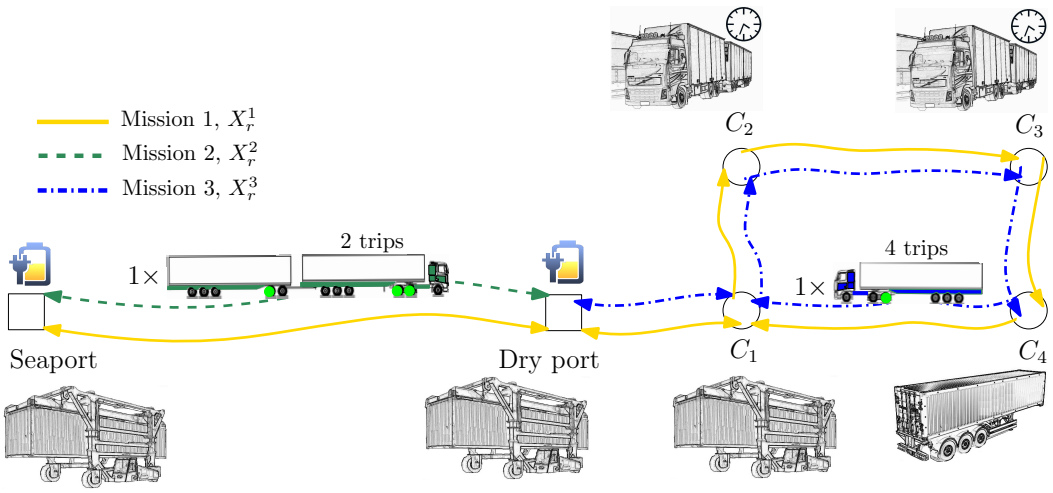

Figure 3.5: An optimum fleet for a maximum daily working time of 10 h and a daily freight flow of 226 m^3. The optimum fleet comprises two vehicles of different sizes working on two different missions. Both vehicles are BEHVs with different types of propulsion, i.e., EMs and batteries. The optimum locations of the charging stations are shown, as is the optimum LU scheme at each node. The LU schemes include using a straddle carrier, additional semitrailer, and on-board waiting. The latter corresponds to the case where the LU is performed by personnel with no extra cost except that related to the waiting time. The propelled axles are the rear axles of the tractor and the rear axle of the dolly (reused from Paper E).

of vehicle average speed, road length, hilliness, vehicle size (shown in Fig. 3.8), vehicle source of power, i.e., battery electric or conventional, and driving system, i.e., driven by ADS or human driver. For each of the transportation scenarios, the vehicle propulsion system and the infrastructure were optimized. It was concluded that the optimum size of the batteries can be different in ADS-DVs and vehicles with human drivers.

Moreover, ADS improved the competitiveness of BEHVs against CHVs. It was shown that, the driving cycle characteristics, e.g., road length, i.e., the distance between LU points (or charging stations), hilliness, the transportation parameters, e.g., utilization, price of fuel and electric energy, ICE efficiency, battery price, discussant rate, and life time, all influence the competitiveness between ADS-D BEHVs and ADS-D CHVs and between BEHVs and CHVs with human drivers. For example, Figs. 3.9 and 3.10 show the influence of road length on the TCO of these vehicles.

Relative sensitivity analyses of the factors contributing to the TCO of different vehicles and driving systems were performed for different transportation scenarios. This process resulted in a large quantity of data that can help practitioners to select the lowest cost vehicle-infrastructure solution for the given transportation scenario. For example, the answers to the following questions can be found by exploring the data:

Figure 3.6: A battery electric ADS-DV (Volvo Group Vera concept, courtesy of Volvo Trucks).

Figure 3.7: The battery electric ADS-DV unloading by a straddle carrier (courtesy of Volvo Trucks).

1. What vehicle size should be used for a specific task?
2. What kind of propulsion system? Fully electric or conventional? Size of the battery, charging infrastructure, loading-unloading?
3. Is it good to use fully and highly automated driving systems, i.e., levels 4 and 5 of DAS?
4. What would be the cost of infrastructure and TMMS?
5. How sensitive is the selected solution to different contributing factors?

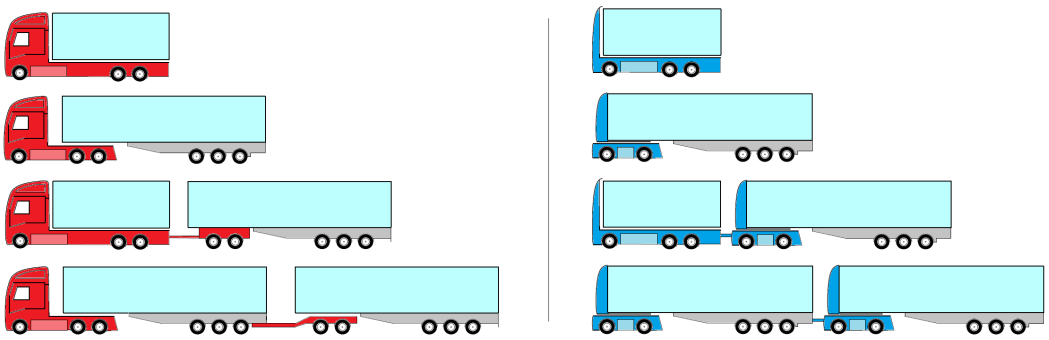

Figure 3.8: Different vehicle sizes with and without human drivers, i.e., ADS-DVs studied in this thesis. From the smallest to the largest, they are a rigid truck, tractor-semitrailer, Nordic combination, and A-double. The semitrailers appear in a different color than the tractor and dolly since they might belong to different operators based on the optimum LU scheme.

An example is shown in Fig. 3.11 for vehicle utilization. An ADS-dedicated battery electric tractor-semitrailer has the lowest TCO if the utilization is high (even though the charging station cost is a part of the TCO), but for utilization less than 70%, the ADS-dedicated conventional tractor-semitrailer yields the lowest TCO. A further reduction in utilization makes the conventional tractor-semitrailer with human driver have the lowest TCO. More details can be found in Papers C and D.

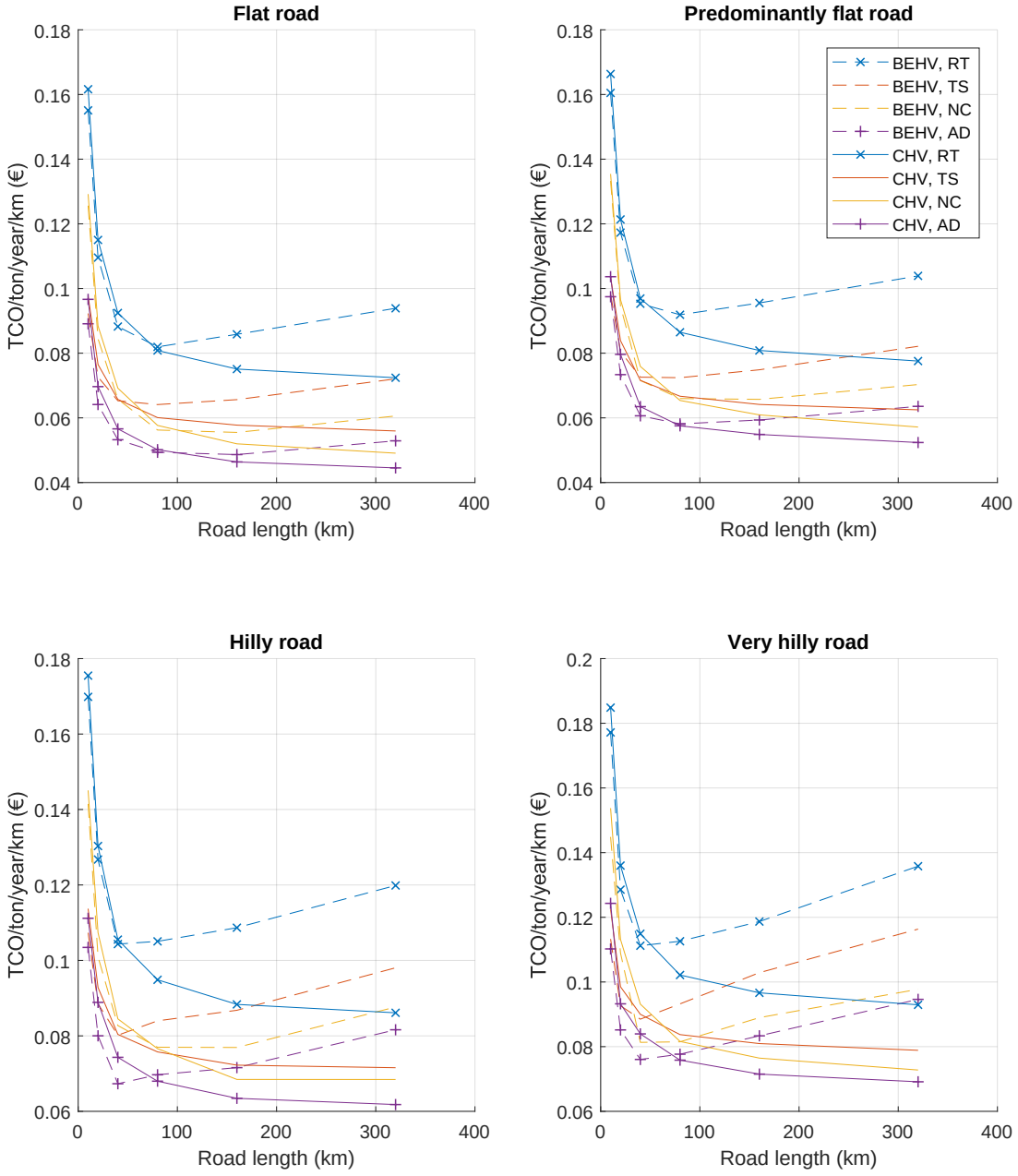

Figure 3.9: The annual TCO per ton freight and kilometer traveled for ADS-DVs of different sizes and power sources, as well as different road hilliness. RT, TS, NC, and AD stand for rigid truck, tractor-semitrailer, Nordic combination, and A-double. For BEHVs, there is a certain road length (i.e., distance between LU nodes and/or charging stations) that yields the minimum TCO. The cost of the infrastructure is included in the TCO calculations. Each data point in the figure corresponds to an optimized vehicle-infrastructure. At certain road lengths, ADS-D BEHVs (automated driving systems-dedicated BEHVs) exhibit a lower TCO than ADS-D CHVs (automated driving systems-dedicated CHVs); reused from publication iv [44].

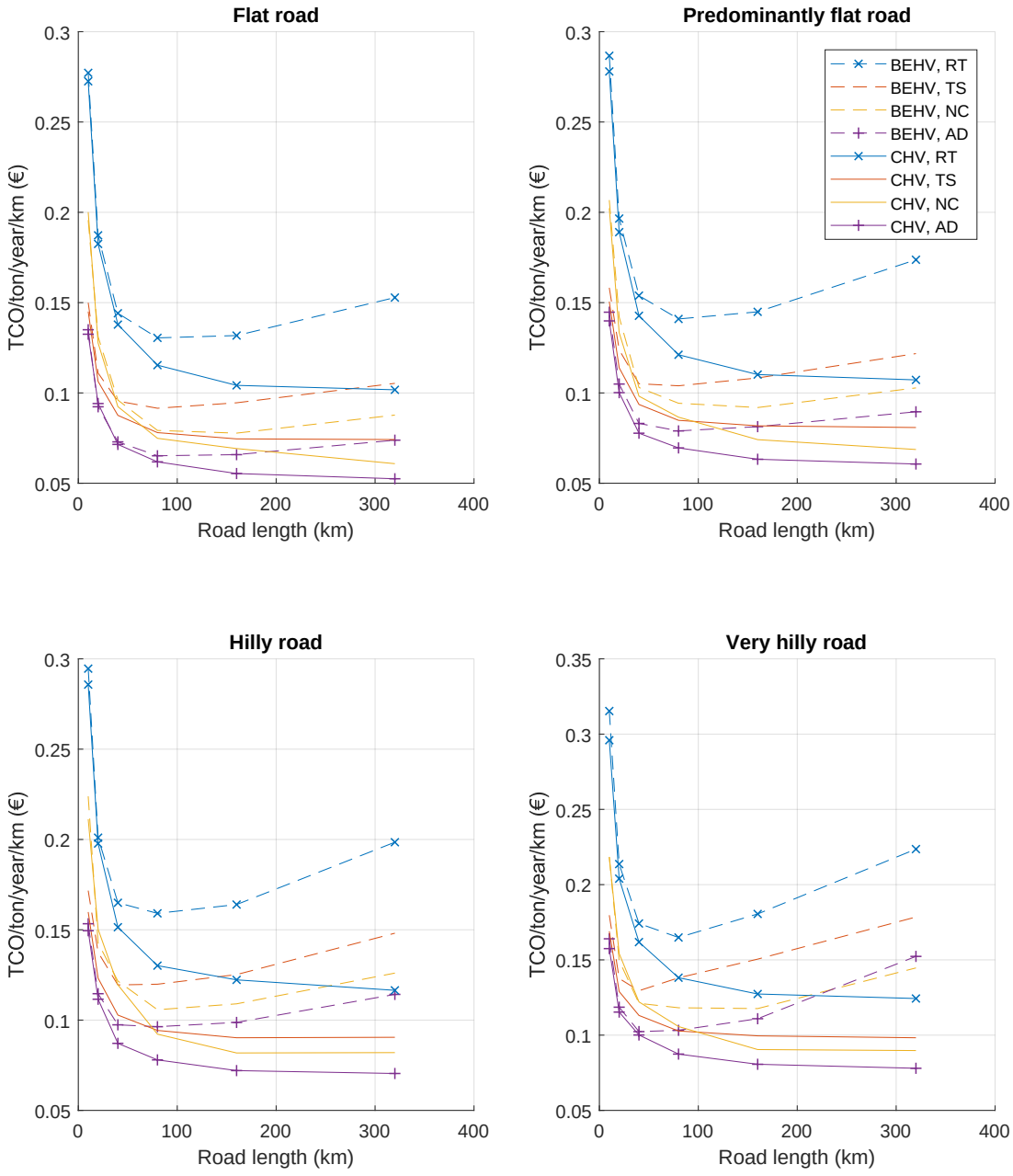

Figure 3.10: The annual TCO per ton freight and kilometer traveled for vehicles with human drivers of different sizes and power sources, as well as different road hilliness. RT, TS, NC, and AD stand for rigid truck, tractor-semitrailer, Nordic combination, and A-double. For BEHVs, there is a certain road length (i.e., distance between LU nodes and/or charging stations) that yields the minimum TCO. The cost of the infrastructure is included in the TCO calculations. Each data point in the figure corresponds to an optimized vehicle-infrastructure. At certain road lengths, BEHVs exhibit a lower TCO than CHVs; reused from publication iv [44].

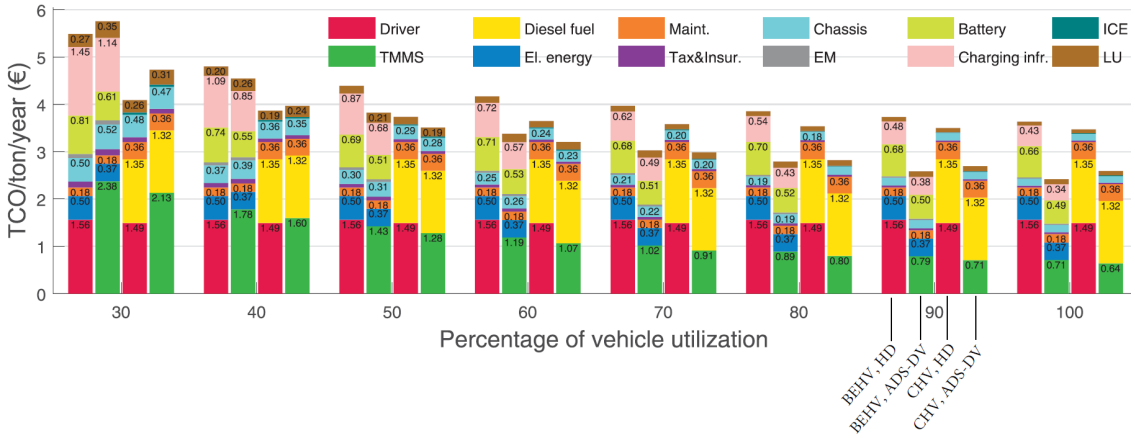

Figure 3.11: The annual TCO per ton freight transported versus different vehicle utilization levels of a tractor-semitrailer that operates on a flat road of 40 km in length at the optimum speed. Also, different cost factors, power sources, and driving systems are compared. Each group of four bars from right to left represents automated CHV (CHV, ADS-DV), CHV with human driver (CHV, HD), automated BEHV (BEHV, ADS-DV), and BEHV with human driver (BEHV, HD), respectively. TMMS stands for transportation mission management system.

Chapter 4

Optimal motion control[1]

The optimal motion controller is responsible for reducing the lateral off-tracking of the vehicle relative to a desired trajectory. This goal can be achieved by either optimal control of the steering angles of different vehicle axles (if they are steerable) or by the combined optimal control of steering, propulsion and braking. As will be discussed in Chapter 5, stable and efficient vehicle motion can be guaranteed by predictive EMS under lateral stability constraints. However, in the optimal EMS framework, minimization of the off-tracking is not part of the cost function nor are the steering angles included as decision variables due to the long prediction horizons, limits in real-time computations and the need for careful tuning of the controller. Instead, it was assumed that the steering control is separated from EMS, and the corresponding optimal controller was introduced in this chapter. In addition, the results of the combined optimal control of the steering, propulsion and braking provided in this chapter serve as building blocks for inclusion of the lateral dynamics constraints in EMS in an efficient manner, i.e., by using LTV-MPC in the next Chapter of this thesis.

According to the vehicle dynamic model of multitrailer vehicles developed in section 2.4 and Paper G, the obtained nonlinear system of implicit ODEs (or DAEs) includes the wheels' longitudinal force and steering angle as input variables. Such a model provides the possibility of controlling the motion of the vehicle using those inputs. As the modeled dynamic system is highly nonlinear with many states and inputs, its real-time optimal control is not a trivial task. However, by means of the procedure proposed in this thesis, the real-time optimal motion control of multitrailer vehicles is possible for long prediction horizons (less than 250 m). The proposed procedure made possible the combined braking, propulsion and steering of these vehicles to ensure safe driving in all driving conditions, provided that sufficient information about the upcoming road and maneuver is available for the controller.

[1]This chapter is based on Paper H.

Figure 4.1: Illustration of the road path available via vehicle localization and the road coordinates in different driving conditions (courtesy of Volvo Trucks, altered from the Volvo original images according to the approval).

The main idea of the optimal control of the nonlinear system in this thesis was converting the dynamics and the defined NOCP into an LTV-OCP (or an LTV-MPC) according to the procedure presented in section 2.3 and Paper H. The dynamic model and all the constraints needed to be linearized around an estimated (i.e. a guess) state-input trajectory that itself satisfies the nonlinear dynamic system. The guess inputs can be generated by solving the problem off-line using a simple control strategy, or they can be taken from the saved OCP solution history of the same or similar route and maneuver. In paper H, it was shown that this strategy resulted in an optimal solution that was very close to the solution of the actual NOCP; whereas an STL vehicle model that was linearized around a fixed operating condition and/or the current operating point resulted in a control law that was far from the solution of the NOCP.

The above approach was tested, by simulation, for the problem of trajectory-following and off-tracking minimization of an A-double with steerable dolly for maneuvers of different characteristics, i.e., low-speed U-turn and high-speed lane change. Notably, this work did not include trajectory planning or lane-change

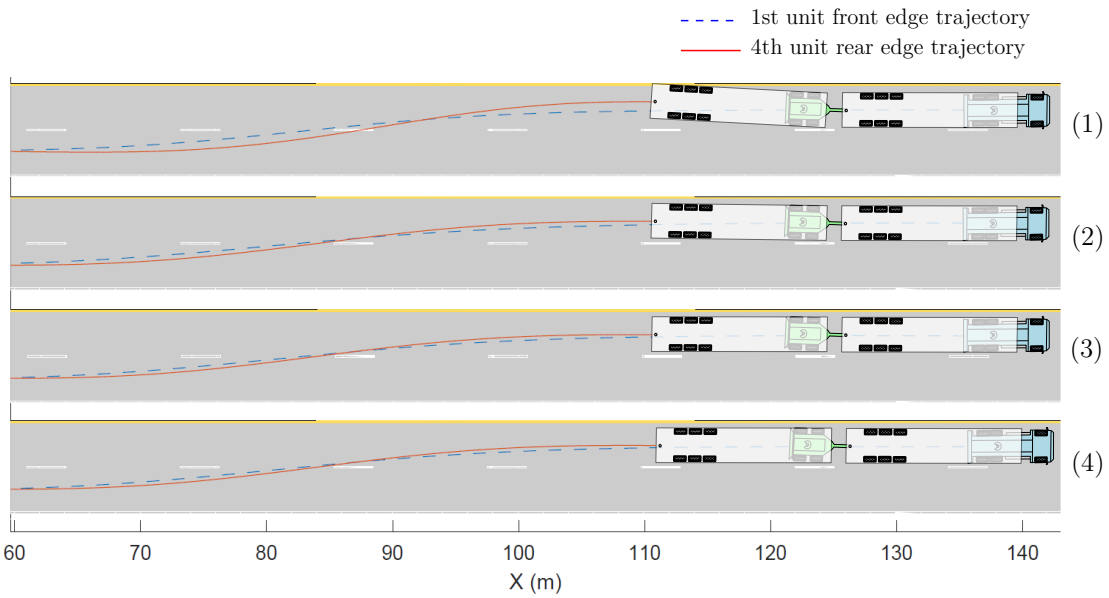

Figure 4.2: Lane-change maneuver at a longitudinal speed of 85 km/h. 1) when no optimal control is involved, with no dolly steering; 2) optimal control of the dolly steering using a linear vehicle model; 3) optimal control of the dolly steering where the vehicle model is linearized around the reference trajectory generated using case (1) with a single iteration of the LTV-MPC; 4) optimal control of the dolly steering using SQP where the iterations were continued until convergence.

decisions. It was assumed that the desired trajectory is either determined by a motion planner or available based on the road coordinates, as illustrated in Fig. 4.1.

Figs. 4.2 and 4.3 compare the high-speed lane changes (85 km/h) of the three methods explained above, together with a lane change without optimal control, i.e.,

1. Lane-change with no off-tracking minimization.

2. LTV-MPC where the nonlinear dynamic system is linearized around a fixed operating condition, that is, all the state-input trajectories are zero, except the longitudinal velocity.

3. LTV-MPC where the nonlinear dynamic system is linearized around the solution of a simple trivial controller, that is, sine steering.

4. NOCP where the optimal control actions were found by directly solving the problem using SQP until convergence.

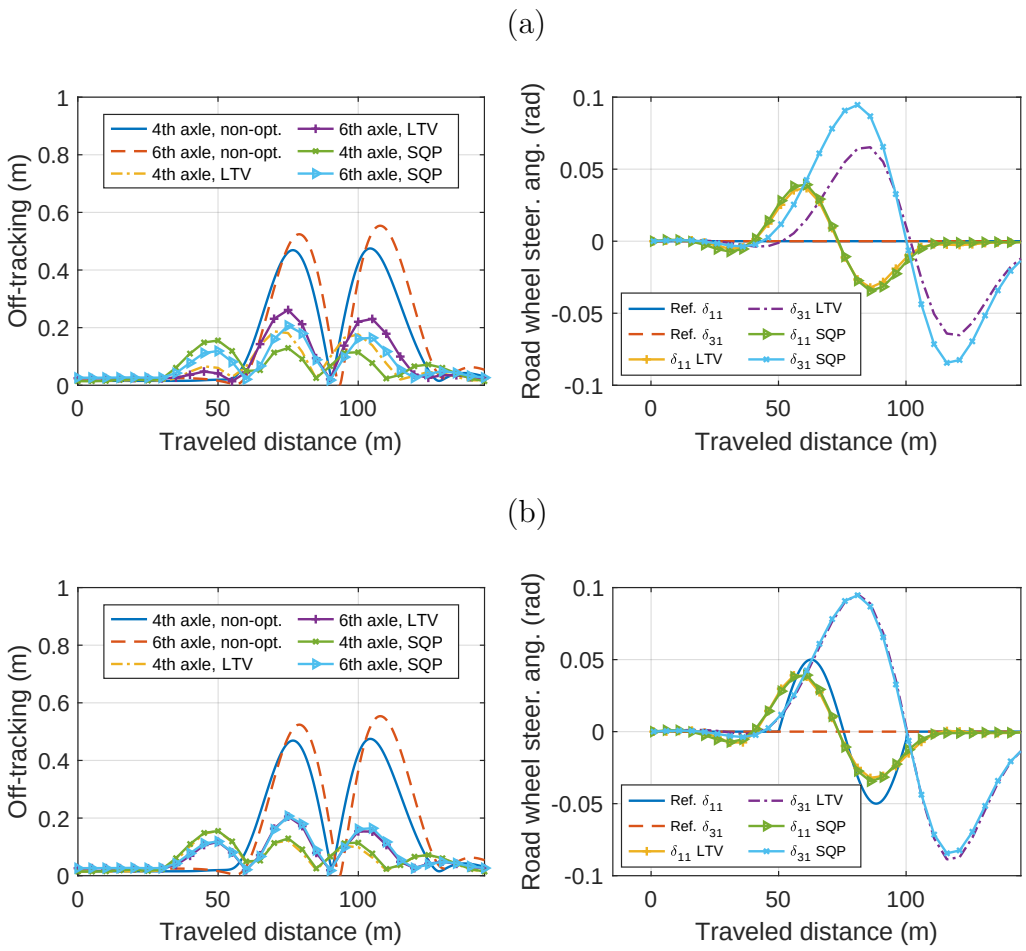

Figure 4.3: Comparison of the off-tracking and optimal steering angles between SQP and LTV optimal control of the steering; a) comparing SQP and LTV, where the vehicle model is linearized around a fixed operating condition, that is, when all the state-input trajectories are zero, except the longitudinal velocity; b) comparing SQP and LTV, where the vehicle model was linearized around a reference trajectory obtained by sine steering. The LTV of case (b) gives a very close solution to the SQP. The LTV of case (a) reduced off-tracking by 50%, whereas in case (b), the LTV reduced the off-tracking by 71%.

Among the above cases, case 4 yields the best possible solution, i.e., optimal steering angle trajectories of the first and third units, which is computationally expensive. Case 3, however, gives a very close solution to case 4 but is computationally efficient and suitable for real-time applications. These two cases reduce the off-tracking by 71% compared to that of the maneuver with no steering of the third unit. The solution in case 2, however, is far from the solution of case 4, resulting in a 50%-reduction in off-tracking. Notably, case 2 uses an STL vehicle model that is widely used in literature in nonoptimal, or short-horizon optimal, motion control of combination vehicles.

The above results lead to an important conclusion: if the nonlinear vehicle model is linearized around representative trajectories that are obtained using a simple controller (in the above example, a lane change via sine steering), then the solution of the LTV-MPC in long prediction horizons is expected to be close to the solution of the NOCP. This result could not be achieved using a linear vehicle model or its linearization around the operating point.

The above conclusion will be used for efficient inclusion of the nonlinear lateral dynamic equations in predictive EMS in the next chapter. More details can be found in Paper H.

Chapter 5

Predictive energy management of distributed propulsion in long combination vehicles[1]

In the previous chapters, it was concluded that battery electric and hybrid heavy vehicles, including long combination vehicles, exhibit a lower TCO than their conventional counterparts in certain transportation scenarios. TCO minimization was performed using simple control strategies to control the gear selection and the split of the total power between the electric and conventional power sources. However, energy management, including speed profile and gear selection optimization for the conventional and battery electric vehicles, and combined speed profile, gear selection and power split optimization in hybrid vehicles, results in considerable fuel and energy savings. The energy savings depend on many parameters, as discussed in paper B using dynamic programming. For example, regarding the vehicle, it depends on the vehicle size, type and size of batteries, EMs, and ICE; and regarding the surrounding environment, it depends on the road profile, speed variations caused by traffic and road legal speed limit, and weather conditions, e.g., wind and road grip. As shown in Paper B, for the tested road profile, predictive energy management of hybrid vehicles, excluding speed profile optimization, resulted in 4-12% fuel savings, depending on the road speed variation and the powertrain. The energy savings can be higher in hilly and very hilly roads and when considering speed profile optimization combined with power split and gear optimization. The speed profile optimization itself leads to fuel savings in CHVs on hilly roads [42]. For battery electric vehicles, however, the savings of predictive energy management on hilly roads are expected to be lower because of the possibility of regenerative braking that is also available in a non-predictive controller.

[1]Parts of this chapter were already presented in Paper F. However, most of the material was not presented in any of the appended papers.

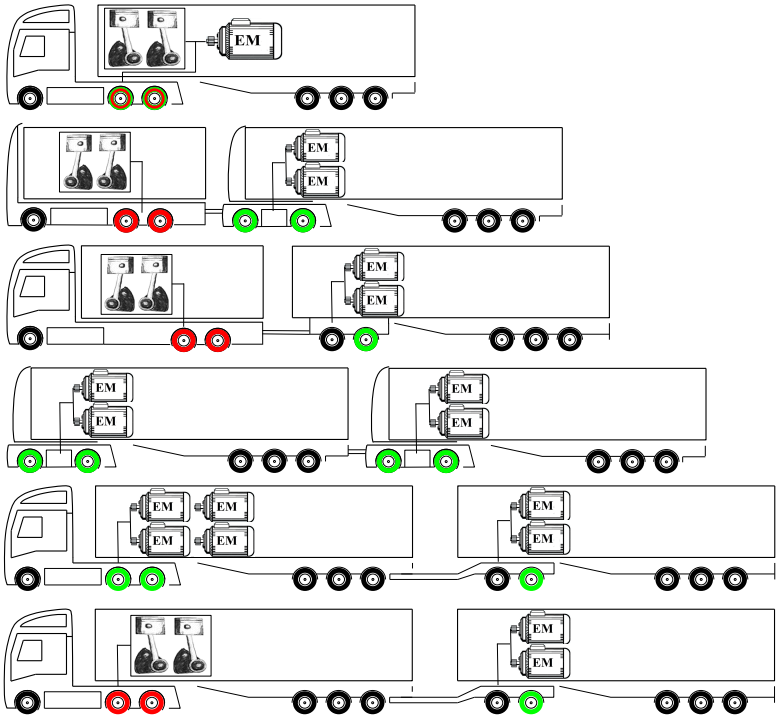

Figure 5.1: Examples of distributed propulsion between different axles of combination vehicles, including vehicles with human drivers and ADS-DVs.

In the sequel, this chapter discusses the predictive, i.e., optimal, energy management of vehicles with hybrid powertrains. Notably, the algorithms are also valid for conventional and battery electric vehicles.

Moreover, according to papers C, D and E, in the case of combination vehicles, e.g., Nordic combination and A-double, the optimum powertrain configuration might include distributed propulsion between axles depending on the vehicle transportation use-case. The distributed propulsion might include different sources of power. Examples of vehicles with hybrid and distributed propulsion are shown in Fig. 5.1.

In these vehicles, the propulsion and braking actuation might act on axles that belong to different units separated by articulation joints. Therefore, the driven axles might be actuated separately from the others based on the request of the optimal energy management controller. For example, the energy management controller might predict that it is more energy efficient to let only the electrically driven axle of the dolly brake, e.g., to reduce the speed or to maintain speed while going downhill, rather than the other axles that have no electric drive, such that more energy can be regenerated. However, such a scenario should be allowed only if the safety and lateral stability are assured. The lateral stability can be compromised by the nonlinear behavior of the tires and because articulation joints (one

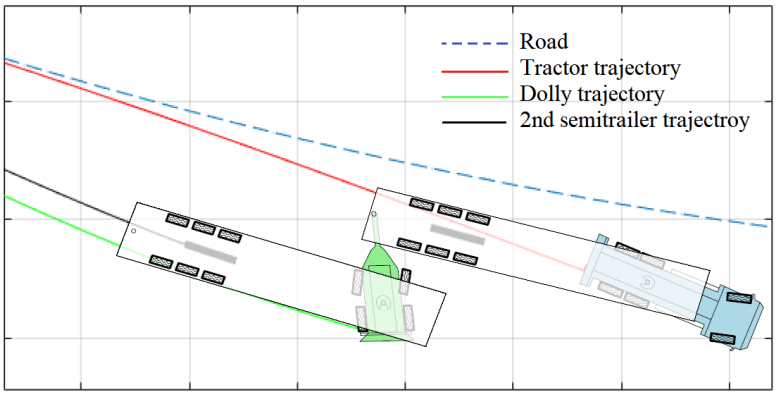

Figure 5.2: Dolly braking on a curved and slightly downhill road. The braked axle loses lateral force due to the combined slip effect of the tires. Then, the push of the second semitrailer causes dolly jack-knifing.

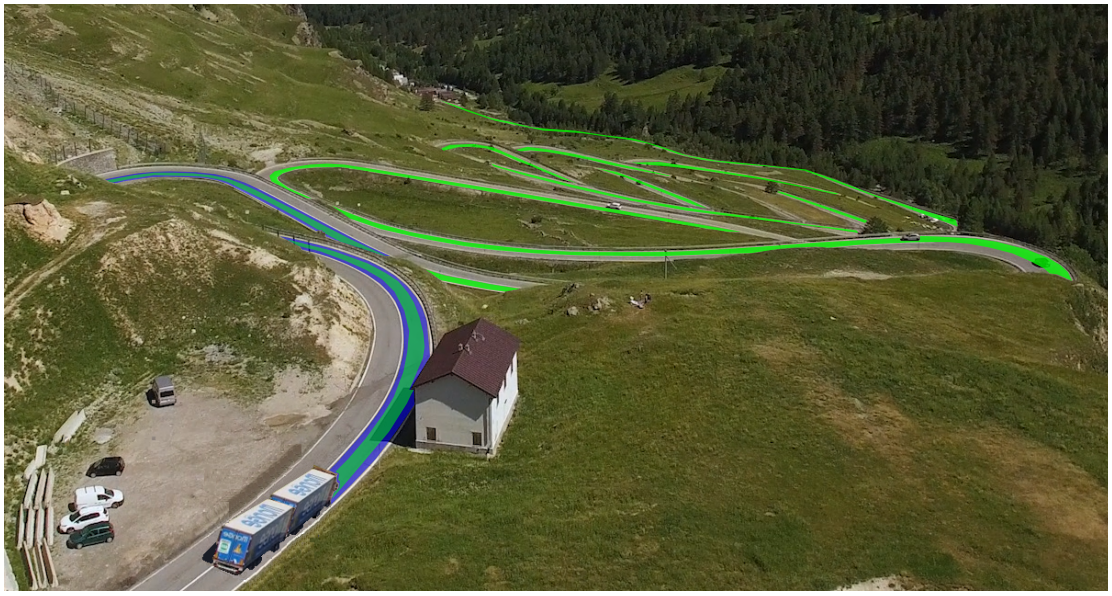

Figure 5.3: Road prediction horizon used for EMS (green lane). The blue section corresponds to the part of the prediction horizon where vehicle lateral stability constraints must be satisfied in the MPC problem (courtesy of Volvo Trucks, altered from the Volvo original image according to the approval).

or more) exist in combination vehicles. For example, if an electrically driven axle is solely actuated because of the energy savings, it pushes the front units during propulsion, and it is pushed by the rear units during braking. Uneven distribution of the load and low road grip contribute to even more critical situations. Such a scenario is simulated, and the result is shown in Fig. 5.2.

A similar instability might occur when the dolly pushes the front units during

propulsion. Therefore, proper constraints should be defined in the energy management controller to avoid such scenarios while maximizing the energy savings. Therefore, this chapter also considers the problem of predictive energy management under lateral stability constraints. The real-time model predictive control of many states and control actions of a highly nonlinear systems in the presence of nonlinear constraints and long prediction horizons, e.g., Fig. 5.3, is challenging.

5.1 Control layer hierarchy[2]

Inclusion of the detailed dynamics of the system in a single control layer requires a high level of computations that cannot be performed in the case of long prediction horizons and real-time applications. A multilayer control hierarchy can help to decompose the complex control system into smaller and computationally efficient subcontrol systems. In this case, each of the subcontrol systems includes a different level of detail regarding the behavior of the overall controlled system and can be solved using different approaches and feedback control laws. In the case of predictive energy management, the control hierarchy in this thesis is shown in Fig. 5.4, where the different control layers exhibit different levels of nonlinearity and require different feedback frequencies.

The vehicle environment block constantly provides information about the upcoming horizon, i.e., the road ahead (and the whole trip, if available) including the topography, traffic, speed limit, and available lanes. Traffic information includes the position and speed of the leading vehicle. The first control layer is thus responsible for planning the vehicle velocity v_{req}, the battery state of charge soc_{req}, the ICE gear $\gamma_{\mathrm{e,req}}$ and the EM gear $\gamma_{\mathrm{m,req}}$ for long prediction horizons. The second and third layers are responsible for tracking the requested states generated by the first layer. In the second layer, the brake and acceleration pedal positions (in case of a vehicle with a human driver), or directly the propulsion power $P_{\mathrm{prop,req}}$ and brake power $P_{\mathrm{brk,req}}$ requests (often in the case of the ADS-DVs), are planned. The control signal selection at this level depends on the signal availability and control hierarchy of the plant model, i.e., the vehicle. For example, the power requests generated in the energy management controller should not override the power requests generated by the vehicle active safety control system. Finally, the third control layer is responsible for following the SOC trajectory generated by the first layer using the equivalent consumption minimization strategy (ECMS).

[2]This section is based on Paper F.

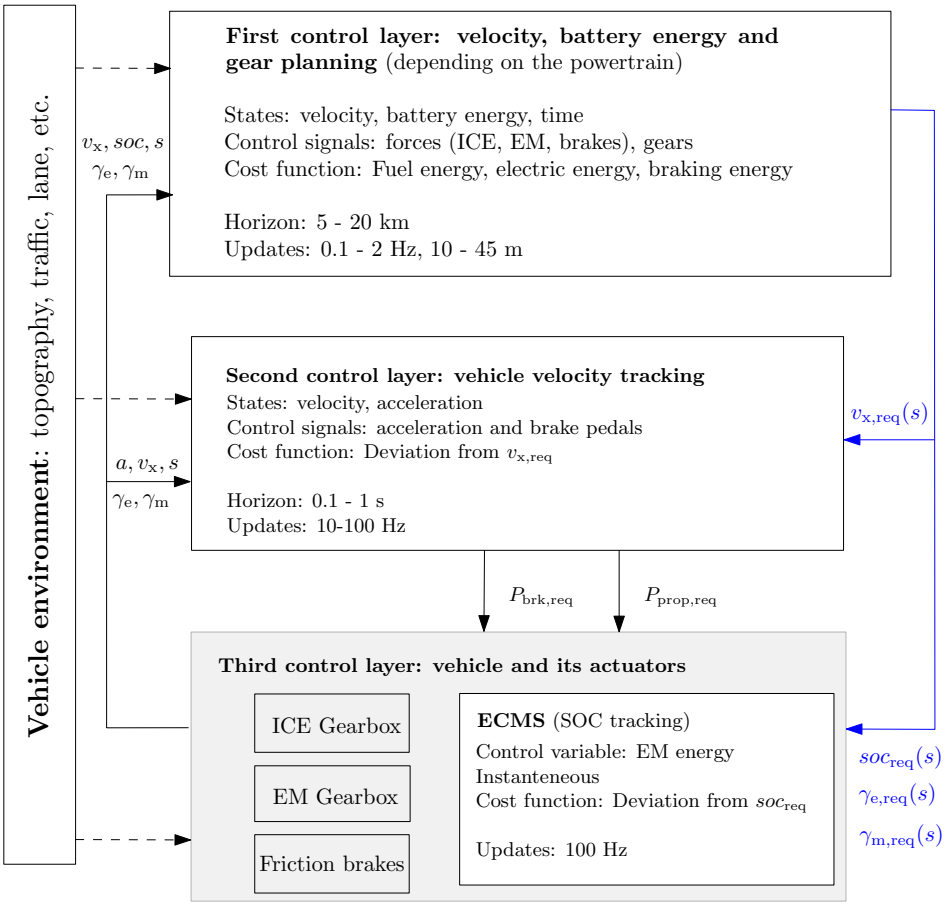

Figure 5.4: Overall control hierarchy, where v_{req}, soc_{req}, $\gamma_{e,req}$, and $\gamma_{m,req}$ denote the optimal profile of the velocity, battery state of charge, ICE gear, and EM gear, respectively; $P_{prop,req}$ and $P_{brk,req}$ denote the propulsion and brake power requests; and signals a, v, s, soc, γ_e and γ_m are the feedback signals, where a denotes acceleration and s denotes the current distance traveled.

5.2 First control layer: velocity, battery and gear planning by solving a nonlinear mixed-integer optimal control problem[3]

Following the NOCP defined in (2.3) and the powertrain model described in section 2.5, the NOCP of energy management of a vehicle driving on a straight road, i.e., neglecting the lateral dynamics, according to Paper F, can be defined as follows, where the state vector is $x = [v_x, soc, t]$ and the input vector is $u = [F_e, F_{mw}, F_{br}, \gamma_e, \gamma_m]$ (see section 2.5 and Fig. 2.10 for definition of the

[3]This section is based on Paper F.

notation):

$$
\begin{aligned}
&\text{Find} && F_{\mathrm{e}}(s), F_{\mathrm{mw}}(s), F_{\mathrm{br}}(s), \gamma_{\mathrm{e}}(s), \gamma_{\mathrm{m}}(s),\\
&\text{to minimize} && J^{nl} = \int_{s=s_0}^{s=s_{\mathrm{f}}} \big(F_{\mathrm{f}}(\cdot) + F_{\mathrm{br}}(s) - F_{\mathrm{mw}}(s) +\\
& && F_{\mathrm{mc}}(s) + \frac{R v_{\mathrm{x}}(s)}{V_{\mathrm{b}}^2}(F_{\mathrm{mc}}(s) + F_{\mathrm{a}}(s))^2\big) ds, && \text{(5.1a)}\\
&\text{subject to} && \textbf{fuel equivalent force:}\\
& && F_{\mathrm{f}}(F_{\mathrm{e}}(s), v_{\mathrm{x}}(s), \gamma_{\mathrm{e}}(s), s) =\\
& && \frac{1}{v_{\mathrm{x}}(s)} \sum_{i=0}^{5}\sum_{j=0}^{5} a_{ij} \big(\frac{r_{\mathrm{e}}(\gamma_{\mathrm{e}}(s))}{R_{\mathrm{w}}} v_{\mathrm{x}}(s)\big)^i \big(\frac{R_{\mathrm{w}}}{r_{\mathrm{e}}(\gamma_{\mathrm{e}}(s))} F_{\mathrm{e}}(s)\big)^j, && \text{(5.1b)}\\
& && \textbf{vehicle longitudinal dynamic:}\\
& && \frac{d v_{\mathrm{x}}(s)}{ds} = \frac{1}{m v_{\mathrm{x}}(s)} \big(F_{\mathrm{br}}(s) - \eta_{\mathrm{te}} F_{\mathrm{e}}(s) - F_{\mathrm{mw}}(s) +\\
& && mg \sin\alpha(s) - mg f_{\mathrm{r}} \cos\alpha(s) - 0.5 \rho_{\mathrm{a}} A_{\mathrm{f}} c_{\mathrm{d}} v_{\mathrm{x}}(s)^2\big), && \text{(5.1c)}\\
& && \textbf{battery SOC dynamic:}\\
& && \frac{dsoc(s)}{ds} = -\frac{1}{E_{\mathrm{bmax}}} \big(F_{\mathrm{mc}}(s) + \frac{R v_{\mathrm{x}}(s)}{V_{\mathrm{b}}^2}(F_{\mathrm{mc}}(s) + F_{\mathrm{a}}(s))^2 + F_{\mathrm{a}}(s)\big), && \text{(5.1d)}\\
& && \textbf{time dynamic:}\\
& && \frac{dt(s)}{ds} = \frac{1}{v_{\mathrm{x}}(s)}, && \text{(5.1e)}\\
& && \textbf{initial and terminal states:}\\
& && v(s_0) = v_0, soc(s_0) = soc_0, t(s_0) = t_0, && \text{(5.1f)}\\
& && soc(s_{\mathrm{f}}) = soc_{\mathrm{f}}, && \text{(5.1g)}\\
& && \textbf{ICE torque upper limit:}\\
& && \frac{R_{\mathrm{w}}}{r_{\mathrm{e}}(\gamma_{\mathrm{e}}(s))} F_{\mathrm{e}}(s) - \min\{\sum_{j=0}^{3} b_{ij}^{e} \big(\frac{r_{\mathrm{e}}(\gamma_{\mathrm{e}}(s))}{R_{\mathrm{w}}} v_{\mathrm{x}}(s)\big)^j,\ i = 1, \ldots, 4\} \le 0, && \text{(5.1h)}\\
& && \textbf{EM torque limits:}\\
& && \frac{R_{\mathrm{w}} F_{\mathrm{mw}}(s)}{r_{\mathrm{m}}(\gamma_{\mathrm{m}}(s)) \eta_{\mathrm{tm}}} - \min\{\sum_{j=0}^{3} b_{ij}^{\mathrm{m}} \big(\frac{r_{\mathrm{m}}(\gamma_{\mathrm{m}}(s))}{R_{\mathrm{w}}} v_{\mathrm{x}}(s)\big)^j,\ i = 1, 2\} \le 0, && \text{(5.1i)}\\
& && -\frac{R_{\mathrm{w}} F_{\mathrm{mw}}(s) \eta_{\mathrm{tm}}}{r_{\mathrm{m}}(\gamma_{\mathrm{m}}(s))} + \max\{\sum_{j=0}^{3} b_{ij}^{\mathrm{m}} \big(\frac{r_{\mathrm{m}}(\gamma_{\mathrm{m}}(s))}{R_{\mathrm{w}}} v_{\mathrm{x}}(s)\big)^j,\ i = 3, 4\} \le 0, && \text{(5.1j)}\\
& && \textbf{arrival time:}\\
& && t(s_{\mathrm{f}}) - t_{\mathrm{tref}}(s_{\mathrm{f}}) \le 0, && \text{(5.1k)}\\
& && \textbf{battery SOC limits:}\\
& && soc_{\min} - soc(s) \le 0, && \text{(5.1l)}\\
& && soc(s) - soc_{\max} \le 0, && \text{(5.1m)}\\
& && \textbf{battery power limits:}
\end{aligned}
$$

$$p_{\text{bmin}} - v_{\text{x}}(s)\big(F_{\text{mc}}(s) + \frac{Rv_{\text{x}}(s)}{V_{\text{b}}^2}(F_{\text{mc}}(s) + F_{\text{a}}(s))^2 + F_{\text{a}}(s)\big) \leq 0, \tag{5.1n}$$

$$v_{\text{x}}(s)\big(F_{\text{mc}}(s) + \frac{Rv_{\text{x}}(s)}{V_{\text{b}}^2}(F_{\text{mc}}(s) + F_{\text{a}}(s))^2 + F_{\text{a}}(s)\big) - p_{\text{bmax}} \leq 0, \tag{5.1o}$$

speed limits:

$$v_{\text{min}}(s) - v_{\text{x}}(s) \leq 0, \tag{5.1p}$$

$$v_{\text{x}}(s) - v_{\text{max}}(s) \leq 0, \tag{5.1q}$$

ICE torque (force) lower limit:

$$-F_{\text{e}}(s) \leq 0, \tag{5.1r}$$

friction brake lower limit:

$$-F_{\text{br}}(s) \leq 0, \tag{5.1s}$$

where the terminal cost $C_{\text{t}}(x(s_{\text{f}}), s_{\text{f}}) = 0$ and, following (2.41), F_{mc} is given according to

$$F_{\text{mc}}(s) = \begin{cases} \frac{1}{v_{\text{x}}(s)} \sum_{i=0}^{5}\sum_{j=0}^{5} \Big(h_{ij}^{+}\big(\frac{r_{\text{m}}(\gamma_{\text{m}}(s))}{R_{\text{w}}} v_{\text{x}}(s)\big)^i \big(\frac{R_{\text{w}}}{r_{\text{m}}(\gamma_{\text{m}}(s))} F_{\text{m}}(s)\big)^j\Big), & F_{mw}(s) > 0 \\ \frac{1}{v_{\text{x}}(s)} \sum_{i=0}^{5}\sum_{j=0}^{5} \Big(h_{ij}^{-}\big(\frac{r_{\text{m}}(\gamma_{\text{m}}(s))}{R_{\text{w}}} v_{\text{x}}(s)\big)^i \big(\frac{R_{\text{w}}}{r_{\text{m}}(\gamma_{\text{m}}(s))} F_{\text{m}}(s)\big)^j\Big), & F_{mw}(s) \leq 0. \end{cases} \tag{5.2}$$

In NOCP (5.1), the cost function includes fuel equivalent force F_{f}, brake force F_{br}, and total equivalent electric dissipation force F_{del}, which are given by the last three terms of the cost function, i.e.,

$$F_{\text{del}} = -F_{\text{mw}}(s) + F_{\text{mc}}(s) + \frac{Rv_{\text{x}}(s)}{V_{\text{b}}^2}(F_{\text{mc}}(s) + F_{\text{a}}(s))^2 \tag{5.3}$$

The primary objective is to reduce fuel consumption. However, the inclusion of the brake force in the cost function led to faster convergence of the NLP. Moreover, the inclusion of the electric dissipation in the cost function was needed to make its later linearization possible, according to Paper F. Therefore, inclusion of both brake and electric dissipation in the cost function, together with the fuel consumption, indirectly discourages deceleration and acceleration, thereby increasing driver comfort.

Furthermore, constraint (5.1c) represents the vehicle longitudinal dynamic system, where the influence of steering, i.e., side slip, is neglected. Constraint (5.1d) represents the battery energy dynamic equation. Constraint (5.1e) represents the time dynamic equation. Constraints (5.1f) and (5.1g) restrict the initial and final states. Constraint (5.1h) enforces the upper limits of the ICE torque (or force). Constraints (5.1i) and (5.1j) limit the positive and negative EM torques. Constraint (5.1k) limits the trip or horizon maximum travel time given the reference

max trip or horizon travel time $t_{\text{tref}}(s)$. Constraints (5.1l) and (5.1m) restrict the battery SOC. Constraints (5.1n) and (5.1o) limit the battery power, and constraints (5.1p)-(5.1s) limit the longitudinal speed and engine and brake forces.

5.2.1 Sequential quadratic programming for solving NOCP of energy management

The nonlinear mixed-integer OCP (5.1) can be solved sequentially, as discussed in section 2.3.1. An SQP can be built by performing discretization and quadratic convex approximation of the cost function, as well as linearization of the constraints. Then, the problem is transformed into a form given by (2.7) that can be iteratively solved by the SLP or SQP until convergence to the solution of the nonlinear problem. However, the SLP or SQP in the form presented in (2.7) are applicable only for continuous variables. Integer variables $\boldsymbol{u}_{\text{d}} = [\boldsymbol{\gamma}_{\text{e}}, \boldsymbol{\gamma}_{\text{m}}]$ are handled by solving a secondary optimization problem to ensure that the best gears are selected in all distance stages to minimize the ICE and EM energy dissipation. The gear optimization is also solved sequentially. The output of the each iteration of gear optimization serves as input to the next iteration of the QP. The detailed procedure is explained in Paper F. Algorithm 2 in section 2.3.2 is updated to include the gear optimization according to the following algorithm. Note that in this algorithm, there are no desired states.

Algorithm 3 SQP and gear optimization for predictive energy management

Input: $\hat{x}, \boldsymbol{x}_0, \boldsymbol{u}_0 = [\boldsymbol{u}_{\text{c}0}, \boldsymbol{u}_{\text{d}0}]$, where $\boldsymbol{u}_{\text{c}0} = [\boldsymbol{F}_{\text{e}0}, \boldsymbol{F}_{\text{mw}0}, \boldsymbol{F}_{\text{br}0}], \boldsymbol{u}_{\text{d}0} = [\boldsymbol{\gamma}_{\text{e}0}, \boldsymbol{\gamma}_{\text{m}0}]$;
Initialization : $j \leftarrow 0$;

1: **while** *not converged* **do**
2: Evaluate Jacobians and linearize the constraints (also perform a convex approximation of the cost function according to Paper F, if needed) to build QP, i.e., $\text{QP}_{\text{NOCP}}(\hat{x}, \boldsymbol{x}_j, \boldsymbol{u}_{\text{c}j}, \boldsymbol{u}_{\text{d}j})$;
3: Solve $\text{QP}_{\text{NOCP}}(\hat{x}, \boldsymbol{x}_j, \boldsymbol{u}_{\text{c}j}, \boldsymbol{u}_{\text{d}j})$ to find $\boldsymbol{x}$ and $\boldsymbol{u}_{\text{c}}$, by calling a QP solver (e.g. [6, 50]);
4: Solve the two-gear optimization problems (one for EM and one for ICE according to Paper F), given $\boldsymbol{x}$ and $\boldsymbol{u}_{\text{c}}$, to find $\boldsymbol{u}_{\text{d}}$;
5: Update the state-input guess $\boldsymbol{x}_j$ and $\boldsymbol{u}_j = [\boldsymbol{u}_{\text{c}j}, \boldsymbol{u}_{\text{d}j}]$ to ensure descent in the Newton direction with step size $\alpha \in]0, 1]$ [105]:
$[\boldsymbol{x}_{(j+1)}, \boldsymbol{u}_{\text{c}(j+1)}] = [\boldsymbol{x}_j, \boldsymbol{u}_{\text{c}j}] + \alpha\big([\boldsymbol{x}, \boldsymbol{u}_{\text{c}}] - [\boldsymbol{x}_j, \boldsymbol{u}_{\text{c}j}]\big)$;
$\boldsymbol{u}_{\text{d}(j+1)} = \boldsymbol{u}_{\text{d}}$
6: $j \leftarrow j + 1$;
7: **end while**
8: **return** $[\boldsymbol{x}, \boldsymbol{u}_{\text{c}}, \boldsymbol{u}_{\text{d}}]$.

5.2.2 Sequential linear programming for solving NOCP of energy management

The difference between SLP and SQP is the approximation of the cost function. In SLP, in each sequential iteration, the cost function is approximated by a linear (affine) function. This can be done by considering F_{del} as a control signal, i.e., $u = [F_{\text{e}}, F_{\text{mw}}, F_{\text{br}}, F_{\text{del}}, \gamma_{\text{e}}, \gamma_{\text{m}}]$. Then, the cost function is

$$J^{nl} = \int_{s_0}^{s_{\text{f}}} \big(F_{\text{f}}(x(s), u(s), s) + F_{\text{br}}(s) + F_{\text{del}}(s)\big) ds. \tag{5.4}$$

Hence, the only nonlinear term in the cost function is $F_f(x(s), u(s), s)$. This term can be linearized according to

$$\begin{aligned} &F_{\text{f0}}^{\text{lin}}(x(s), u(s), s) = F_f(x_0(s), u_0(s)) + \\ &\frac{\partial F_{\text{f}}(\cdot)}{\partial x}|_{(x_0(s), u_0(s))}(x(s) - x_0(s)) + \\ &\frac{\partial F_{\text{f}}(\cdot)}{\partial u}|_{(x_0(s), u_0(s))}(u(s) - u_0(s)). \end{aligned} \tag{5.5}$$

Therefore, a linear cost function is obtained as follows.

$$J_0^{\text{lin}} = \int_{s_0}^{s_{\text{f}}} \big(F_{\text{f0}}^{\text{lin}}(x(s), u(s), s) + F_{\text{br}}(s) + F_{\text{del}}(s)\big) ds. \tag{5.6}$$

The linearization of the cost function is sequentially updated with the updates of the constraints. The rest of the SLP algorithm and gear optimization is the same as Algorithm 3.

In addition, the introduction of F_{del} as a control signal linearizes the battery energy dynamic equation (5.1d) and simplifies the constraints on the battery power (5.1n) and (5.1o).

5.3 Predictive lateral stability and energy management in long prediction horizons as a part of the first control layer[4]

The predictive energy management presented previously did not include lateral motion. Direct application of the energy management strategy explained above in applications with distributed propulsion causes safety issues. The reasons include the higher risks of side slip, roll-over, and pushing the towing unit. A quick remedy

[4]This section was not presented in any of the appended papers.

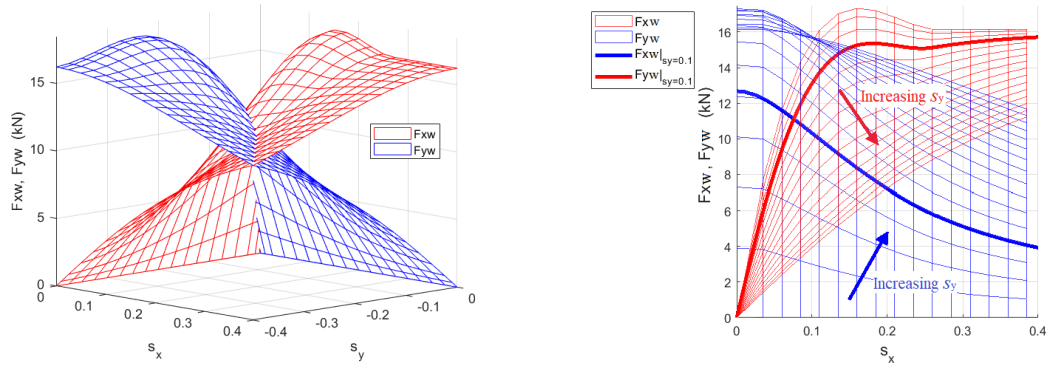

Figure 5.5: Tire longitudinal and lateral forces, F_{xw} and F_{yw}, as functions of longitudinal and lateral slip, i.e., s_{x} and s_{y}, using a combined slip tire brush model.

for the safety problem is to use a large safety factor and to limit the propulsion and braking forces of the driven axles to a small portion of the maximum available tire longitudinal force. Another solution is limiting the longitudinal speed based on the curvature of the road. However, these approaches may not be sufficient to ensure safety, as they do not take into account different contributing factors, such as road friction, vehicle configuration, load distribution, and the combination of the curvature, road grade, and road banking angle, unless by being too conservative, which can result in less efficient energy management. Therefore, the optimal distribution of propulsion and braking considering the dynamics of the vehicle combination is necessary to ensure safety and energy efficiency simultaneously.

One of the main reasons for the increased safety risk of distributed propulsion is the combined tire slip effect. The tire longitudinal and lateral forces are interrelated because the total force that a tire can provide is limited. For example, a high longitudinal tire force reduces the maximum lateral force that the tire can develop, and vice versa. This characteristic is shown in Fig. 5.5 using an anisotropic tire brush model with parabolic pressure and a stick and slip friction [65], where the lateral and longitudinal forces are shown as functions of the tire lateral and longitudinal slips, i.e., s_{x} and s_{y}.

In this thesis, the tire longitudinal forces serve as inputs to the dynamic system, whereas the required slip for generating these forces is not calculated in the first control layer. Moreover, the combined slip equations as functions of the slips, e.g., the brush tire model or Pacejka tire model [107], are not invertible. Therefore, if the longitudinal force and lateral slip are known, the longitudinal slip and the lateral force cannot be easily calculated. A combined slip model that is simpler than the brush and Pacejka models is the friction ellipse model [107, 65]. This model directly relates the longitudinal and lateral forces, rather than the

longitudinal and lateral slips, based on the Pythagorean theorem, according to

$$F_{\mathrm{yw}} = \sqrt{1 - (\frac{F_{\mathrm{xw}}}{e\ \mu\ F_{\mathrm{z}}})^2}\ F_{\mathrm{yw}}|_{(s_{\mathrm{x}}=0)}, \tag{5.7}$$

where F_{yw} denotes the tire lateral force, F_{xw} denotes the tire longitudinal force caused by actuation (the input of dynamic system (2.12) or (2.13) according to (2.15)), neglecting the rolling resistance, μ is the road friction, F_{z} denotes the tire normal force, and e is a scaling factor that defines the shape of the combined slip model; i.e., if $e = 1$, then the model is a friction circle. The friction ellipse model (5.7) shows that the lateral force decreases if the longitudinal slip or longitudinal force is nonzero. A comparison of the friction ellipse combined slip model and the anisotropic tire brush model with a parabolic pressure and stick and slip friction is illustrated in Figs. 5.6-5.8. The brush combined slip tire model is defined as

$$F_{\mathrm{xw}} = C_{\mathrm{x}} s_{\mathrm{x}} (\frac{\xi_{\mathrm{c}}}{L})^2 + \mu_{\mathrm{slip}} F_{\mathrm{z}} \frac{s_{\mathrm{x}}}{s} (1 - 3(\frac{\xi_{\mathrm{c}}}{L})^2 + 2(\frac{\xi_{\mathrm{c}}}{L})^3) \tag{5.8}$$

$$F_{\mathrm{yw}} = -\big(C_{\mathrm{y}} s_{\mathrm{y}} (\frac{\xi_{\mathrm{c}}}{L})^2 + \mu_{\mathrm{slip}} F_{\mathrm{z}} \frac{s_{\mathrm{y}}}{s} (1 - 3(\frac{\xi_{\mathrm{c}}}{L})^2 + 2(\frac{\xi_{\mathrm{c}}}{L})^3)\big), \tag{5.9}$$

where

$$s_{\mathrm{x}} = \frac{R\ \omega - v_{\mathrm{wx}}}{|R\ \omega|}, \tag{5.10}$$

$$s_{\mathrm{y}} = \frac{v_{\mathrm{wy}}}{|R\ \omega|}, \tag{5.11}$$

$$s = \sqrt{s_{\mathrm{x}}^2 + s_{\mathrm{y}}^2}$$

$$s_k = \sqrt{(\frac{C_{\mathrm{x}}}{C_{\mathrm{y}}}\ s_{\mathrm{x}})^2 + s_{\mathrm{y}}^2}$$

$$\xi_{\mathrm{c}} = (1 - \frac{C_{\mathrm{y}}\ s_k}{3\ \mu_{\mathrm{stick}}\ F_{\mathrm{z}}})\ L,$$

where R denotes the tire radius, ω denotes the tire rotational speed, v_{wy} and v_{wx} denote the wheel hub velocity components in the wheel local coordinate system, C_{x} and C_{y} denote the longitudinal and lateral tire stiffness, μ_{slip} and μ_{stick} denote the road friction at nonzero slip and the road friction at zero slip, respectively, L denotes the road-tire contact length, and F_{z} denotes the tire vertical force. Equations (5.8) and (5.9) are valid if the tire rotational speed and the vehicle longitudinal speed have the same sign. The figures were generated using $C_{\mathrm{x}} = 270$ kN, $C_{\mathrm{y}} = 180$ kN, $\mu_{\mathrm{slip}} = 0.9$, $\mu_{\mathrm{stick}} = 1.35$, $L = 0.1$ m, and $F_{\mathrm{z}} = 18$ kN. More details are provided in Paper G and [65].

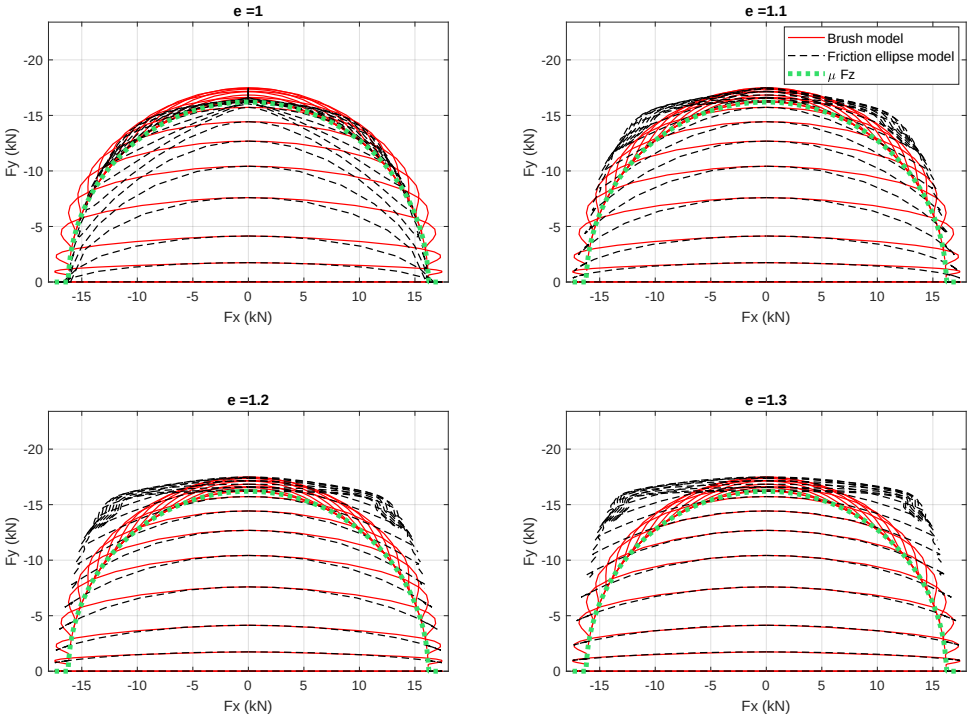

Figure 5.6: The lateral force F_{y} versus the longitudinal force F_{x} modeled with two different combined slip tire models, i.e., the brush and the friction ellipse models, and for different values of scaling factor e. The friction ellipse results in a lower lateral force for most combinations of F_{x} and F_{y}. The line for $\sqrt{F_{\mathrm{x}}^2 + F_{\mathrm{y}}^2} = \mu F_{\mathrm{z}}$ is also shown. F_{z} refers to the tire vertical load, and μ refers to the road friction at a large slip.

The nonlinear equations of motion of multitrailer vehicles described in section 2.4 and Paper G can include the tire combined slip effect and distributed propulsion and braking, as well as steering. Therefore, the vehicle dynamic equation (5.1c) can be replaced with the nonlinear equations of motion of multitrailer vehicles (2.13) with the addition of constraints related to the axles' lateral force and acceleration to obtain a new NOCP that considers predictive energy management of LHVs with distributed propulsion, where the lateral stability is taken into account. However, the applicability of such an energy management method in real-time applications is not guaranteed because the equations of motion of the combined lateral and longitudinal dynamics are highly nonlinear and stiff compared to the longitudinal dynamic equation (5.1c), where the lateral dynamics are neglected. For example, the Euler method for the approximation of the derivatives can be used to discretize the NOCP in (5.1) with an arbitrary step size, whereas the step size of an NOCP that includes the lateral dynamics can barely exceed

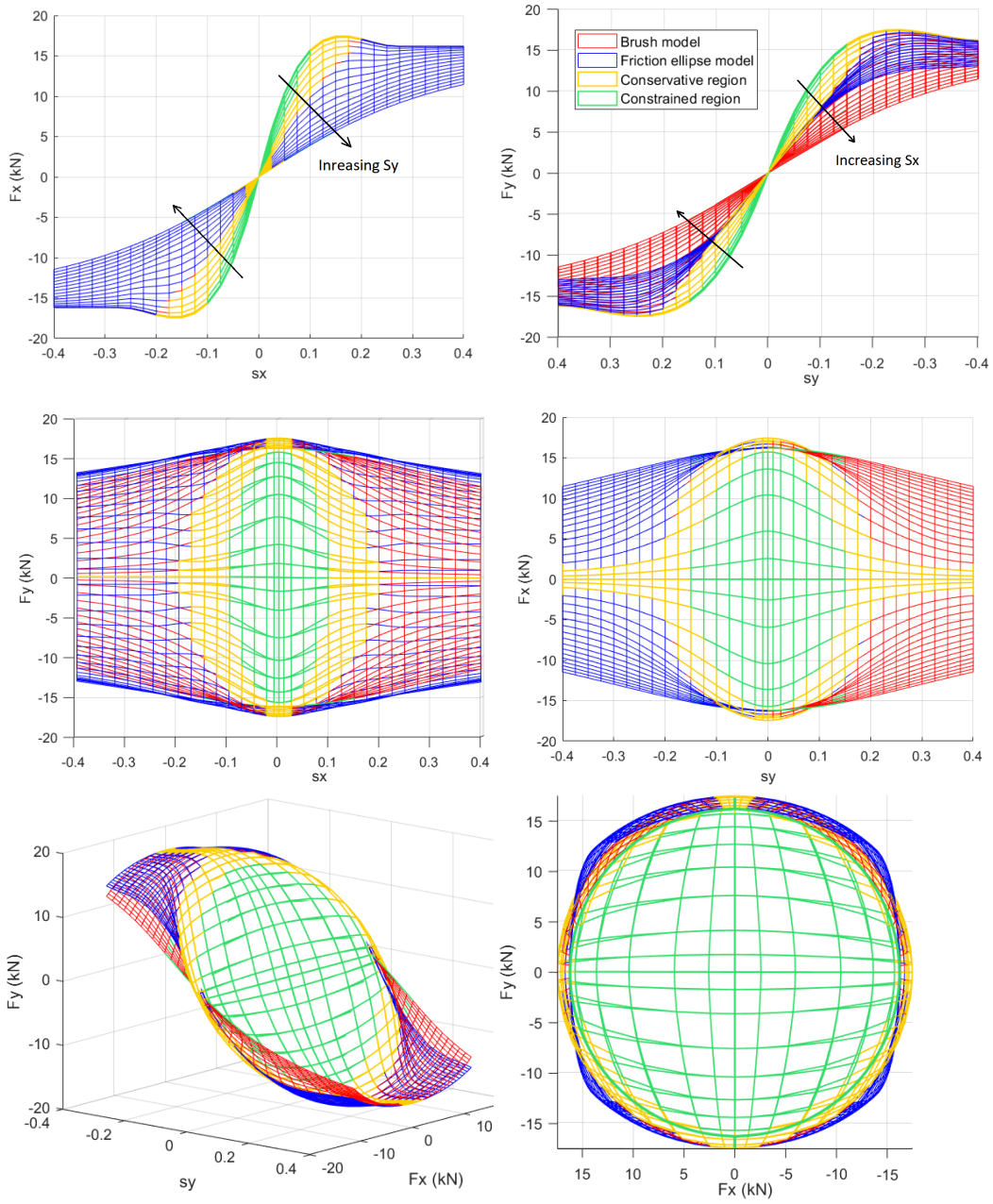

Figure 5.7: The combined slip using brush and friction ellipse models, where $e = 1.2$ is used for the friction ellipse. The region where the friction ellipse model yields a lower F_y than the one modeled by the brush model is called the conservative region. Additionally, the region where $\sqrt{F_x^2 + F_y^2} \leq \mu F_z$, i.e., the constrained region, is shown. The constrained region is a subregion of the conservative region. F_z refers to the tire vertical load, and μ refers to the road friction at a large slip.

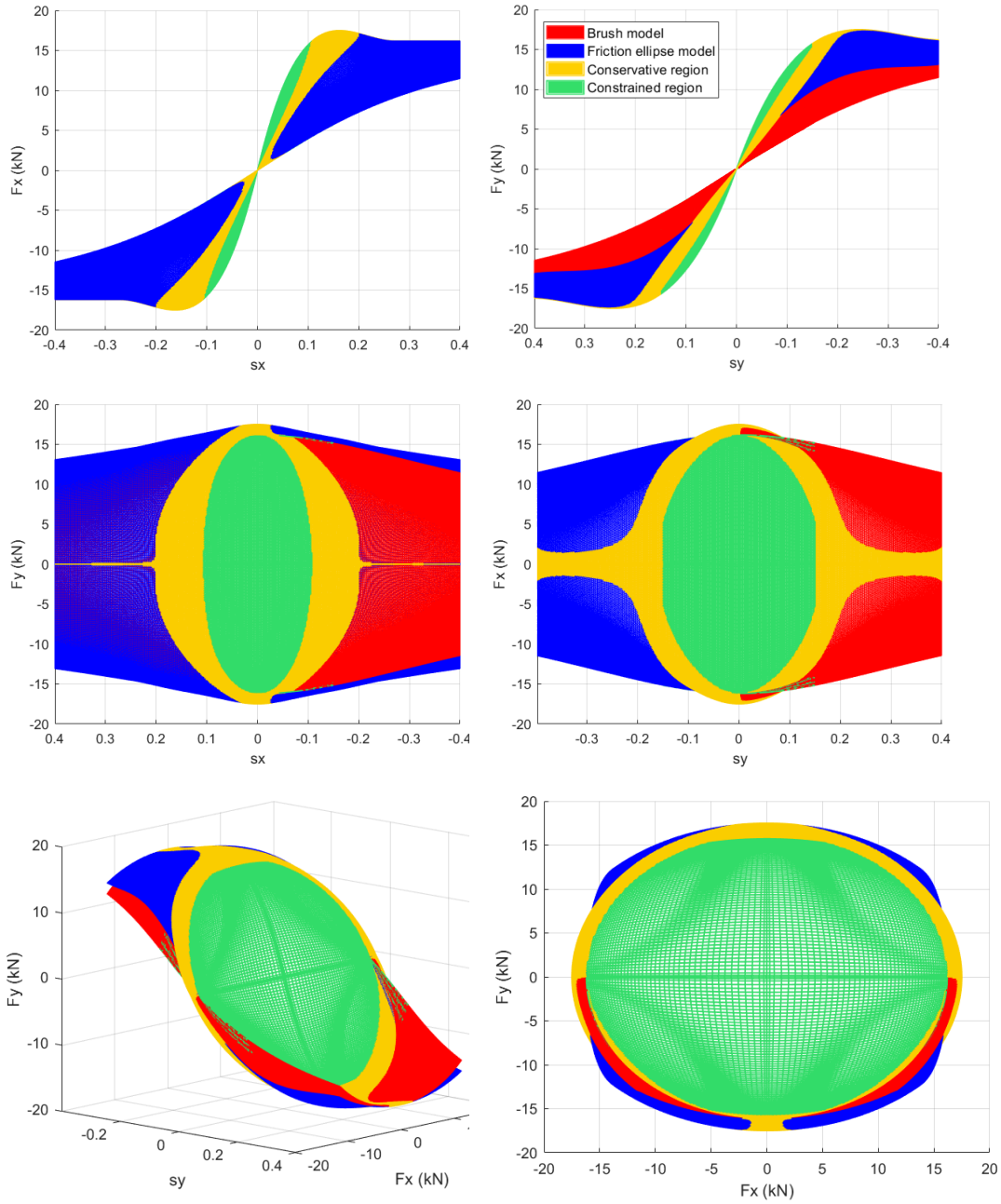

Figure 5.8: Similar to Fig. 5.7 but with a high resolution to better illustrate the conservative and constrained regions.

0.5 m for nonzero steering since the ODEs are highly nonlinear. In addition, the number of states in dynamic equation (2.13) is considerably larger than that in (5.1c), i.e., the state vector given in (2.14) versus v_{x}. Moreover, the number of control inputs in dynamic equation (2.13) is also considerably larger than that in (5.1c). Therefore, directly solving an NOCP that includes lateral dynamics for prediction horizons of 5-20 km is computationally expensive, which makes it unsuitable for real-time applications.

In this thesis, a five-step problem simplification is proposed to reduce the computational burden of solving the NOCP of predictive energy management that includes lateral stability constraints:

1. use a nonlinear single-track vehicle model with lumped axle groups, as described in Paper G, as apposed to a two-track model;

2. reduce the number of states in the longitudinal dynamics equation, as described in section 2.4.2;

3. use a rule-based strategy to reduce the number of dynamic system inputs in the longitudinal dynamics equation, e.g., the total friction brake is distributed proportionally among the nonelectrified axles;

4. use two different discretizations for the longitudinal and lateral dynamics equations, i.e., a coarse discretization for longitudinal dynamics and a fine discretization for lateral dynamics;

5. use an LTV version of the lateral dynamics that is linearized around a reference guess trajectory close to the nonlinear solution, as described in section 2.3.1 and Paper H. The LTV model does not need to be updated in every iteration of the sequential program.

Furthermore, the lateral stability constraints derived from the nonlinear lateral dynamic equations can be active for a shorter horizon than that used for energy management, e.g., for 500 m instead of 10 km, as illustrated in Fig. 5.3, to further reduce the computational burden. The above simplifications in the NOCP, including the lateral dynamics, makes this approach suitable for real-time energy management of distributed propulsion in combination vehicles.

5.3.1 Criteria for LHV stability

There are several criteria that can be used to limit the lateral motion of a vehicle, each with its own pros and cons. The objective here is to avoid vehicle instability and loss of control caused by the vehicle velocity and the braking and propulsion of the axles when the vehicle is in autonomous or cruising mode using constraints in

the optimization problem. Inclusion of the stability objectives in the cost function was discussed in Chapter 4 and is part of the motion control and active safety functions that override the control actions of the energy management whenever necessary. However, inclusion of lateral constraints in the energy management helps to reduce the number of interventions made by the active safety functions other than steering control. In this context, optimal control refers to energy optimality, and, for example, reduction in off-tracking by active steering of the axles is not included. Nevertheless, with the proposed algorithm, it is possible to include the axle steering as control variables and to add weighted terms to the cost function to account for minimizing the off-tracking, which then requires additional computational effort.

The criteria that can be used for limiting lateral motion include (but are not limited to) the following:

Availability of the additional tire lateral force of all the axles during all driving scenarios

High tire side slip might occur when the tire reaches its peak lateral force. The loss of control due to lateral motion and the excessive increase in the articulation angles can be avoided if the required tire lateral force, e.g., for the safe negotiation of a curve, remains less than the peak lateral force a tire can provide. Such a constraint ensures that an increase in the lateral slip to greater than that needed for negotiating a curve always results in an increase in the lateral force. This means that there is always an additional lateral force available. The tire longitudinal force affects the tire peak lateral force due to the tire combined slip effect, and the vehicle longitudinal speed affects the lateral force needed for safe negotiation of a curve. With the proposed predictive energy management algorithm, which includes constraints on the lateral motion, both factors, i.e., the vehicle velocity and the tire longitudinal force, are optimally controlled to ensure that the lateral forces of all the axles do not reach their peak, within a safety margin, to avoid jack-knifing, swinging, increased overshoot and rearward amplification.

The availability of the lateral force can be ensured by constraining the longitudinal and lateral forces of the tires to remain in the green region shown in Figs. 5.6-5.8, i.e.,

$$\sqrt{F_{\mathrm{x}}^2 + F_{\mathrm{y}}^2} \leq \frac{1}{S}\,\mu F_{\mathrm{z}} \tag{5.12}$$

where $S \geq 1$ denotes the safety factor. The safety factor is needed due to possible disturbances and uncertainties of road friction estimation and the error caused by the linearization and simplification of the system dynamics along the road. When using the friction ellipse combined slip tire model, depending on the scale factor

e, the estimated lateral force F_{y} is smaller than that estimated by a more sophisticated combined slip tire model, i.e., the brush model, for a certain combination of lateral and longitudinal forces. Those combinations belong to the conservative region, which is marked in the Figs. 5.6-5.8. The region that satisfies (5.12), i.e., the constrained region for $S = 1$, is a subregion of the conservative region. This means that the friction ellipse tire model can be safely used in the vehicle dynamic model without risking safety if the magnitude of the slips s_{x} and s_{x} remain bounded, e.g., less than 0.2. Constraint (5.12) also ensures that such a bound is met.

The benefit of using constraint (5.12) is that it does not include a variable that is calculated using the reference vehicle (except the reference guess trajectories used for system linearization). The drawbacks of using (5.12) are that it does not avoid an increase in off-tracking and it does not account for roll-over prevention. Moreover, in the case of a large lateral slip imposed by a sharp road curvature at low speeds, constraint (5.12) cannot be satisfied for all tires of an axle group with any choice of control inputs, as some of the tires in an axle group experience a large lateral slip that requires exceeding the peak lateral force, which contradicts constraint (5.12). Therefore, constraint (5.12) should only be active if the vehicle does not perform low-speed full steering turns or if each of the axle groups is lumped into a single axle; e.g., when the lateral slips of the different axles are not larger than 0.15, depending on the safety factor and the tire model.

The increase in off-tracking can be handled by the motion controller described in Chapter 4. In the case of high-speed driving with a constant speed, the increase in the off-tracking occurs because the propulsion and braking of an axle reduce the lateral force, as shown in Fig. 5.5. Therefore, a larger lateral slip is needed to achieve the same lateral force as that in the absence of the longitudinal force and, consequently, a larger yaw angle. Such an increase in the lateral slip Δs_{y} is shown in Fig. 5.9. The maximum increase in lateral slip within the constraint region is approximately 25%. In the case of a reduction in speed, the off-tracking might increase because of the smaller lateral acceleration that reduces the effect of "shooting" the trailers towards the outer side of the curve.

Finally, the roll-over prevention can be enforced by adding a constraint on the lateral acceleration of each of the vehicle units.

Limiting the change in the articulation angle compared to a reference vehicle

Limiting the change in the articulation angle compared to a reference vehicle is an alternative or complementary approach to the constraint of the availability of the lateral force. The benefit of using such a constraint is that the off-tracking can be limited. Therefore, this constraint avoids the change in the speed to some

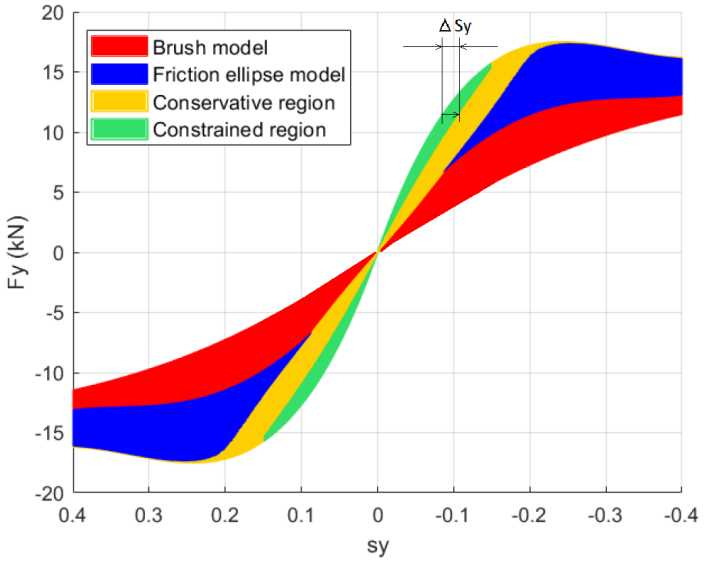

Figure 5.9: An increase in lateral slip by Δs_y caused by an increase in the longitudinal force within the constrained region while the lateral force is constant.

extent due to the fact that the change in speed results in a change in articulation angles. Hence, this constraint contradicts the energy management objectives in situations where the optimal speed is largely different from the reference speed. Another important drawback is that this constraint depends on the reference vehicle performance, which might not be well controlled and stable by itself. Moreover, the model and the numerical method used for simulating the performance of a well-controlled reference vehicle should have similar characteristics to those of the one used in the optimization problem; otherwise, the constraint might be infeasible due to the mismatch of the model solutions. In addition, this constraint alone cannot prevent roll-over or side slip.

Limiting the lateral acceleration of the individual vehicle units

Limiting the lateral acceleration works well for avoiding roll-overs in situations when there is sufficient lateral force available and the vehicle might roll-over because of the high lateral acceleration (and a high height of the COG) since a roll-over might occur sooner than a skid on a dry road. Moreover, a low lateral acceleration improves driver comfort. This constraint does not depend on the reference vehicle performance (except for linearization). However, this constraint alone cannot prevent the side slip caused by the tire combined slip effect and does not take into account an increase in the low-speed off-tracking. More explanation of this constraint can be found later in this section.

Limiting the yaw rate of the individual vehicle units A critical yaw rate might occur at high speeds and relatively high lateral accelerations. Therefore, the constraints on the tire forces and the lateral acceleration might become active sooner than that on the yaw rate. Moreover, limiting the yaw rate cannot avoid low-speed side slip. However, the yaw rate is used in the electronic stability control of the today's vehicles as a part of active safety functions, where there is no long horizon (i.e., look ahead) stability controller. The look-ahead stability controller presented in this thesis stops critical situations before they actually become critical.

Ensuring that all the vehicle units stay in the lane

Such a constraint requires a good driver model of the reference vehicle, i.e., its feasibility depends on the driver model and the width of the lane. There might be situations in which the vehicle cannot stay in the lane no matter how it is controlled. A virtual lane can be defined around the swept path of the reference vehicle and can be used as a limit for the vehicle position. Such a constraint, however, works similarly to limiting the articulation angles compared to that of the reference vehicle, thereby demonstrating similar benefits and drawbacks.

Limiting the lateral off-tracking

This constraint works similarly to limiting the articulation angles and stay-in-lane constraint. High-speed off-tracking can be reduced by the energy management via controlling the speed; however, low-speed off-tracking cannot be minimized by energy management, unless it is penalized in the cost function. In this thesis, however, low-speed off-tracking is not included in the energy management cost function, and it is only minimized by the motion controller based on steering inputs.

Following the above discussion, in the sequel, the vehicle stability constraints in the energy management strategy include the availability of the additional lateral force, limits on the lateral acceleration of the individual vehicle units, and limits on the change in the articulation angles compared to those of the reference vehicle. These constraints together ensure lateral stability of the vehicle along the trip. The latter constraint, however, was not used in the case study.

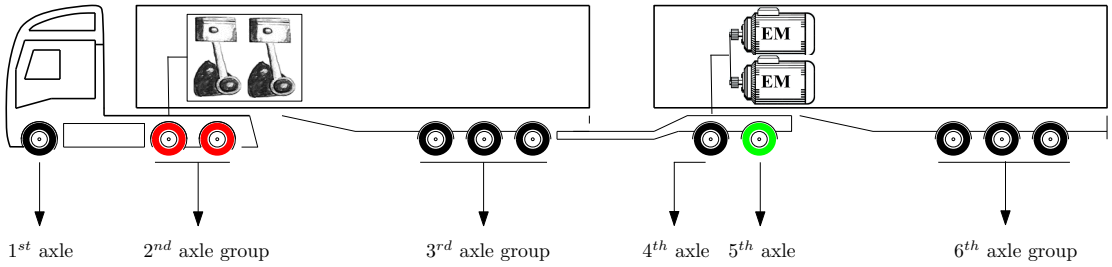

Figure 5.10: The subject hybrid A-double used for the predictive lateral stability control and energy management. The second axle group and the fifth axle are driven by ICE and EMs, respectively.

5.3.2 A case study for predictive lateral stability and energy management of an A-double with an electrified dolly

The subject vehicle for testing the algorithm of predictive stability control and energy management is the A-double shown in Fig. 5.10. The real-world vehicle has 11 axles and 26 tires. The tractor was propelled by an ICE, and the dolly was driven by EMs. The vehicle was modeled by a single-track model, as shown in Fig. 2.3, where some axles were grouped, as shown in Fig. 5.10. The single-track model included 26 tires, the same number of tires as in the real-world vehicle.

The NOCP defined in (5.1) is modified to include the lateral stability constraints and the additional state variables. It includes 12 states, i.e.,

$$x = [\phi_1, v_{\mathrm{x}}, v_{\mathrm{y}}, \dot{\phi}_1, \theta_1, \theta_2, \theta_3, \dot{\theta}_1, \dot{\theta}_2, \dot{\theta}_3, soc, t] \tag{5.13}$$

where v_x and v_y denote the longitudinal and lateral velocities of the first unit and θ_1, θ_2 and θ_3 denote the articulation angles. The input vector remains similar to that in NOCP (5.1), i.e., $u = [F_{\mathrm{e}}, F_{\mathrm{mw}}, F_{\mathrm{br}}, \gamma_{\mathrm{e}}, \gamma_{\mathrm{m}}]$. Here, the criteria for lateral stability comprise the availability of the additional lateral and longitudinal forces and the lateral acceleration of each of the vehicle units, evaluated at the unit's COG. Therefore, the following changes in (5.1) must be made to include the above lateral stability constraints:

longitudinal dynamics equation:

$$\frac{dv_{\mathrm{x}}(s)}{ds} = \frac{1}{mv_{\mathrm{x}}(s)}\big(F_{\mathrm{br}}(s) - \eta_{\mathrm{te}}F_{\mathrm{e}}(s) - F_{\mathrm{mw}}(s) + mg\sin\alpha(s) - mgf_{\mathrm{r}}\cos\alpha(s) - 0.5\rho_{\mathrm{a}}A_{\mathrm{f}}c_{\mathrm{d}}v_{\mathrm{x}}(s)^2 + c\ v_{\mathrm{x}}(s)\ \delta_{11}(s)^2\big), \tag{5.14a}$$

lateral dynamic equations:

$$F\big(x(s), \frac{dx(s)}{ds}, A_{\mathrm{u}}(s)u(s), s\big) = 0, \tag{5.14b}$$

friction ellipse total force constraints:

$$\sqrt{F_{\mathrm{xw}ij}^2(A_{\mathrm{u}}(s)u(s)) + F_{\mathrm{yw}ij}^2(x(s), A_{\mathrm{u}}(s)u(s))} \leq \frac{1}{S}\,\mu F_{\mathrm{z}ij}(s), \tag{5.14c}$$

$$i = 1, \ldots, n_{\mathrm{u}}, \quad j = 1, \ldots, n_{\mathrm{a}}, \quad ua_{ij} \neq 0,$$

lateral acceleration constraints:

$$|a_{\mathrm{y}i}(x(s), A_{\mathrm{u}}(s)u(s))| \leq a_{\mathrm{ymax}i}, \quad i = 1, \ldots, n_{\mathrm{u}}, \tag{5.14d}$$

where compared to (5.1), the constraints (5.14b), (5.14c) and (5.14d) were added, as well as the term $c\ v_{\mathrm{x}}\ \delta_{11}^2$, according to (2.30), which was added to the longitudinal dynamic equation (5.14a). The rest of the constraints and the cost function remain the same as in NOCP (5.1). Constraint (5.14b) accounts for the lateral dynamics, according to the model explained in section 2.4, where A_{u} maps the EMS inputs to the input forces used in the lateral dynamics model. Notably, the steering angles act as known inputs to the NOCP defined above. Constraint (5.14c) limits the sum of the lateral and longitudinal forces experienced by each of the tires (or axles), where $F_{\mathrm{xw}ij}$ and $F_{\mathrm{yw}ij}$ denote the tire (or axle) longitudinal and lateral forces in the wheel coordinate system and $F_{\mathrm{z}ij}$ denotes the tire (or axle) vertical force, which considers the road grade. The safety factor S is used to account for measurement uncertainties and modeling imperfections. Constraint (5.14d) limits the lateral acceleration of each of the units, where $a_{\mathrm{y}i}$ denotes the lateral acceleration of the COG of unit i.

Is using a simple bound on the lateral acceleration sufficient for lateral stability?

The maximum lateral acceleration of each of the vehicle units $a_{\mathrm{ymax}i}$ depends on the unit's COG height h_i and track width $t_{\mathrm{w}i}$ [135, 65], according to

$$a_{\mathrm{y,max,roll},i} = g\,\frac{t_{\mathrm{w}i}}{2h_i}. \tag{5.15}$$

The above maximum acceleration is a simplified equation for predicting the roll-over acceleration of a single-unit rigid vehicle. In this thesis the roll motion was not modeled in order to reduce the number of states. A safety factor $S_{\mathrm{a}} > 1$,

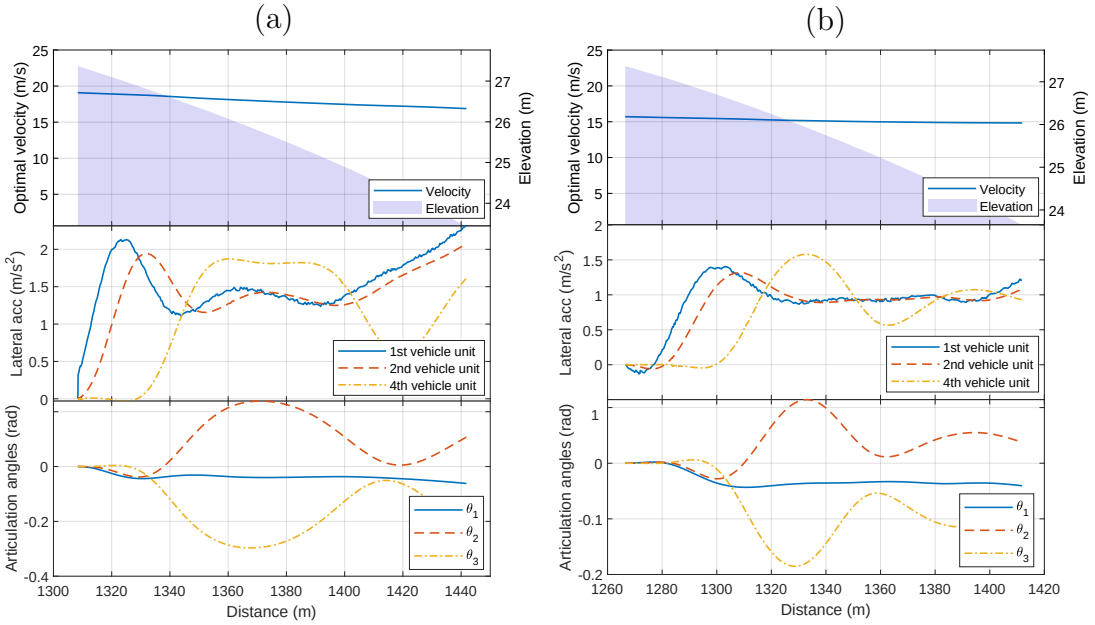

Figure 5.11: a) Simulation of the jack-knifing situation on a wet road ($\mu = 0.6$) at a low lateral acceleration caused by full braking of the dolly second axle; b) a similar situation on an icy road ($\mu = 0.35$). In both cases, the combined slip model (5.7) based on the friction ellipse with $e = 1$ has been used in the vehicle model. Note that the dolly jack-knifing is detected when the two articulation angles θ_2 and θ_3 increase in opposite directions (see Fig. 5.2). The jack-knifing situation cannot be avoided by limiting the lateral acceleration alone to be less than is 2.94 m/s^2 and 1.72 m/s^2 for the wet and icy roads, respectively; however, it can be avoided by using constraint (5.14c).

however, accounts for possible environment uncertainties, state prediction error, and roll motion model simplification. In addition, the maximum lateral acceleration should also be limited by the side slip at low friction. A simple point mass model can be used to show that $ma_{\mathrm{y,max}} = F_{\mathrm{y,max}} = \mu F_{\mathrm{z}} = \mu mg$; thus, $a_{\mathrm{y,max}} = \mu\, g$. Therefore, a rough estimate for the upper bound of the lateral acceleration using the safety factor is

$$a_{\mathrm{y,max},i} = \frac{1}{S_{\mathrm{a}}} \min(\mu\, g, a_{\mathrm{y,max,roll},i}). \tag{5.16}$$

The limit on the lateral acceleration alone cannot prevent instability, jack-knifing and swinging unless a very conservative safety factor is used because of the tire combined slip effect, where the maximum lateral force drops considerably if a high longitudinal force is actuated. It might often occur that the maximum braking and propulsion is preferable on the electrified axle, as decided by the EMS. For example, in the scenario shown in Fig. 5.2, the A-double drives downhill on a slightly curved road, and the lateral acceleration is low. Therefore, the constraints

on the lateral acceleration are not active, yet the vehicle loses stability. Fig. 5.11 illustrates this scenario for two different values of road friction coefficient, i.e., $\mu = 0.6$ and $\mu = 0.35$, corresponding to wet and icy roads, respectively. Considering a safety factor of 2, the maximum acceleration according to (5.16) is 2.94 m/s^2 and 1.72 m/s^2 for the wet and icy roads, respectively. By contrast, in Fig. 5.11, the loss of stability triggers at 1.8 m/s^2 and 1.3 m/s^2 lateral acceleration. Similar instability might occur on dry asphalt at higher lateral acceleration. Moreover, an uneven load distribution can cause an even more unstable situation. Such an unstable situation could be prevented by using constraint (5.14c), which takes into account both the longitudinal and lateral forces based on the tire combined slip effect. Therefore, using a simple bound on the lateral acceleration is not sufficient to ensure lateral stability.

Comparison of the solutions: EMS with and without lateral stability constraints

Algorithm 3 can be used to obtain real-time solutions of the NOCP (5.1) by means of the MPC approach and using SLP or SQP, where the constraints related to the lateral stability (5.14) are checked only for the beginning of the prediction horizon, i.e., 5-10 % of the length of the prediction horizon, whereas they are relaxed for the rest of the prediction horizon. As previously explained, the discretization of the lateral equations is considerably finer than that used in other dynamic equations of NOCP (5.1).

The lateral equations are highly nonlinear, and the set of nonlinear equations has many terms that are not included in this thesis. The set of equations can be generated using the code provided in [43] as a part of the work done in this thesis. The equations for the axle lateral forces and COG lateral accelerations in the space domain, however, are provided in the Appendix.

The NOCP problem (5.1) with and without constraints (5.14) is solved in a single horizon, and the results of the two cases are compared in Figs. 5.12-5.16. The driving cycle included two turns in the road, as illustrated in Fig. 2.18. Fig. 5.12 shows the first 400 m of the prediction horizon, where the lateral stability constraints (5.14) were active.

Fig. 5.13 illustrates the optimal trajectories of the vehicle longitudinal velocity, ICE gear, and SOC, and the road topography, speed limit and regions where the vehicle eco-rolls, i.e., where it rolls down-hill while the ICE is off, the clutch is disengaged, or the gearbox is in the neutral state. The speed limit was generated by preprocessing the driving cycle and limiting the speed based on the road curvature and the legal speed limit. The speed limit is updated together with the receding horizon. Therefore, the impact of the surrounding traffic in limiting the vehicle speed can also be considered. In Fig. 5.13.b, the optimal velocity

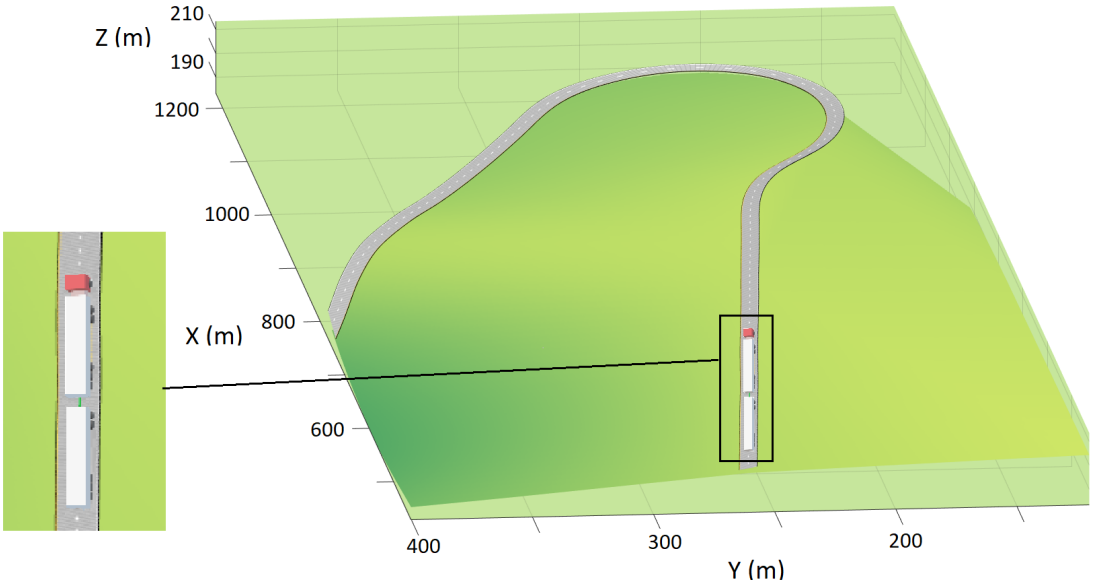

Figure 5.12: The beginning of the prediction horizon where the lateral stability constraints are checked.

decreases at the beginning of the horizon where the lateral stability constraints are active. Later in the horizon, the optimal velocity of the vehicle with lateral stability constraints is higher than that of the vehicle without lateral stability constraints to compensate for the time lost at the beginning of the horizon because of the lower speed. This occurs since the arrival time is also constrained in the two NOCPs. The arrival time is the time spent by the reference vehicle to travel the horizon. The reference vehicle is similar to the controlled vehicle but with a conventional powertrain that tries to maintain the speed limit as far as the vehicle powertrain allows. However, the motion of this reference vehicle should not be used for the linearization of the lateral dynamics equations, as its performance might be very different from the optimal performance of the controlled vehicle. The linearization reference trajectories were obtained using the inputs generated by solving the NOCP without lateral stability constraints. The obtained axle forces were then used to simulate the full vehicle dynamics nonlinear model to generate the final state-input reference trajectories used for linearization of the lateral equations and generating the Jacobians. The Jacobians do not need to be updated frequently unless the hardware computational capacity allows. Moreover, the nonlinear vehicle dynamics model included a driver model that decided the steering input required to follow the road lane.

In addition, the horizon final SOC was constrained to have the same value as that at the beginning of the horizon, the so-called charge sustaining strategy. Such a hard constraint can be used for long horizons. For short horizons, however,

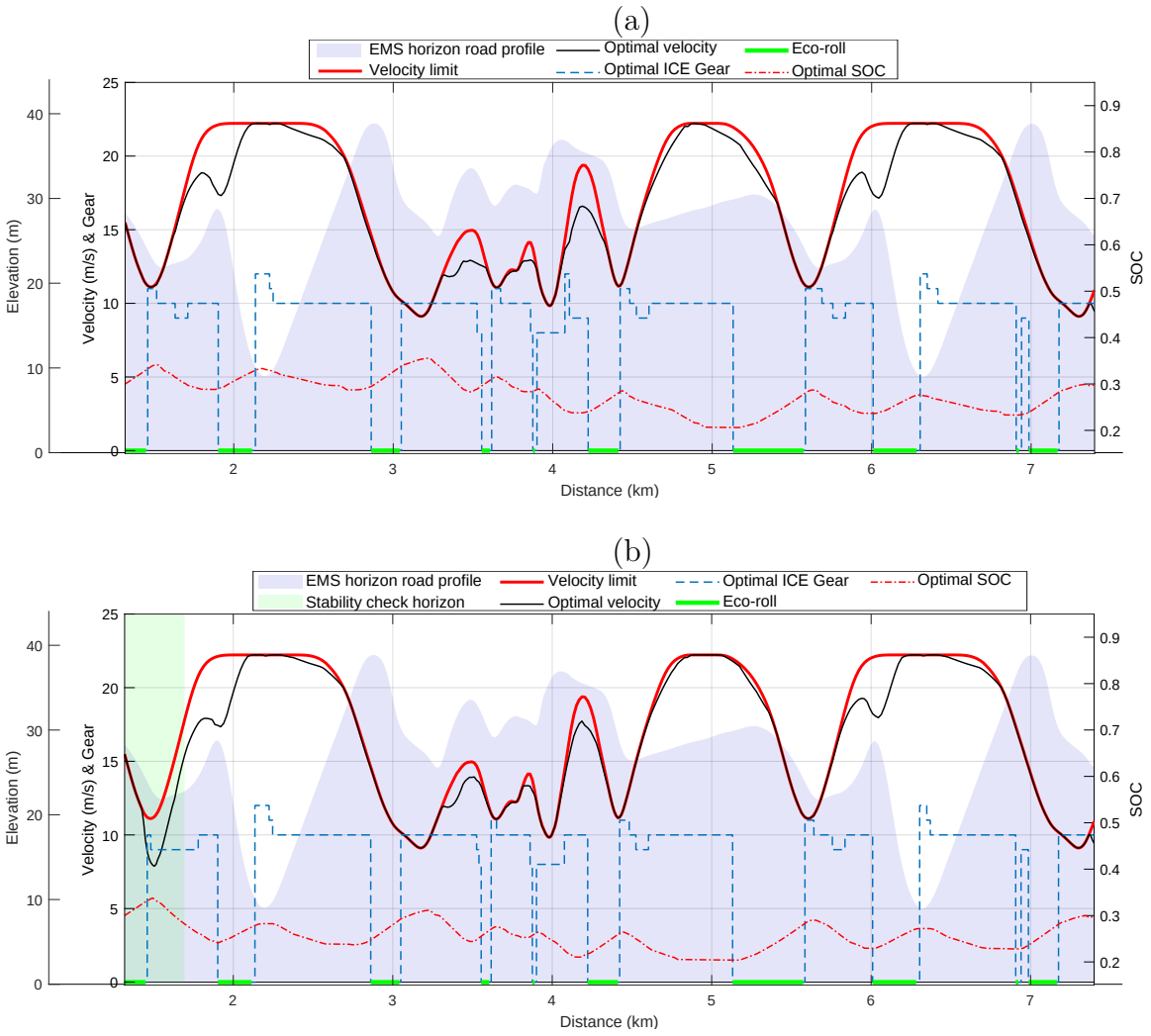

Figure 5.13: a) The solution of the NOCP excluding the lateral stability constraints; b) the solution of the NOCP including the lateral stability constraints for the first 400 m. When the lateral stability constraints are included, the optimal velocity decreases at the beginning of the horizon to keep the vehicle stable, and the optimal ICE gear is different than that in the case when the stability constraints are not included. Moreover, later in the horizon, the vehicle goes faster compared to the case when the stability constraints are not included to compensate for the time lost as a result of the velocity drop at the beginning of the horizon.

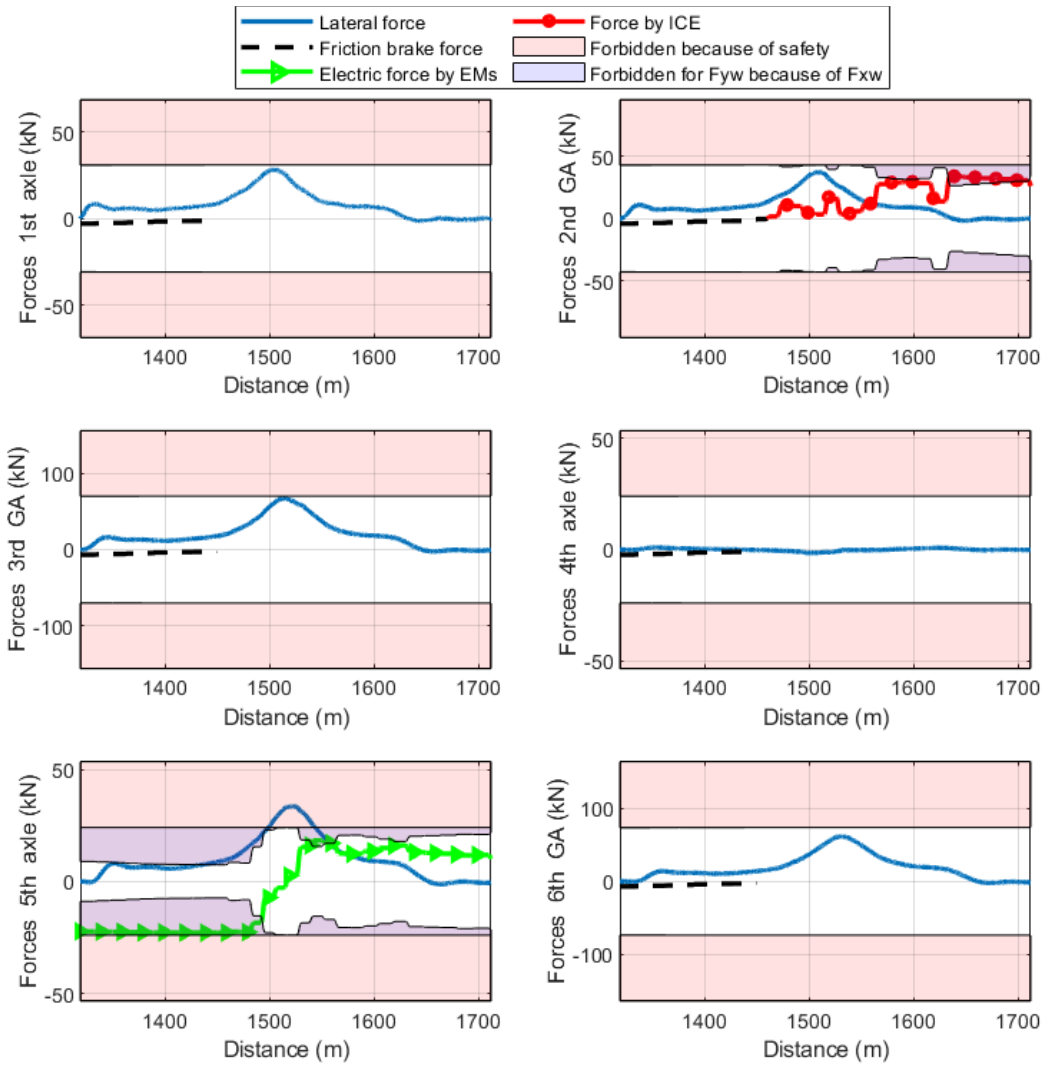

Figure 5.14: The optimal lateral and longitudinal forces acting on different axles in a part of the driving cycle. GA refers to the axle group. The force region that is forbidden because of safety concerns refers to sums of the lateral and longitudinal forces that violate the condition $\sqrt{F_{\mathrm{xw}}^2 + F_{\mathrm{yw}}^2} \leq \frac{1}{S}\mu F_{\mathrm{Z}}$, where $S = 2$. The forbidden region of F_{yw} because of F_{xw} refers to the values of F_{yw} that violate the condition $F_{\mathrm{yw}} \leq \sqrt{(\frac{1}{S}\mu F_{\mathrm{Z}})^2 - F_{\mathrm{xw}}^2}$. The constraints are violated at the fifth axle between distances 1440 m and 1570 m. Note that the region that violates $F_{\mathrm{xw}} \leq \sqrt{(\frac{1}{S}\mu F_{\mathrm{Z}})^2 - F_{\mathrm{yw}}^2}$ is not shown. Moreover, only the nonzero values of the forces are shown.

it might be more energy efficient to not have a hard constraint on the SOC at the end of the horizon; instead, a terminal cost can be included to penalize deviation of the SOC from the set value at the end of the horizon. The same strategy could

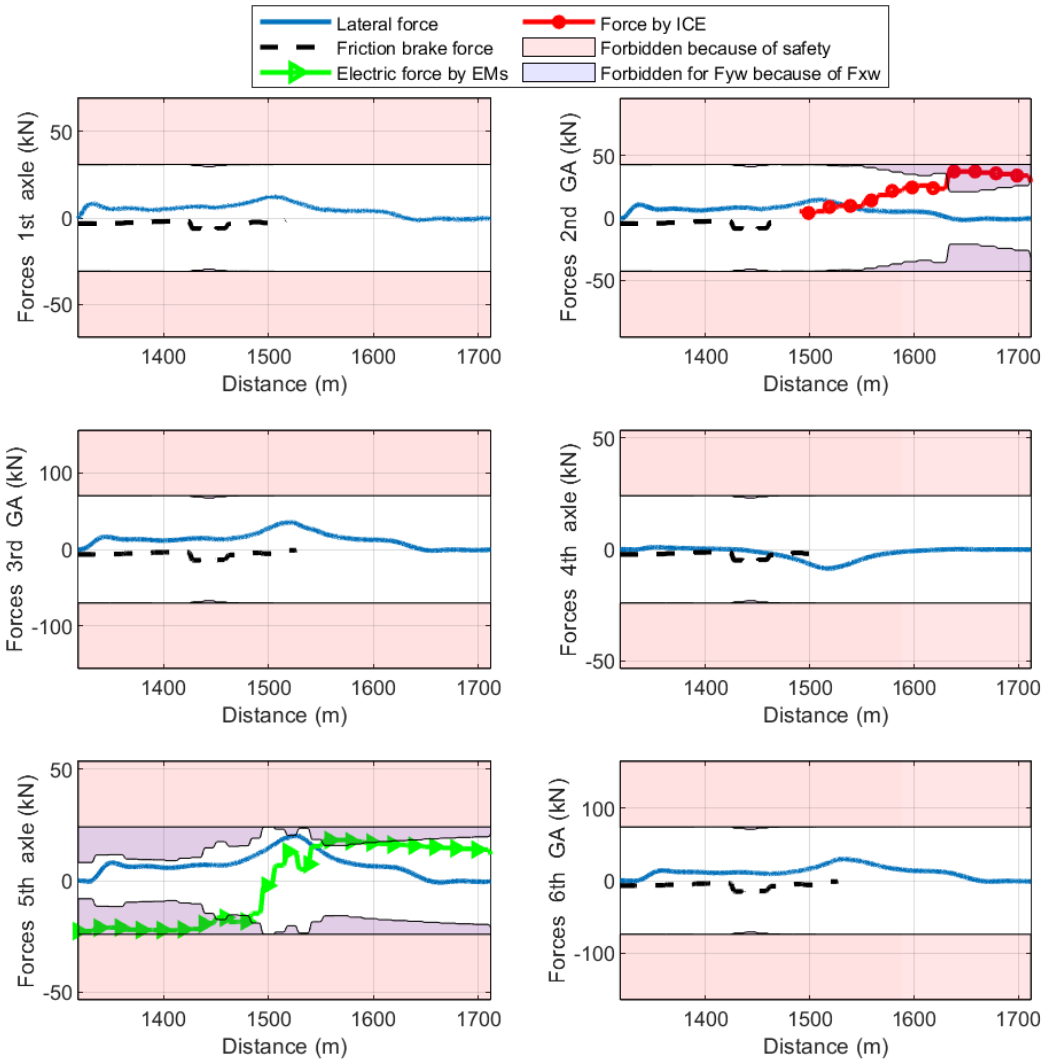

Figure 5.15: Similar to Fig. 5.14 but the NOCP included the lateral stability constraints. Higher friction brakes were used in addition to less electric regenerative braking and propulsion forces to meet all the constraints on all the axles.

be used for the vehicle velocity at the end of the horizon or for the arrival time.

The optimal tire forces generated by solving the two NOCPs are shown in Figs. 5.14 and 5.15. These figures show the axle lateral and longitudinal forces and the force limits because of the safety concerns and tire maximum available force. The solution of the NOCP includes the optimal trajectories of the ICE propulsion force on the second axle group, the electric drive force (positive or negative) on the fifth axle, and a single friction brake force distributed between all the axles, except the fifth one, proportionally to the axle vertical force. If the lateral constraint is not included in the NOCP, the limits of the lateral force are

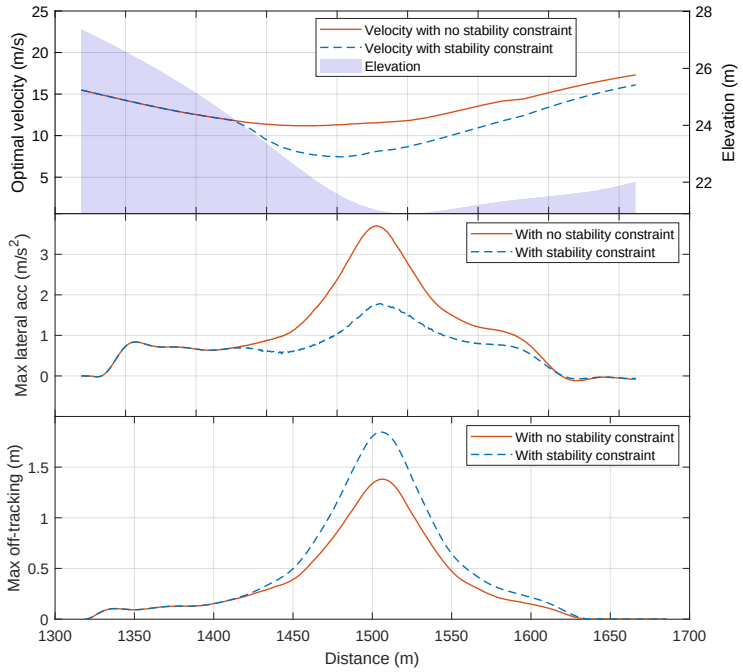

Figure 5.16: A comparison between the optimal longitudinal velocity, maximum lateral acceleration, and the maximum off-tracking of the two NOCPs.

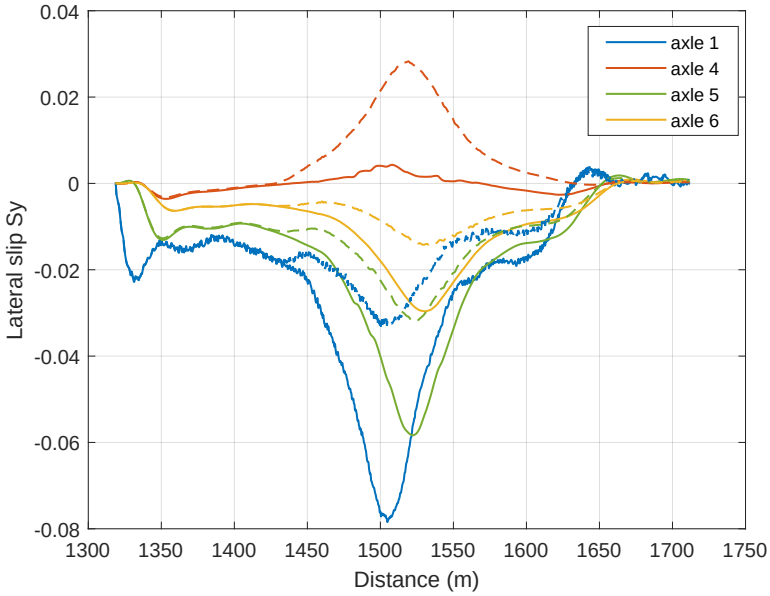

Figure 5.17: A comparison between the tire lateral slips on different axles obtained by solving the two different NOCPs. The solid line is the case with no lateral stability constraints, and the dashed lines represent the case with the lateral stability constraints.

violated by the fifth axle. When the lateral constraints are included, the optimizer attempts to optimally distribute the propulsion and brake forces between axles such that the tire forces remain in the safe region, as shown in Fig. 5.15 for the lateral force. The vehicle velocity is not reduced unless necessary since the forces can be distributed differently between axles to maintain the stability constraints while the sum of the forces is constant.

The performance of the vehicle is better illustrated in Fig. 5.16, where the optimal longitudinal speed, maximum lateral acceleration and maximum off-tracking are shown for the two cases. The lateral acceleration is reduced considerably when the lateral stability constraints are included in NOCP. However, the off-tracking increases when the lateral stability constraints are included. This is because of the reduction in the longitudinal velocity and, consequently, the reduction in the lateral acceleration, which reduced the effect of "shooting" the trailers towards the outer side of the road curve, thereby increasing the off-tracking on the inner side.

Finally, the lateral slips of the axles are shown in Fig. 5.17 for the two different cases.

5.4 Second and third control layers: speed and state of charge tracking[5]

5.4.1 Acceleration and brake pedals control

Using the requested speed, this control layer regulates the acceleration and pedal positions or, alternatively, the total propulsion and brake power. The advantage of controlling the pedal positions is that, in a real vehicle, there is no need to directly send propulsion and brake request signals to the actuators, in which case, additional care would be required to coordinate the same actuation signals coming from active safety functions. This control layer is based on an MPC with a simple first-order vehicle model that generates desired acceleration, inspired by [149]. Then, a simple inverse vehicle model is used to calculate the propulsion and brake power together with a request for neutral (gear 0) and automatic (gear non-zero) gearbox states. Constraints on smooth driving can be imposed in this layer by limiting acceleration and jerk. The control structure is depicted in Fig. 5.18.

The first-order vehicle model used in the receding horizon control block (RHC)

[5]This section was not presented in any of the appended papers.

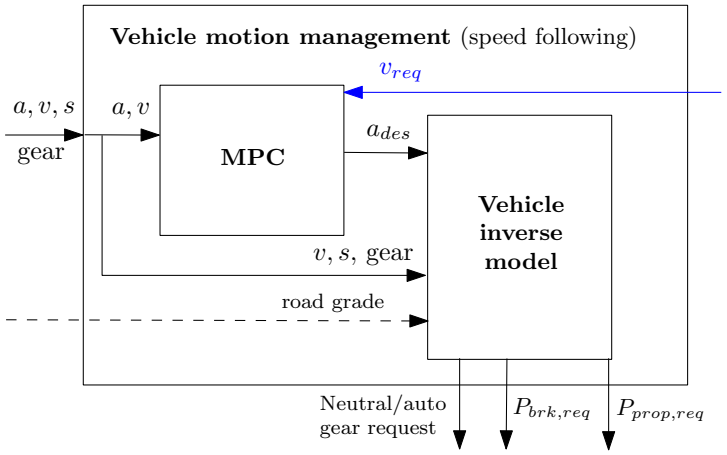

Figure 5.18: Second control layer; acceleration and brake pedals together with ICE gearbox state control.

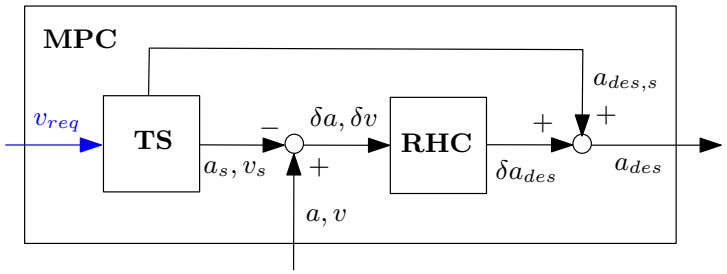

Figure 5.19: MPC block of the second control layer.

of the MPC is described by the following system.

$$\begin{cases} \dot{v} = a \\ \dot{a} = \dfrac{-a}{\tau} + \dfrac{K}{\tau} a_{\text{des}}, \end{cases} \tag{5.17}$$

where the input of the first-order system is $u = a_{\text{des}}$ and the system states are $x = [v, a]^{\text{T}}$; τ and K are the system time constant and gain. Discretization in time, with time index k and time step T, yields

$$x_{k+1} = Ax_k + Bu_k, A = \begin{bmatrix} 1 & T \\ 0 & 1 - \frac{T}{\tau} \end{bmatrix}, B = \begin{bmatrix} 1 \\ \frac{KT}{\tau} \end{bmatrix}, \tag{5.18}$$

$$y_k = Cx_k, \quad C = [1 \;\; 0], \tag{5.19}$$

where the system output y_k is selected to be the vehicle speed. The above system is stable for $0 < T \leq 2\tau$. It can be shown that the same system is valid for the deviation variables, i.e.,

$$\delta x_{k+1} = A\delta x_k + B\delta u_k, \tag{5.20}$$

$$\delta x_k = x_k - x_\mathrm{s}, \quad \delta u_k = u_k - u_s,$$

where $(x_\mathrm{s}, u_\mathrm{s})$ are steady states of the system given the set point v_req and satisfying the equation

$$\begin{bmatrix} I - A & -B \\ C & 0 \end{bmatrix} \begin{bmatrix} x_\mathrm{s} \\ u_\mathrm{s} \end{bmatrix} = \begin{bmatrix} \mathbf{0} \\ v_\mathrm{req} \end{bmatrix}. \tag{5.21}$$

In this case, the speed set point is v_req, and the acceleration set point is zero. The MPC block is shown in Fig. 5.19. The target selector (TS) block solves Eq. (5.21). The values of T and τ should be carefully tuned. Here, $T = 0.5$ and $\tau = 0.5$.

Based on the definitions above, the RHC optimization problem with the objective of minimizing the speed tracking error is defined as follows. To simplify the notation, the optimization problem is shown for a single horizon with prediction length H_p.

Find	$\delta u_k \qquad k = 1 \dots H_\mathrm{p}$	
to minimize	$J(\delta x_0) = \sum_{k=1}^{H_\mathrm{p}} (C \delta x_k)^2$	(5.22a)
subject to	$\forall k = 1 \dots H_\mathrm{p}$	
	Eq. (5.20),	
	$\delta u_\mathrm{min} \leq \delta u_k \leq \delta u_\mathrm{max}$	(5.22b)

where δx_0 is the state deviation at the beginning of the horizon. Additional terms can be added to the objective function and set of constraints to minimize and limit the acceleration variation and, consequently, increase the ride comfort.

The above controller yields high-quality speed tracking.

The vehicle inverse model simply includes Eq. (2.31).

$$F_\mathrm{w}(t) = m a_\mathrm{des}(t) + F_\mathrm{g}(s(t)) + F_\mathrm{roll}(s(t)) + F_\mathrm{air}(v(t)) + F_\mathrm{steer}^\mathrm{approx}(s(t)). \tag{5.23}$$

where $v(t) \approx v_\mathrm{x}(t)$ and

$$P_\mathrm{prop,req} = \begin{cases} F_\mathrm{w}(t) v(t), & a_\mathrm{des} > 0 \\ 0, & a_\mathrm{des} \leq 0 \end{cases} \tag{5.24}$$

$$P_\mathrm{brk,req} = \begin{cases} F_\mathrm{w}(t) v(t), & a_\mathrm{des} < 0 \\ 0, & a_\mathrm{des} \geq 0 \end{cases} \tag{5.25}$$

As a part of the doctoral studies, this speed-tracking controller was programmed, tuned and tested on a real tractor at low speeds up to 30 km/h and showed high-quality speed-tracking performance. The details of the real-world test are expected to be published in future.

5.4.2 Tracking the requested state of charge

The third control layer uses the reference SOC trajectory generated in the first layer to split the power between the engine and electric machines in an instantaneous optimum manner using ECMS. ECMS, introduced by [110] and [109], reduces the optimal control problem to an instantaneous optimization problem using a nonlinear powertrain model and state feedback from vehicle sensors to compensate for the imperfections of the simplified powertrain model used in the first layer. Therefore, the nonlinear properties of the system that have not been considered in the predictive optimization are taken into account in an instantaneous optimization. The equivalent consumption function $\dot{C}_{\text{eqv}}(t)$ to be minimized at each instant is defined as

$$\dot{C}_{\text{eqv}}(t) = \dot{C}_{\text{f}}(t) + \frac{1}{e_{\text{f}}} P_{\text{b}}(t) s(soc(t)) \tag{5.26}$$

where $\dot{C}_{\text{f}}(t)$ is the fuel consumption rate given by Eq. (2.40), e_{f} is the energy content per gram of fuel, $soc(t)$ is the current state of charge, which is a state variable, P_{b} is battery power and $s(soc(t))$ is the equivalence factor or a correction function that penalizes the deviation of the current SOC $soc(t)$ from the reference SOC $soc_{\text{ref}}(t)$. The penalty function is defined as

$$s(soc(t)) = -10^6 \big(tan(2\frac{soc(t) - soc_{\text{req}}(t)}{SOC_{\max} - SOC_{\min}})\big)^3 + 1 \tag{5.27}$$

which can be further tuned. The state equation is given by

$$\dot{soc}(t) = \frac{-P_{\text{b}}(t)}{E_{\text{b,max}}} \tag{5.28}$$

where $E_{\text{b,max}}$ is the maximum energy that can be stored in the battery. According to [126], equivalent consumption function (5.26) is the same as the Hamiltonian derived using PMP and the reference SOC is similar to the reference co-state. However, physical interpretation of the co-state and Hamiltonian function is better described by Eq. (5.26), which is preferred in this thesis. Penalty function $s(soc(t))$ favors the use of the battery energy according to the reference SOC, giving a high weight to the battery equivalent consumption if the SOC is below the reference and a smaller weight if it is higher than the reference. Given the total power request at the wheels from the second layer, the power split is achieved by minimizing Eq. (5.26) with respect to $P_{\text{b}}(t)$. At each instant, $soc(t)$ is calculated by integrating Eq. (5.28) and taking the actual vehicle SOC determined by sensors as the initial SOC. Since the optimization problem has a single variable $(P_{\text{b}}(t))$, finding a solution is rather quick using either an analytical approach, as

explained in [23, 126], nonlinear programming, or implementing PSO according to section 2.2.

The above three-layer predictive energy management controller was tested in simulations using a high-fidelity in-house vehicle model. However, the lateral stability constraints were not included in that work. The results were reported in Paper F.

Chapter 6

Concluding remarks

By implementing mathematical optimization methods and tailoring the propulsion system of a fleet of freight vehicles, this thesis proposed methodologies to enhance road freight transportation efficiency and minimize the fleet TCO. The propulsion systems included conventional, battery electric, and hybrid powertrains. Coupling the infrastructure design to the propulsion system tailoring helped to reduce the TCO. This thesis showed that the optimum vehicle-infrastructure depends on many factors related to the operational design domain and the prices of energy and different components, utilization level, etc. Moreover, the competitiveness of different road freight transportation solutions, including vehicles without human drivers, was compared for different transportation scenarios, and sensitivity analyses of TCO were performed for the contributing factors to help practitioners select a vehicle that suits their needs.

As a result of the propulsion system tailoring, LHVs with distributed propulsion on different axles were found to be viable solutions for certain transportation scenarios. Therefore, this thesis proposed a methodology for predictive and optimal control of distributed propulsion, where safe and energy-efficient driving were assured. As the proposed methodology was model based and included the overall vehicle motion, combined optimal control of the steering, propulsion and braking in long prediction horizons was also achieved.

The following section includes some of the important highlights of the thesis and the appended papers.

6.1 Highlights

Vehicle-infrastructure design (based on Paper A)

– LHVs are not cost-efficient in missions with relatively short driving time, i.e., with a low utilization level. In such missions, the costs of the hardware

and driver are the deciding factors.
- Vehicle performance-based characteristics acting as constraints reduce the size of the vehicle-infrastructure design problem substantially by disqualifying many vehicles.
- If strong performance-based characteristics are required, the routing problem can be separated from propulsion design for certain transportation tasks. Otherwise, the vehicle-infrastructure design problem is coupled with the routing problem.
- Considering route-specific performance-based standards, i.e., adopting the performance-based standards for the routes of the vehicle missions, results in designing cheaper vehicles for those missions.

Automation and electrification (based on Papers C and D)

- Poor vehicle customization results in an increase in TCO, e.g., if an electric vehicle designed to operate in a travel range of 80 km is used instead in missions with a travel range of 10 km.
- The optimum propulsion setup differs between BEHVs equipped with ADS and such vehicles with a human driver, whereas no difference in ICE optimum size was observed in CHVs with different driving systems.
- ADS make BEHVs more competitive with CHVs compared to BEHVs driven by human drivers.
- The reduction in TCO caused by ADS was between 27% and 46% for BEHVs and between 11% and 41% for CHVs for transportation missions with different characteristics.
- The reduction in TCO caused by ADS with a very low cost of transport mission management system was between 40% and 78% for BEHVs and between 20% and 70% for CHVs for transportation missions with different characteristics.
- BEHVs equipped with ADS tend to have lower optimal speeds than those vehicles with human drivers.
- It is less expensive for BEHVs equipped with ADS than CHVs equipped with ADS to drive at low speeds, i.e., an increase in TCO up to 10% was observed in BEHVs equipped with ADS if they were driven at a speed of 50 km/h, whereas the increase in TCO was up to 25% for CHVs equipped with ADS. Therefore, if the speed of vehicles equipped with ADS must be limited for safety reasons, this limitation is less expensive for BEHVs.
- If a similar propulsion hardware as in a BEHV with a human driver is used in a BEHV equipped with ADS, the TCO might increase between zero and 25%, depending on the transportation mission and vehicle size.

- Larger vehicles have lower profit margins when employing ADS, mainly because of the lower share of the driver cost compared to the total cost.
- Increased hilliness of the road negatively affects the competitiveness of BEHVs, mainly because of the high power needed to travel uphill, which requires large batteries.
- Large vehicle sizes yield lower TCO in all missions, including the ones with short travel distances down to 10 km, in the case of quick LU and high utilization.
- BEHVs of all the sizes, regardless of the driving system, show a minimum TCO at certain travel ranges. The optimum travel range differs depending on the vehicle size, hardware and mission.

Fleet vehicle-infrastructure design (based on Paper E)

- Integrated fleet vehicle-infrastructure optimization can substantially reduce the TCO, e.g., a reduction of 50% in the case of a fleet and 35% in the case of a single battery electric vehicle, e.g., a fleet of LHVs with the optimized propulsion system could result in an approximately 50% lower TCO than that in a fleet of rigid trucks.
- The optimum fleet composition and optimum vehicle hardware are sensitive to the daily operation time and freight volume/mass flow.
- In LHVs, additional semitrailers show up as solutions for LU, in many missions, giving the priority of having propelled axles to the converter-dolly.
- Charging power and the durations of charging and LU, along with other factors, affect the optimum battery size.
- Low-density freight improves the competitiveness of BEHVs against CHVs since the gross combination mass is not reached, even if large batteries are used, i.e., in that case, the batteries do not reduce the vehicle volume-loading capacity.
- If many vehicles are included in a mission, then infrastructure can be shared among them, affecting the optimum size of the batteries and the competitiveness of the BEHVs in a positive manner.
- BEHVs benefit more than hybrid vehicles from improvements in battery quality.
- For missions involving long stop times, CHVs result in a lower TCO than that of BEHVs and hybrid vehicles, mainly due to the high depreciation of the purchase cost of hybrid and electric vehicles and low utilization.
- Future reduction in battery prices, increased battery quality, diesel price, and tax incentives, and extension of the vehicle service life and battery second life also contribute to the competitiveness of BHEVs against CHVs.

Energy management of hybrid vehicles (based on Papers B and F)

- Optimal (predictive) EMS helps to reduce costs and energy consumption.
- Traffic flow has a considerable influence on the optimal (predictive) EMS.
- Optimal EMS of hybrid vehicles, excluding the optimal speed optimization, i.e., predictive split of the power between EMs and ICE considering the upcoming road horizon and traffic, yields up to a 4% reduction in fuel consumption in smooth traffic (RMS acceleration of 0.166 m/s^2) on the given road profile, whereas in traffic with a relatively high variation in speed (RMS acceleration of 0.261 m/s^2), the reduction can reach up to 12% compared to a reference consumption obtained by optimizing the power split but not in a predictive manner.
- Including the battery degradation in the cost function decreases battery wear of small batteries, whereas the total operational cost, i.e., the sum of the energy cost and the battery degradation cost, remains almost unchanged.
- The optimal power split, i.e., the value, i.e., the merit, of the predictive control, is not highly sensitive to the vehicle total mass variation.
- The optimal power split is more effective for a certain range of battery sizes.
- The value of the predictive control is higher for larger ICEs, especially in nonsmooth traffic.
- The value of the predictive control cannot be precisely reported unless the vehicle parameters and the driving cycle, as well as the reference vehicle, i.e., the baseline, and its control strategies, are precisely known.

Optimal energy management and vehicle stability (based on Paper H and Chapter 5)

- Sequential programming was an effective method for real-time solving of nonlinear predictive energy management problems comprising many states and inputs (three states: longitudinal speed, SOC, and time; and five inputs: ICE force, EMs force, friction brake force, gear of ICE, gear of EM).
- The SLP yields similar results as the SQP while being computationally more efficient.
- The convex quadratic approximation of the ICE fuel consumption map does not need to be updated sequentially if it is closely fitted to the actual map. A close fit can be obtained using the vehicle longitudinal speed as a state. Consideration of the vehicle longitudinal speed as a state also helps the inclusion of the lateral stability constraints.
- Consideration a full model of lateral dynamics in predictive EMS is possible; for example, the resulting problem for an A-double has 12 states and five inputs.

- Lateral stability is best assured by limiting the tire forces such that they always remain less than a maximum limit, as well as limiting the lateral acceleration.
- In long-horizon predictive energy and lateral stability control, vehicle speed and the propulsion and braking of different axles are optimally controlled in such a way that the vehicle remains stable under all road conditions while the energy usage is optimal.
- The derived vehicle dynamics model is nonlinear with a nonlinear tire model considering the combined slip. Such a model is essential for predicting vehicle behavior in long prediction horizons, in contrast to linear models, which are suitable for very short prediction horizons.
- Combined optimal control of the steering, braking and propulsion of multitrailer vehicles is possible in real time if the NOCP is converted into an LTV-OCP by linearizing the nonlinear equation around the reference trajectories. Linearization around the operating conditions or a fixed trajectory results in a poor controller.
- The derived nonlinear vehicle models can predict vehicle behavior close to the experimental data in maneuvers with low lateral acceleration, and the nonlinear single-track model was also shown to be efficient.
- The proposed LTV-OCPs can be used for efficient and safe motion and energy control of any road vehicle.
- As the derived NOCPs involved the least simplifications in the vehicle model, they can be used as benchmarks for validation of simpler controllers.

6.2 Future works

This thesis assumed that a clear description of future transportation assignments is already available in the conceptual design stage of fleet vehicles, which resulted in deterministic problems. Inclusion of uncertainty and stochastic operations in vehicle-infrastructure design can be a subject of future work. However, large uncertainties result in less vehicle customization, which yields higher TCO.

The sources of power of propulsion systems in this thesis were limited to conventional diesel and battery electric. Alternative power sources, such as fuel cells, can be included as design variables in vehicle-infrastructure optimization, and their competitiveness against the CHVs and BEHVs can be studied in the future.

At the time of writing this thesis, the vehicle concept of a real-world A-double with an electrified dolly was not ready. Future work could involve testing the proposed algorithms on the concept vehicle and determining the least number of signals and sensors required.

The combined optimal control of the steering, propulsion, and braking based on the proposed algorithm can be tested for reverse vehicle motion in the future.

The proposed NOCPs are very large and have many states and inputs that, in the case of long prediction horizons, makes them suitable only for the top control layer, which does not require an update frequency greater than 10 Hz. Moreover, the upcoming road must be known to the controller. When the human driver takes over vehicle control, the role of the controller for combined steering, braking and propulsion must change to active steering, and the upcoming road is unknown. Such a scenario was not studied in the thesis. In that case, for example, for an A-double with a steerable dolly, the dolly active steering must rely on the first axle steering input. The proposed NOCP in this thesis can be tested by generating the optimal dolly steering angle using a prediction horizon that is the same size as the distance between the first axle of the first unit and the first axle of the dolly. Such a controller is expected to generate a valid control action under any operating conditions.

Moreover, the proposed optimal controller can be used for supervised training of a motion controller with the purpose of generating optimal control actions with a high frequency that can also be used in the lower control layers.

Finally, the proposed speed-tracking controller in the second control layer of the predictive energy management was tested on a real-world truck at low speed and showed good speed-tracking performance. The results are expected to be published in the future.

Appendix A

Equations of lateral forces and accelerations

Most of the notation used in this section is defined in section 2.4. In addition, the parameters that are related to the nonlinear tire model defined in Paper G include the following: $F_{\mathrm{z}0ij}$ denotes the nominal tire normal force of axle j on vehicle unit i, $C^{\mathrm{s}}_{\mathrm{cy}0}$ and $C^{\mathrm{us}}_{\mathrm{cy}0}$ denote the cornering coefficient at the nominal tire normal force for steered and unsteered tires, respectively, $u^{\mathrm{s}}_{\mathrm{yg}}$ and $u^{\mathrm{us}}_{\mathrm{yg}}$ denote the maximum lateral force gradient for steered and unsteered tires, respectively.

A.1 Axle lateral force equations of an A-double vehicle

$$
\begin{aligned}
F_{\mathrm{yw11}} = &- F_{\mathrm{Z11}} \sin((2916457339141729 \tan^{-1}((1125899906842624\, C^{\mathrm{s}}_{\mathrm{cy0}} \\
&\tan^{-1}((\cos(\delta_{11}+\phi_1)(v_{\mathrm{y}}\cos(\phi_1) + v_{\mathrm{x}}\sin(\phi_1) + \frac{d\phi_1}{ds} v_{\mathrm{x}} x_{\mathrm{a11}} \cos(\phi_1)) + \\
&\sin(\delta_{11}+\phi_1)(v_{\mathrm{y}}\sin(\phi_1) - v_{\mathrm{x}}\cos(\phi_1) + \frac{d\phi_1}{ds} v_{\mathrm{x}} x_{\mathrm{a11}} \sin(\phi_1)))/|\sin(\delta_{11}+ \\
&\phi_1)(v_{\mathrm{y}}\cos(\phi_1) + v_{\mathrm{x}}\sin(\phi_1) + \frac{d\phi_1}{ds} v_{\mathrm{x}} x_{\mathrm{a11}} \cos(\phi_1)) - \cos(\delta_{11}+ \\
&\phi_1)(v_{\mathrm{y}}\sin(\phi_1) - v_{\mathrm{x}}\cos(\phi_1) + \frac{d\phi_1}{ds} v_{\mathrm{x}} x_{\mathrm{a11}} \sin(\phi_1))|)((F_{\mathrm{z011}}/10- \\
&(F_{\mathrm{Z11}}\cos(\lambda_{\mathrm{b1}})\cos(\lambda_{\mathrm{p1}}))/(10 n_{\mathrm{w11}}))/F_{\mathrm{z011}} + 1))/((11665829356566916 \\
&u^{\mathrm{s}}_{\mathrm{yg}}(F_{\mathrm{z011}} - (F_{\mathrm{Z11}}\cos(\lambda_{\mathrm{b1}})\cos(\lambda_{\mathrm{p1}}))/n_{\mathrm{w11}}))/(5F_{\mathrm{z011}}) - \\
&11665829356566916/5)))/1125899906842624)\cos(\lambda_{\mathrm{b1}}) \\
&\cos(\lambda_{\mathrm{p1}})((4u^{\mathrm{s}}_{\mathrm{yg}}(F_{\mathrm{z011}} - (F_{\mathrm{Z11}}\cos(\lambda_{\mathrm{b1}})\cos(\lambda_{\mathrm{p1}}))/n_{\mathrm{w11}}))/(5F_{\mathrm{z011}}) - 4/5)
\end{aligned}
$$

$$(1 - F_{\mathrm{xw11}}^2/(F_{\mathrm{Z11}}^2 e^2 \mu_{11}^2 \cos(\lambda_{\mathrm{b1}})^2 \cos(\lambda_{\mathrm{p1}})^2))^{1/2}, \tag{A.1}$$

$$\begin{aligned}
F_{\mathrm{yw12}} = &- F_{\mathrm{Z12}} \sin((2916457339141729 \tan^{-1}((1125899906842624\, C_{\mathrm{cy0}}^{\mathrm{us}} \\
&\tan^{-1}((\cos(\phi_1)(v_{\mathrm{y}} \cos(\phi_1) + v_{\mathrm{x}} \sin(\phi_1) + \frac{d\phi_1}{ds} v_{\mathrm{x}} x_{\mathrm{a12}} \cos(\phi_1)) + \\
&\sin(\phi_1)(v_{\mathrm{y}} \sin(\phi_1) - v_{\mathrm{x}} \cos(\phi_1) + \\
&\frac{d\phi_1}{ds} v_{\mathrm{x}} x_{\mathrm{a12}} \sin(\phi_1)))/|\sin(\phi_1)(v_{\mathrm{y}} \cos(\phi_1) + v_{\mathrm{x}} \sin(\phi_1) + \\
&\frac{d\phi_1}{ds} v_{\mathrm{x}} x_{\mathrm{a12}} \cos(\phi_1)) - \cos(\phi_1)(v_{\mathrm{y}} \sin(\phi_1) - \\
&v_{\mathrm{x}} \cos(\phi_1) + \frac{d\phi_1}{ds} v_{\mathrm{x}} x_{\mathrm{a12}} \sin(\phi_1))|)((F_{\mathrm{z012}}/10 - \\
&(F_{\mathrm{Z12}} \cos(\lambda_{\mathrm{b1}}) \cos(\lambda_{\mathrm{p1}}))/(10 n_{\mathrm{w12}}))/F_{\mathrm{z012}} + 1)) \\
&/((11665829356566916\, u_{\mathrm{yg}}^{\mathrm{us}}(F_{\mathrm{z012}} - (F_{\mathrm{Z12}} \cos(\lambda_{\mathrm{b1}}) \\
&\cos(\lambda_{\mathrm{p1}}))/n_{\mathrm{w12}}))/(5F_{\mathrm{z012}}) - 11665829356566916/5))) \\
&/1125899906842624) \cos(\lambda_{\mathrm{b1}}) \cos(\lambda_{\mathrm{p1}})((4u_{\mathrm{yg}}^{\mathrm{us}}(F_{\mathrm{z012}} - \\
&(F_{\mathrm{Z12}} \cos(\lambda_{\mathrm{b1}}) \cos(\lambda_{\mathrm{p1}}))/n_{\mathrm{w12}}))/(5F_{\mathrm{z012}}) - 4/5) \\
&(1 - F_{\mathrm{xw12}}^2/(F_{\mathrm{Z12}}^2 e^2 \mu_{12}^2 \cos(\lambda_{\mathrm{b1}})^2 \cos(\lambda_{\mathrm{p1}})^2))^{1/2},
\end{aligned} \tag{A.2}$$

$$\begin{aligned}
F_{\mathrm{yw21}} = &- F_{\mathrm{Z21}} \sin((2916457339141729 \tan^{-1}((1125899906842624\, C_{\mathrm{cy0}}^{\mathrm{us}} \\
&\tan^{-1}((\cos(\phi_1 - \theta_1)(v_{\mathrm{y}} \cos(\phi_1) + v_{\mathrm{x}} \sin(\phi_1) + \\
&x_{\mathrm{a21}} \cos(\phi_1 - \theta_1)(\frac{d\phi_1}{ds} v_{\mathrm{x}} - \frac{d\theta_1}{ds} v_{\mathrm{x}}) - x_{\mathrm{c21}} \cos(\phi_1 - \\
&\theta_1)(\frac{d\phi_1}{ds} v_{\mathrm{x}} - \frac{d\theta_1}{ds} v_{\mathrm{x}}) + \frac{d\phi_1}{ds} v_{\mathrm{x}} x_{\mathrm{c12}} \cos(\phi_1)) + \sin(\phi_1 - \theta_1)(v_{\mathrm{y}} \sin(\phi_1) - \\
&v_{\mathrm{x}} \cos(\phi_1) + x_{\mathrm{a21}} \sin(\phi_1 - \theta_1)(\frac{d\phi_1}{ds} v_{\mathrm{x}} - \frac{d\theta_1}{ds} v_{\mathrm{x}}) - \\
&x_{\mathrm{c21}} \sin(\phi_1 - \theta_1)(\frac{d\phi_1}{ds} v_{\mathrm{x}} - \frac{d\theta_1}{ds} v_{\mathrm{x}}) + \\
&\frac{d\phi_1}{ds} v_{\mathrm{x}} x_{\mathrm{c12}} \sin(\phi_1)))/|\sin(\phi_1 - \theta_1)(v_{\mathrm{y}} \cos(\phi_1) + v_{\mathrm{x}} \sin(\phi_1) + \\
&x_{\mathrm{a21}} \cos(\phi_1 - \theta_1)(\frac{d\phi_1}{ds} v_{\mathrm{x}} - \frac{d\theta_1}{ds} v_{\mathrm{x}}) - x_{\mathrm{c21}} \cos(\phi_1 - \\
&\theta_1)(\frac{d\phi_1}{ds} v_{\mathrm{x}} - \frac{d\theta_1}{ds} v_{\mathrm{x}}) + \frac{d\phi_1}{ds} v_{\mathrm{x}} x_{\mathrm{c12}} \cos(\phi_1)) - \cos(\phi_1 - \\
&\theta_1)(v_{\mathrm{y}} \sin(\phi_1) - v_{\mathrm{x}} \cos(\phi_1) + x_{\mathrm{a21}} \sin(\phi_1 - \theta_1)(\frac{d\phi_1}{ds} v_{\mathrm{x}} - \\
&\frac{d\theta_1}{ds} v_{\mathrm{x}}) - x_{\mathrm{c21}} \sin(\phi_1 - \theta_1)(\frac{d\phi_1}{ds} v_{\mathrm{x}} - \frac{d\theta_1}{ds} v_{\mathrm{x}}) +
\end{aligned}$$

$$\frac{d\phi_1}{ds}v_{\mathrm{x}}x_{\mathrm{c12}}\sin(\phi_1))|)((F_{\mathrm{z021}}/10-(F_{\mathrm{Z21}}\cos(\lambda_{\mathrm{b2}})\cos(\lambda_{\mathrm{p2}}))/(10n_{\mathrm{w21}}))$$
$$/F_{\mathrm{z021}}+1))/((11665829356566916\,u_{\mathrm{yg}}^{\mathrm{us}}(F_{\mathrm{z021}}-$$
$$(F_{\mathrm{Z21}}\cos(\lambda_{\mathrm{b2}})\cos(\lambda_{\mathrm{p2}}))/n_{\mathrm{w21}}))/(5F_{\mathrm{z021}})-$$
$$11665829356566916/5)))/1125899906842624)\cos(\lambda_{\mathrm{b2}})$$
$$\cos(\lambda_{\mathrm{p2}})((4u_{\mathrm{yg}}^{\mathrm{us}}(F_{\mathrm{z021}}-(F_{\mathrm{Z21}}\cos(\lambda_{\mathrm{b2}})\cos(\lambda_{\mathrm{p2}}))/n_{\mathrm{w21}}))/(5F_{\mathrm{z021}})-4/5)$$
$$(1-F_{\mathrm{xw21}}^2/(F_{\mathrm{Z21}}^2e^2\mu_{21}^2\cos(\lambda_{\mathrm{b2}})^2\cos(\lambda_{\mathrm{p2}})^2))^{1/2}, \tag{A.3}$$

$$\begin{aligned}
F_{\mathrm{yw31}} = &-F_{\mathrm{Z31}}\sin((2916457339141729\tan^{-1}((1125899906842624\,C_{\mathrm{cy0}}^{\mathrm{s}}\\
&\tan^{-1}((\cos(\delta_{31}+\phi_1-\theta_1-\theta_2)(v_{\mathrm{y}}\cos(\phi_1)+v_{\mathrm{x}}\sin(\phi_1)-x_{\mathrm{a31}}\cos(\theta_1-\\
&\phi_1+\theta_2)(\frac{d\theta_1}{ds}v_{\mathrm{x}}-\frac{d\phi_1}{ds}v_{\mathrm{x}}+\frac{d\theta_2}{ds}v_{\mathrm{x}})+x_{\mathrm{c31}}\\
&\cos(\theta_1-\phi_1+\theta_2)(\frac{d\theta_1}{ds}v_{\mathrm{x}}-\frac{d\phi_1}{ds}v_{\mathrm{x}}+\frac{d\theta_2}{ds}v_{\mathrm{x}})-\\
&x_{\mathrm{c21}}\cos(\phi_1-\theta_1)(\frac{d\phi_1}{ds}v_{\mathrm{x}}-\frac{d\theta_1}{ds}v_{\mathrm{x}})+x_{\mathrm{c22}}\cos(\phi_1-\theta_1)\\
&(\frac{d\phi_1}{ds}v_{\mathrm{x}}-\frac{d\theta_1}{ds}v_{\mathrm{x}})+\frac{d\phi_1}{ds}v_{\mathrm{x}}x_{\mathrm{c12}}\cos(\phi_1))+\sin(\delta_{31}+\phi_1-\theta_1-\theta_2)(v_{\mathrm{y}}\sin(\phi_1)-\\
&v_{\mathrm{x}}\cos(\phi_1)+x_{\mathrm{a31}}\sin(\theta_1-\phi_1+\theta_2)(\frac{d\theta_1}{ds}v_{\mathrm{x}}-\frac{d\phi_1}{ds}v_{\mathrm{x}}+\frac{d\theta_2}{ds}v_{\mathrm{x}})-\\
&x_{\mathrm{c31}}\sin(\theta_1-\phi_1+\theta_2)(\frac{d\theta_1}{ds}v_{\mathrm{x}}-\frac{d\phi_1}{ds}v_{\mathrm{x}}+\frac{d\theta_2}{ds}v_{\mathrm{x}})-x_{\mathrm{c21}}\sin(\phi_1-\\
&\theta_1)(\frac{d\phi_1}{ds}v_{\mathrm{x}}-\frac{d\theta_1}{ds}v_{\mathrm{x}})+x_{\mathrm{c22}}\sin(\phi_1-\theta_1)(\frac{d\phi_1}{ds}v_{\mathrm{x}}-\frac{d\theta_1}{ds}v_{\mathrm{x}})+\\
&\frac{d\phi_1}{ds}v_{\mathrm{x}}x_{\mathrm{c12}}\sin(\phi_1)))/|\sin(\delta_{31}+\phi_1-\theta_1-\theta_2)(v_{\mathrm{y}}\cos(\phi_1)+v_{\mathrm{x}}\sin(\phi_1)-\\
&x_{\mathrm{a31}}\cos(\theta_1-\phi_1+\theta_2)(\frac{d\theta_1}{ds}v_{\mathrm{x}}-\frac{d\phi_1}{ds}v_{\mathrm{x}}+\frac{d\theta_2}{ds}v_{\mathrm{x}})+\\
&x_{\mathrm{c31}}\cos(\theta_1-\phi_1+\theta_2)(\frac{d\theta_1}{ds}v_{\mathrm{x}}-\frac{d\phi_1}{ds}v_{\mathrm{x}}+\frac{d\theta_2}{ds}v_{\mathrm{x}})-x_{\mathrm{c21}}\cos(\phi_1-\theta_1)(\frac{d\phi_1}{ds}v_{\mathrm{x}}-\\
&\frac{d\theta_1}{ds}v_{\mathrm{x}})+x_{\mathrm{c22}}\cos(\phi_1-\theta_1)(\frac{d\phi_1}{ds}v_{\mathrm{x}}-\frac{d\theta_1}{ds}v_{\mathrm{x}})+\frac{d\phi_1}{ds}v_{\mathrm{x}}x_{\mathrm{c12}}\cos(\phi_1))-\\
&\cos(\delta_{31}+\phi_1-\theta_1-\theta_2)(v_{\mathrm{y}}\sin(\phi_1)-v_{\mathrm{x}}\cos(\phi_1)+\\
&x_{\mathrm{a31}}\sin(\theta_1-\phi_1+\theta_2)(\frac{d\theta_1}{ds}v_{\mathrm{x}}-\frac{d\phi_1}{ds}v_{\mathrm{x}}+\\
&\frac{d\theta_2}{ds}v_{\mathrm{x}})-x_{\mathrm{c31}}\sin(\theta_1-\phi_1+\theta_2)(\frac{d\theta_1}{ds}v_{\mathrm{x}}-\frac{d\phi_1}{ds}v_{\mathrm{x}}+\frac{d\theta_2}{ds}v_{\mathrm{x}})-\\
&x_{\mathrm{c21}}\sin(\phi_1-\theta_1)(\frac{d\phi_1}{ds}v_{\mathrm{x}}-\frac{d\theta_1}{ds}v_{\mathrm{x}})+x_{\mathrm{c22}}\sin(\phi_1-\theta_1)(\frac{d\phi_1}{ds}v_{\mathrm{x}}-\frac{d\theta_1}{ds}v_{\mathrm{x}})+
\end{aligned}$$

$$\frac{d\phi_1}{ds}v_{\mathrm{x}}x_{\mathrm{c12}}\sin(\phi_1))|)((F_{\mathrm{z031}}/10-(F_{\mathrm{Z31}}\cos(\lambda_{\mathrm{b3}})\cos(\lambda_{\mathrm{p3}}))/(10n_{\mathrm{w31}}))$$
$$/F_{\mathrm{z031}}+1))/((11665829356566916\,u^{\mathrm{s}}_{\mathrm{yg}}(F_{\mathrm{z031}}-$$
$$(F_{\mathrm{Z31}}\cos(\lambda_{\mathrm{b3}})\cos(\lambda_{\mathrm{p3}}))/n_{\mathrm{w31}}))/(5F_{\mathrm{z031}})-11665829356566916/5)))$$
$$/1125899906842624)\cos(\lambda_{\mathrm{b3}})\cos(\lambda_{\mathrm{p3}})((4u^{\mathrm{s}}_{\mathrm{yg}}(F_{\mathrm{z031}}-$$
$$(F_{\mathrm{Z31}}\cos(\lambda_{\mathrm{b3}})\cos(\lambda_{\mathrm{p3}}))/n_{\mathrm{w31}}))/(5F_{\mathrm{z031}})-4/5)$$
$$(1-F^2_{\mathrm{xw31}}/(F^2_{\mathrm{Z31}}e^2\mu^2_{31}\cos(\lambda_{\mathrm{b3}})^2\cos(\lambda_{\mathrm{p3}})^2))^{1/2}, \tag{A.4}$$

$$\begin{aligned}
F_{\mathrm{yw32}} = &-F_{\mathrm{Z32}}\sin((2916457339141729\tan^{-1}((1125899906842624\,C^{\mathrm{us}}_{\mathrm{cy0}}\\
&\tan^{-1}((\cos(\theta_1-\phi_1+\theta_2)(v_{\mathrm{y}}\cos(\phi_1)+v_{\mathrm{x}}\sin(\phi_1)-x_{\mathrm{a32}}\\
&\cos(\theta_1-\phi_1+\theta_2)(\frac{d\theta_1}{ds}v_{\mathrm{x}}-\frac{d\phi_1}{ds}v_{\mathrm{x}}+\frac{d\theta_2}{ds}v_{\mathrm{x}})+\\
&x_{\mathrm{c31}}\cos(\theta_1-\phi_1+\theta_2)(\frac{d\theta_1}{ds}v_{\mathrm{x}}-\frac{d\phi_1}{ds}v_{\mathrm{x}}+\frac{d\theta_2}{ds}v_{\mathrm{x}})-\\
&x_{\mathrm{c21}}\cos(\phi_1-\theta_1)(\frac{d\phi_1}{ds}v_{\mathrm{x}}-\frac{d\theta_1}{ds}v_{\mathrm{x}})+x_{\mathrm{c22}}\cos(\phi_1-\theta_1)(\frac{d\phi_1}{ds}v_{\mathrm{x}}-\\
&\frac{d\theta_1}{ds}v_{\mathrm{x}})+\frac{d\phi_1}{ds}v_{\mathrm{x}}x_{\mathrm{c12}}\cos(\phi_1))-\sin(\theta_1-\phi_1+\theta_2)(v_{\mathrm{y}}\sin(\phi_1)-\\
&v_{\mathrm{x}}\cos(\phi_1)+x_{\mathrm{a32}}\sin(\theta_1-\phi_1+\theta_2)(\frac{d\theta_1}{ds}v_{\mathrm{x}}-\frac{d\phi_1}{ds}v_{\mathrm{x}}+\frac{d\theta_2}{ds}v_{\mathrm{x}})-\\
&x_{\mathrm{c31}}\sin(\theta_1-\phi_1+\theta_2)(\frac{d\theta_1}{ds}v_{\mathrm{x}}-\frac{d\phi_1}{ds}v_{\mathrm{x}}+\frac{d\theta_2}{ds}v_{\mathrm{x}})-x_{\mathrm{c21}}\sin(\phi_1-\theta_1)\\
&(\frac{d\phi_1}{ds}v_{\mathrm{x}}-\frac{d\theta_1}{ds}v_{\mathrm{x}})+x_{\mathrm{c22}}\sin(\phi_1-\theta_1)(\frac{d\phi_1}{ds}v_{\mathrm{x}}-\frac{d\theta_1}{ds}v_{\mathrm{x}})+\\
&\frac{d\phi_1}{ds}v_{\mathrm{x}}x_{\mathrm{c12}}\sin(\phi_1)))/|\sin(\theta_1-\phi_1+\theta_2)(v_{\mathrm{y}}\cos(\phi_1)+v_{\mathrm{x}}\sin(\phi_1)-x_{\mathrm{a32}}\\
&\cos(\theta_1-\phi_1+\theta_2)(\frac{d\theta_1}{ds}v_{\mathrm{x}}-\frac{d\phi_1}{ds}v_{\mathrm{x}}+\frac{d\theta_2}{ds}v_{\mathrm{x}})+x_{\mathrm{c31}}\cos(\theta_1-\phi_1+\\
&\theta_2)(\frac{d\theta_1}{ds}v_{\mathrm{x}}-\frac{d\phi_1}{ds}v_{\mathrm{x}}+\frac{d\theta_2}{ds}v_{\mathrm{x}})-x_{\mathrm{c21}}\cos(\phi_1-\theta_1)(\frac{d\phi_1}{ds}v_{\mathrm{x}}-\frac{d\theta_1}{ds}v_{\mathrm{x}})+\\
&x_{\mathrm{c22}}\cos(\phi_1-\theta_1)(\frac{d\phi_1}{ds}v_{\mathrm{x}}-\frac{d\theta_1}{ds}v_{\mathrm{x}})+\frac{d\phi_1}{ds}v_{\mathrm{x}}x_{\mathrm{c12}}\cos(\phi_1))+\\
&\cos(\theta_1-\phi_1+\theta_2)(v_{\mathrm{y}}\sin(\phi_1)-v_{\mathrm{x}}\cos(\phi_1)+x_{\mathrm{a32}}\sin(\theta_1-\phi_1+\theta_2)\\
&(\frac{d\theta_1}{ds}v_{\mathrm{x}}-\frac{d\phi_1}{ds}v_{\mathrm{x}}+\frac{d\theta_2}{ds}v_{\mathrm{x}})-x_{\mathrm{c31}}\sin(\theta_1-\phi_1+\theta_2)(\frac{d\theta_1}{ds}v_{\mathrm{x}}-\frac{d\phi_1}{ds}v_{\mathrm{x}}+\\
&\frac{d\theta_2}{ds}v_{\mathrm{x}})-x_{\mathrm{c21}}\sin(\phi_1-\theta_1)(\frac{d\phi_1}{ds}v_{\mathrm{x}}-\frac{d\theta_1}{ds}v_{\mathrm{x}})+x_{\mathrm{c22}}\sin(\phi_1-\theta_1)(\frac{d\phi_1}{ds}v_{\mathrm{x}}-\\
&\frac{d\theta_1}{ds}v_{\mathrm{x}})+\frac{d\phi_1}{ds}v_{\mathrm{x}}x_{\mathrm{c12}}\sin(\phi_1))|)((F_{\mathrm{z032}}/10-\\
&(F_{\mathrm{Z32}}\cos(\lambda_{\mathrm{b3}})\cos(\lambda_{\mathrm{p3}}))/(10n_{\mathrm{w32}}))/F_{\mathrm{z032}}+1))
\end{aligned}$$

$$
\begin{aligned}
&/((11665829356566916\,u_{\mathrm{yg}}^{\mathrm{us}}(F_{\mathrm{z032}}- \\
&(F_{\mathrm{Z32}}\cos(\lambda_{\mathrm{b3}})\cos(\lambda_{\mathrm{p3}}))/n_{\mathrm{w32}}))/(5F_{\mathrm{z032}})- \\
&11665829356566916/5)))/1125899906842624)\cos(\lambda_{\mathrm{b3}}) \\
&\cos(\lambda_{\mathrm{p3}})((4u_{\mathrm{yg}}^{\mathrm{us}}(F_{\mathrm{z032}}-(F_{\mathrm{Z32}}cos(\lambda_{\mathrm{b3}})cos(\lambda_{\mathrm{p3}}))/n_{\mathrm{w32}})) \\
&/(5F_{\mathrm{z032}})-4/5)(1-F_{\mathrm{xw32}}^2/(F_{\mathrm{Z32}}^2e^2\mu_{32}^2\cos(\lambda_{\mathrm{b3}})^2\cos(\lambda_{\mathrm{p3}})^2))^{1/2}, \qquad \text{(A.5)}
\end{aligned}
$$

$$
\begin{aligned}
F_{\mathrm{yw41}} =& F_{\mathrm{Z41}}\sin((2916457339141729\tan^{-1}((1125899906842624 \\
&C_{\mathrm{cy0}}^{\mathrm{us}}\tan^{-1}((\sin(\theta_1-\phi_1+\theta_2+\theta_3)(v_{\mathrm{y}}\sin(\phi_1)- \\
&v_{\mathrm{x}}\cos(\phi_1)+x_{\mathrm{a41}}\sin(\theta_1-\phi_1+\theta_2+\theta_3)(\frac{d\theta_1}{ds}v_{\mathrm{x}}-\frac{d\phi_1}{ds}v_{\mathrm{x}}+ \\
&\frac{d\theta_2}{ds}v_{\mathrm{x}}+\frac{d\theta_3}{ds}v_{\mathrm{x}})-x_{\mathrm{c41}}\sin(\theta_1-\phi_1+\theta_2+\theta_3)(\frac{d\theta_1}{ds}v_{\mathrm{x}}-\frac{d\phi_1}{ds}v_{\mathrm{x}}+ \\
&\frac{d\theta_2}{ds}v_{\mathrm{x}}+\frac{d\theta_3}{ds}v_{\mathrm{x}})-x_{\mathrm{c31}}\sin(\theta_1-\phi_1+\theta_2)(\frac{d\theta_1}{ds}v_{\mathrm{x}}- \\
&\frac{d\phi_1}{ds}v_{\mathrm{x}}+\frac{d\theta_2}{ds}v_{\mathrm{x}})+x_{\mathrm{c32}}\sin(\theta_1-\phi_1+\theta_2)(\frac{d\theta_1}{ds}v_{\mathrm{x}}- \\
&\frac{d\phi_1}{ds}v_{\mathrm{x}}+\frac{d\theta_2}{ds}v_{\mathrm{x}})-x_{\mathrm{c21}}\sin(\phi_1-\theta_1)(\frac{d\phi_1}{ds}v_{\mathrm{x}}-\frac{d\theta_1}{ds}v_{\mathrm{x}})+x_{\mathrm{c22}}\sin(\phi_1- \\
&\theta_1)(\frac{d\phi_1}{ds}v_{\mathrm{x}}-\frac{d\theta_1}{ds}v_{\mathrm{x}})+\frac{d\phi_1}{ds}v_{\mathrm{x}}x_{\mathrm{c12}}\sin(\phi_1))-\cos(\theta_1-\phi_1+\theta_2+ \\
&\theta_3)(v_{\mathrm{y}}\cos(\phi_1)+v_{\mathrm{x}}\sin(\phi_1)-x_{\mathrm{a41}}\cos(\theta_1-\phi_1+\theta_2+\theta_3)(\frac{d\theta_1}{ds}v_{\mathrm{x}}- \\
&\frac{d\phi_1}{ds}v_{\mathrm{x}}+\frac{d\theta_2}{ds}v_{\mathrm{x}}+\frac{d\theta_3}{ds}v_{\mathrm{x}})+x_{\mathrm{c41}}\cos(\theta_1-\phi_1+\theta_2+ \\
&\theta_3)(\frac{d\theta_1}{ds}v_{\mathrm{x}}-\frac{d\phi_1}{ds}v_{\mathrm{x}}+\frac{d\theta_2}{ds}v_{\mathrm{x}}+\frac{d\theta_3}{ds}v_{\mathrm{x}})+x_{\mathrm{c31}}\cos(\theta_1-\phi_1+ \\
&\theta_2)(\frac{d\theta_1}{ds}v_{\mathrm{x}}-\frac{d\phi_1}{ds}v_{\mathrm{x}}+\frac{d\theta_2}{ds}v_{\mathrm{x}})-x_{\mathrm{c32}}\cos(\theta_1-\phi_1+ \\
&\theta_2)(\frac{d\theta_1}{ds}v_{\mathrm{x}}-\frac{d\phi_1}{ds}v_{\mathrm{x}}+\frac{d\theta_2}{ds}v_{\mathrm{x}})-x_{\mathrm{c21}}\cos(\phi_1-\theta_1)(\frac{d\phi_1}{ds}v_{\mathrm{x}}-\frac{d\theta_1}{ds}v_{\mathrm{x}})+ \\
&x_{\mathrm{c22}}\cos(\phi_1-thet1)(\frac{d\phi_1}{ds}v_{\mathrm{x}}-\frac{d\theta_1}{ds}v_{\mathrm{x}})+\frac{d\phi_1}{ds}v_{\mathrm{x}}x_{\mathrm{c12}}\cos(\phi_1)))/abs(\cos(\theta_1-\phi_1+ \\
&\theta_2+\theta_3)(v_{\mathrm{y}}\sin(\phi_1)-v_{\mathrm{x}}\cos(\phi_1)+x_{\mathrm{a41}}\sin(\theta_1-\phi_1+\theta_2+\theta_3)(\frac{d\theta_1}{ds}v_{\mathrm{x}}-\frac{d\phi_1}{ds}v_{\mathrm{x}}+ \\
&\frac{d\theta_2}{ds}v_{\mathrm{x}}+\frac{d\theta_3}{ds}v_{\mathrm{x}})-x_{\mathrm{c41}}\sin(\theta_1-\phi_1+\theta_2+\theta_3)(\frac{d\theta_1}{ds}v_{\mathrm{x}}-\frac{d\phi_1}{ds}v_{\mathrm{x}}+ \\
&\frac{d\theta_2}{ds}v_{\mathrm{x}}+\frac{d\theta_3}{ds}v_{\mathrm{x}})-x_{\mathrm{c31}}\sin(\theta_1-\phi_1+\theta_2)(\frac{d\theta_1}{ds}v_{\mathrm{x}}- \\
&\frac{d\phi_1}{ds}v_{\mathrm{x}}+\frac{d\theta_2}{ds}v_{\mathrm{x}})+x_{\mathrm{c32}}\sin(\theta_1-\phi_1+\theta_2)(\frac{d\theta_1}{ds}v_{\mathrm{x}}-\frac{d\phi_1}{ds}v_{\mathrm{x}}+\frac{d\theta_2}{ds}v_{\mathrm{x}})-
\end{aligned}
$$

$$
\begin{aligned}
&x_{\mathrm{c21}}\sin(\phi_1-\theta_1)(\frac{d\phi_1}{ds}v_{\mathrm{x}}-\frac{d\theta_1}{ds}v_{\mathrm{x}})+x_{\mathrm{c22}}\sin(\phi_1-\\
&\theta_1)(\frac{d\phi_1}{ds}v_{\mathrm{x}}-\frac{d\theta_1}{ds}v_{\mathrm{x}})+\frac{d\phi_1}{ds}v_{\mathrm{x}}x_{\mathrm{c12}}\sin(\phi_1))+\sin(\theta_1-\\
&\phi_1+\theta_2+\theta_3)(v_{\mathrm{y}}\cos(\phi_1)+v_{\mathrm{x}}\sin(\phi_1)-x_{\mathrm{a41}}\cos(\theta_1-\phi_1+\theta_2+\theta_3)(\frac{d\theta_1}{ds}v_{\mathrm{x}}-\\
&\frac{d\phi_1}{ds}v_{\mathrm{x}}+\frac{d\theta_2}{ds}v_{\mathrm{x}}+\frac{d\theta_3}{ds}v_{\mathrm{x}})+x_{\mathrm{c41}}\cos(\theta_1-\phi_1+\theta_2+\\
&\theta_3)(\frac{d\theta_1}{ds}v_{\mathrm{x}}-\frac{d\phi_1}{ds}v_{\mathrm{x}}+\frac{d\theta_2}{ds}v_{\mathrm{x}}+\frac{d\theta_3}{ds}v_{\mathrm{x}})+x_{\mathrm{c31}}\cos(\theta_1-\phi_1+\theta_2)\\
&(\frac{d\theta_1}{ds}v_{\mathrm{x}}-\frac{d\phi_1}{ds}v_{\mathrm{x}}+\frac{d\theta_2}{ds}v_{\mathrm{x}})-x_{\mathrm{c32}}\cos(\theta_1-\phi_1+\theta_2)(\frac{d\theta_1}{ds}v_{\mathrm{x}}-\\
&\frac{d\phi_1}{ds}v_{\mathrm{x}}+\frac{d\theta_2}{ds}v_{\mathrm{x}})-\\
&x_{\mathrm{c21}}\cos(\phi_1-\theta_1)(\frac{d\phi_1}{ds}v_{\mathrm{x}}-\frac{d\theta_1}{ds}v_{\mathrm{x}})+x_{\mathrm{c22}}\\
&\cos(\phi_1-\theta_1)(\frac{d\phi_1}{ds}v_{\mathrm{x}}-\frac{d\theta_1}{ds}v_{\mathrm{x}})+\frac{d\phi_1}{ds}v_{\mathrm{x}}x_{\mathrm{c12}}\cos(\phi_1))))\\
&((F_{\mathrm{z041}}/10-(F_{\mathrm{Z41}}\cos(\lambda_{\mathrm{b4}})\cos(\lambda_{\mathrm{p4}}))/(10n_{\mathrm{w41}}))/F_{\mathrm{z041}}+1))\\
&/((11665829356566916\,u_{\mathrm{yg}}^{\mathrm{us}}(F_{\mathrm{z041}}-(F_{\mathrm{Z41}}\cos(\lambda_{\mathrm{b4}})\\
&\cos(\lambda_{\mathrm{p4}}))/n_{\mathrm{w41}}))/(5F_{\mathrm{z041}})-11665829356566916/5)))/1125899906842624)\\
&\cos(\lambda_{\mathrm{b4}})\cos(\lambda_{\mathrm{p4}})((4u_{\mathrm{yg}}^{\mathrm{us}}(F_{\mathrm{z041}}-\\
&(F_{\mathrm{Z41}}\cos(\lambda_{\mathrm{b4}})\cos(\lambda_{\mathrm{p4}}))/n_{\mathrm{w41}}))/(5F_{\mathrm{z041}})-4/5)(1-F_{\mathrm{xw41}}^2\\
&/(F_{\mathrm{Z41}}^2e^2\mu_{41}^2\cos(\lambda_{\mathrm{b4}})^2\cos(\lambda_{\mathrm{p4}})^2))^{1/2}. \qquad \text{(A.6)}
\end{aligned}
$$

A.2 Lateral acceleration equations of vehicle units of an A-double vehicle

The lateral acceleration equations of COGs are provided for units 1, 2 and 4.

$$a_{\mathrm{y1}}=\frac{dv_{\mathrm{y}}}{ds}v_{\mathrm{x}}+\frac{d\phi_1}{ds}v_{\mathrm{x}}^2, \qquad \text{(A.7)}$$

$$
\begin{aligned}
a_{\mathrm{y2}}=&x_{\mathrm{c21}}(\frac{d^2\theta_1}{ds^2}v_{\mathrm{x}}^2+\frac{dv_{\mathrm{x1}}}{ds}\frac{d\theta_1}{ds}v_{\mathrm{x}})-x_{\mathrm{c21}}(\frac{d^2\phi_1}{ds^2}v_{\mathrm{x}}^2+\frac{dv_{\mathrm{x1}}}{ds}\frac{d\phi_1}{ds}v_{\mathrm{x}})+\\
&\frac{dv_{\mathrm{y}}}{ds}v_{\mathrm{x}}\cos(\theta_1)+\frac{dv_{\mathrm{x1}}}{ds}v_{\mathrm{x}}\sin(\theta_1)+x_{\mathrm{c12}}\cos(\theta_1)(\frac{d^2\phi_1}{ds^2}v_{\mathrm{x}}^2+\\
&\frac{dv_{\mathrm{x1}}}{ds}\frac{d\phi_1}{ds}v_{\mathrm{x}})+\frac{d\phi_1}{ds}v_{\mathrm{x}}^2\cos(\theta_1)-\frac{d\phi_1}{ds}^2v_{\mathrm{x}}^2x_{\mathrm{c12}}\sin(\theta_1)-\frac{d\phi_1}{ds}v_{\mathrm{x}}v_{\mathrm{y}}\sin(\theta_1), \qquad \text{(A.8)}
\end{aligned}
$$

$$
\begin{aligned}
a_{\mathrm{y4}} =& x_{\mathrm{c41}}\left(\frac{d^2\theta_1}{ds^2}v_{\mathrm{x}}^2 + \frac{dv_{\mathrm{x1}}}{ds}\frac{d\theta_1}{ds}v_{\mathrm{x}}\right) - x_{\mathrm{c41}}\left(\frac{d^2\phi_1}{ds^2}v_{\mathrm{x}}^2 + \right.\\
&\left.\frac{dv_{\mathrm{x1}}}{ds}\frac{d\phi_1}{ds}v_{\mathrm{x}}\right) + x_{\mathrm{c41}}\left(\frac{d^2\theta_2}{ds^2}v_{\mathrm{x}}^2 + \frac{dv_{\mathrm{x1}}}{ds}\frac{d\theta_2}{ds}v_{\mathrm{x}}\right) +\\
&x_{\mathrm{c41}}\left(\frac{d^2\theta_3}{ds^2}v_{\mathrm{x}}^2 + \frac{dv_{\mathrm{x1}}}{ds}\frac{d\theta_3}{ds}v_{\mathrm{x}}\right) - x_{\mathrm{c21}}\cos(\theta_2+\theta_3)\left(\frac{d^2\phi_1}{ds^2}v_{\mathrm{x}}^2 + \right.\\
&\left.\frac{dv_{\mathrm{x1}}}{ds}\frac{d\phi_1}{ds}v_{\mathrm{x}}\right) + x_{\mathrm{c22}}\cos(\theta_2+\theta_3)\left(\frac{d^2\phi_1}{ds^2}v_{\mathrm{x}}^2 + \right.\\
&\left.\frac{dv_{\mathrm{x1}}}{ds}\frac{d\phi_1}{ds}v_{\mathrm{x}}\right) + x_{\mathrm{c21}}\cos(\theta_2+\theta_3)\left(\frac{d^2\theta_1}{ds^2}v_{\mathrm{x}}^2 + \frac{dv_{\mathrm{x1}}}{ds}\frac{d\theta_1}{ds}v_{\mathrm{x}}\right)\\
&- x_{\mathrm{c22}}\cos(\theta_2+\theta_3)\left(\frac{d^2\theta_1}{ds^2}v_{\mathrm{x}}^2 + \frac{dv_{\mathrm{x1}}}{ds}\frac{d\theta_1}{ds}v_{\mathrm{x}}\right) - x_{\mathrm{c31}}\cos(\theta_3)\left(\frac{d^2\phi_1}{ds^2}v_{\mathrm{x}}^2 + \right.\\
&\left.\frac{dv_{\mathrm{x1}}}{ds}\frac{d\phi_1}{ds}v_{\mathrm{x}}\right) + x_{\mathrm{c32}}\cos(\theta_3)\left(\frac{d^2\phi_1}{ds^2}v_{\mathrm{x}}^2 + \frac{dv_{\mathrm{x1}}}{ds}\frac{d\phi_1}{ds}v_{\mathrm{x}}\right) +\\
&x_{\mathrm{c31}}\cos(\theta_3)\left(\frac{d^2\theta_1}{ds^2}v_{\mathrm{x}}^2 + \frac{dv_{\mathrm{x1}}}{ds}\frac{d\theta_1}{ds}v_{\mathrm{x}}\right) - x_{\mathrm{c32}}\cos(\theta_3)\left(\frac{d^2\theta_1}{ds^2}v_{\mathrm{x}}^2 + \frac{dv_{\mathrm{x1}}}{ds}\frac{d\theta_1}{ds}v_{\mathrm{x}}\right) +\\
&x_{\mathrm{c31}}\cos(\theta_3)\left(\frac{d^2\theta_2}{ds^2}v_{\mathrm{x}}^2 + \frac{dv_{\mathrm{x1}}}{ds}\frac{d\theta_2}{ds}v_{\mathrm{x}}\right) - x_{\mathrm{c32}}\cos(\theta_3)\left(\frac{d^2\theta_2}{ds^2}v_{\mathrm{x}}^2 + \frac{dv_{\mathrm{x1}}}{ds}\frac{d\theta_2}{ds}v_{\mathrm{x}}\right) +\\
&\frac{dv_{\mathrm{y}}}{ds}v_{\mathrm{x}}\cos(\theta_1+\theta_2+\theta_3) + \frac{dv_{\mathrm{x1}}}{ds}v_{\mathrm{x}}\sin(\theta_1+\theta_2+\theta_3) +\\
&x_{\mathrm{c12}}\cos(\theta_1+\theta_2+\theta_3)\left(\frac{d^2\phi_1}{ds^2}v_{\mathrm{x}}^2 + \frac{dv_{\mathrm{x1}}}{ds}\frac{d\phi_1}{ds}v_{\mathrm{x}}\right) +\\
&\frac{d\phi_1}{ds}v_{\mathrm{x}}^2\cos(\theta_1+\theta_2+\theta_3) + \frac{d\phi_1}{ds}^2 v_{\mathrm{x}}^2 x_{\mathrm{c21}}\sin(\theta_2+\theta_3) -\\
&\frac{d\phi_1}{ds}^2 v_{\mathrm{x}}^2 x_{\mathrm{c22}}\sin(\theta_2+\theta_3) + \frac{d\theta_1}{ds}^2 v_{\mathrm{x}}^2 x_{\mathrm{c21}}\sin(\theta_2+\theta_3) -\\
&\frac{d\theta_1}{ds}^2 v_{\mathrm{x}}^2 x_{\mathrm{c22}}\sin(\theta_2+\theta_3) + \frac{d\phi_1}{ds}^2 v_{\mathrm{x}}^2 x_{\mathrm{c31}}\sin(\theta_3) -\\
&\frac{d\phi_1}{ds}^2 v_{\mathrm{x}}^2 x_{\mathrm{c32}}\sin(\theta_3) + \frac{d\theta_1}{ds}^2 v_{\mathrm{x}}^2 x_{\mathrm{c31}}\sin(\theta_3) -\\
&\frac{d\theta_1}{ds}^2 v_{\mathrm{x}}^2 x_{\mathrm{c32}}\sin(\theta_3) + \frac{d\theta_2}{ds}^2 v_{\mathrm{x}}^2 x_{\mathrm{c31}}\sin(\theta_3) -\\
&\frac{d\theta_2}{ds}^2 v_{\mathrm{x}}^2 x_{\mathrm{c32}}\sin(\theta_3) - \frac{d\phi_1}{ds}^2 v_{\mathrm{x}}^2 x_{\mathrm{c12}}\sin(\theta_1+\theta_2+\theta_3) -\\
&\frac{d\phi_1}{ds}v_{\mathrm{x}}v_{\mathrm{y}}\sin(\theta_1+\theta_2+\theta_3) - 2\frac{d\phi_1}{ds}\frac{d\theta_1}{ds}v_{\mathrm{x}}^2 x_{\mathrm{c21}}\sin(\theta_2+\theta_3) +\\
&2\frac{d\phi_1}{ds}\frac{d\theta_1}{ds}v_{\mathrm{x}}^2 x_{\mathrm{c22}}\sin(\theta_2+\theta_3) - 2\frac{d\phi_1}{ds}\frac{d\theta_1}{ds}v_{\mathrm{x}}^2 x_{\mathrm{c31}}\sin(\theta_3) +\\
&2\frac{d\phi_1}{ds}\frac{d\theta_1}{ds}v_{\mathrm{x}}^2 x_{\mathrm{c32}}\sin(\theta_3) - 2\frac{d\phi_1}{ds}\frac{d\theta_2}{ds}v_{\mathrm{x}}^2 x_{\mathrm{c31}}\sin(\theta_3) +
\end{aligned}
$$

$$2\frac{d\phi_1}{ds}\frac{d\theta_2}{ds}v_{\mathrm{x}}^2 x_{\mathrm{c32}}\sin(\theta_3) + 2\frac{d\theta_1}{ds}\frac{d\theta_2}{ds}v_{\mathrm{x}}^2 x_{\mathrm{c31}}\sin(\theta_3) - 2\frac{d\theta_1}{ds}\frac{d\theta_2}{ds}v_{\mathrm{x}}^2 x_{\mathrm{c32}}\sin(\theta_3) \tag{A.9}$$

Bibliography

[1] *OxTS RT3000. Oxford Technical Solutions ltd.* Accessed: 2020.

[2] Advanced Industries McKinsey, *Delivering change - the transformation of commercial transport by 2025*, tech. rep., sep 2016.

[3] A. Alessandrini, A. Campagna, P. Delle Site, F. Filippi, and L. Persia, *Automated vehicles and the rethinking of mobility and cities*, Transportation Research Procedia, 5 (2015), pp. 145–160.

[4] R. W. Allen, H. T. Szostak, T. J. Rosenthal, and D. H. Klyde, *Field testing and computer simulation analysis of ground vehicle dynamic stability*, SAE transactions, (1990), pp. 102–125.

[5] J. M. Anderson, K. Nidhi, K. D. Stanley, P. Sorensen, C. Samaras, and O. A. Oluwatola, *Autonomous vehicle technology: A guide for policymakers*, Rand Corporation, Santa Monica, California, 2014.

[6] J. A. Andersson, J. Gillis, G. Horn, J. B. Rawlings, and M. Diehl, *Casadi: a software framework for nonlinear optimization and optimal control*, Mathematical Programming Computation, 11 (2019), pp. 1–36.

[7] R. Baldacci, P. Toth, and D. Vigo, *Recent advances in vehicle routing exact algorithms*, 4OR, 5 (2007), pp. 269–298.

[8] R. E. Bellman and S. E. Dreyfus, *Applied dynamic programming*, Princeton university press, 2015.

[9] Y. Bin, T. Shim, N. Feng, and D. Zhou, *Path tracking control for backing-up tractor-trailer system via model predictive control*, in 2012 24th Chinese Control and Decision Conference (CCDC), IEEE, 2012, pp. 198–203.

[10] H. G. Bock, M. Diehl, E. Kostina, and J. P. Schlöder, *Constrained optimal feedback control of systems governed by large differential algebraic*

equations, in Real-Time PDE-constrained optimization, SIAM, 2007, pp. 3–24.

[11] H. G. Bock, M. Diehl, P. Kühl, E. Kostina, J. P. Schlöder, and L. Wirsching, *Numerical methods for efficient and fast nonlinear model predictive control*, in Assessment and future directions of nonlinear model predictive control, Springer, 2007, pp. 163–179.

[12] C. Botsford and A. Szczepanek, *Fast charging vs. slow charging: Pros and cons for the new age of electric vehicles*, in International Battery Hybrid Fuel Cell Electric Vehicle Symposium, 2009.

[13] Z. Brock, J. Nelson, and R. L. Hatton, *A comparison of lateral dynamic models for tractor-trailer systems*, in 2019 IEEE Intelligent Vehicles Symposium (IV), IEEE, 2019, pp. 2052–2059.

[14] A. Brown, J. Gonder, and B. Repac, *An analysis of possible energy impacts of automated vehicles*, in Road vehicle automation, Springer, Cham, 2014, pp. 137–153.

[15] J. C. Butcher and N. Goodwin, *Numerical methods for ordinary differential equations*, vol. 2, Wiley Online Library, 2008.

[16] S. Canto, A. de Madrid, and S. Bencomo, *Dynamic programming on clusters for solving control problems*, in Proc. of the 4th Asian Control Conference ASCC, vol. 2, Citeseer, 2002, pp. 25–27.

[17] C.-Y. Chan, *Advancements, prospects, and impacts of automated driving systems*, International journal of transportation science and technology, 6 (2017), pp. 208–216.

[18] P. Christidis, G. Leduc, et al., *Longer and heavier vehicles for freight transport*, JRC European Commission, (2009), pp. 1–40.

[19] M. P. Czechowicz and G. Mavros, *Analysis of vehicle rollover dynamics using a high-fidelity model*, Vehicle System Dynamics, 52 (2014), pp. 608–636.

[20] B. A. Davis and M. A. Figliozzi, *A methodology to evaluate the competitiveness of electric delivery trucks*, Transportation Research Part E: Logistics and Transportation Review, 49 (2013), pp. 8–23.

[21] B. De Jager, T. Van Keulen, and J. Kessels, *Optimal control of hybrid vehicles*, Springer, 2013.

[22] A. De Madrid, S. Dormido, and F. Morilla, *Reduction of the dimensionality of dynamic programming: A case study*, in American Control Conference, 1999. Proceedings of the 1999, vol. 4, IEEE, 1999, pp. 2852–2856.

[23] S. Delprat, T.-M. Guerra, and J. Rimaux, *Optimal control of a parallel powertrain: from global optimization to real time control strategy*, in Vehicular Technology Conference, 2002. VTC Spring 2002. IEEE 55th, vol. 4, IEEE, 2002, pp. 2082–2088.

[24] E. Demir, T. Bektaş, and G. Laporte, *A review of recent research on green road freight transportation*, European Journal of Operational Research, 237 (2014), pp. 775–793.

[25] W. Deng and X. Kang, *Parametric study on vehicle-trailer dynamics for stability control*, SAE transactions, (2003), pp. 1411–1419.

[26] G. Desaulniers, F. Errico, S. Irnich, and M. Schneider, *Exact algorithms for electric vehicle-routing problems with time windows*, Operations Research, 64 (2016), pp. 1388–1405.

[27] M. Diehl, R. Findeisen, F. Allgöwer, H. G. Bock, and J. P. Schlöder, *Nominal stability of real-time iteration scheme for nonlinear model predictive control*, IEE Proceedings-Control Theory and Applications, 152 (2005), pp. 296–308.

[28] B. Duprey, M. Sayers, and T. Gillespie, *Simulation of the performance based standards (pbs) low-speed 90 turn test in trucksim by jumping back in time*, tech. rep., SAE Technical Paper, 2013.

[29] J. Edgar, H. Prem, and F. Calvert, *Applying performance standards to the australian heavy vehicle fleet*, in Proceedings of the 7th International Symposium on Heavy Vehicle Weights & Dimensions, 2002, pp. 73–96.

[30] S. Edlund and P.-O. Fryk, *The right truck for the job with global truck application descriptions*, tech. rep., SAE technical paper, 2004.

[31] E. Eich-Soellner and C. Führer, *Numerical methods in multibody dynamics*, vol. 45, Springer, 1998.

[32] European Commission, *Road transport: Reducing co_2 emissions from vehicles*, tech. rep., 2016.

[33] ——, *Traffic safety basic facts 2018 – heavy goods vehicles and buses*, tech. rep., 2018.

[34] ——, *Freight transport statistics*, tech. rep., 2020.

[35] P. Falcone, F. Borrelli, H. E. Tseng, J. Asgari, and D. Hrovat, *Linear time-varying model predictive control and its application to active steering systems: Stability analysis and experimental validation*, International Journal of Robust and Nonlinear Control: IFAC-Affiliated Journal, 18 (2008), pp. 862–875.

[36] P. Falcone, H. E. Tseng, J. Asgari, F. Borrelli, and D. Hrovat, *Integrated braking and steering model predictive control approach in autonomous vehicles*, IFAC Proceedings Volumes, 40 (2007), pp. 273–278.

[37] P. Falcone, M. Tufo, F. Borrelli, J. Asgari, and H. E. Tseng, *A linear time varying model predictive control approach to the integrated vehicle dynamics control problem in autonomous systems*, in 2007 46th IEEE Conference on Decision and Control, IEEE, 2007, pp. 2980–2985.

[38] P. Fancher and C. Winkler, *Directional performance issues in evaluation and design of articulated heavy vehicles*, Vehicle System Dynamics, 45 (2007), pp. 607–647.

[39] P. Fancher, C. Winkler, R. Ervin, and H. Zhang, *Using braking to control the lateral motions of full trailers*, Vehicle System Dynamics, 29 (1998), pp. 462–478.

[40] W. Feng and M. Figliozzi, *An economic and technological analysis of the key factors affecting the competitiveness of electric commercial vehicles: A case study from the usa market*, Transportation Research Part C: Emerging Technologies, 26 (2013), pp. 135–145.

[41] H. Flämig, *Autonomous vehicles and autonomous driving in freight transport*, in Autonomous driving, Springer, Berlin, Heidelberg, 2016, pp. 365–385.

[42] A. Fröberg, E. Hellström, and L. Nielsen, *Explicit fuel optimal speed profiles for heavy trucks on a set of topographic road profiles*, SAE World Congress, (2006).

[43] T. Ghandriz, *Multitrailer vehicle simulation: Generation and integration of differential equations*. Accessed: 2020, November 6.

[44] ——, *Transportation Mission Based Optimization of Heavy Vehicle Fleets including Propulsion Tailoring*, licentiate thesis, no 2018:17, Chalmers University of Technology, 2018.

[45] T. Ghandriz and B. Jacobson, *A vehicle longitudinal dynamical model for propulsion component tailoring*, Tech. Rep. 2020:03, 2020.

[46] F. Ghilardelli, G. Lini, and A. Piazzi, *Path generation using η^4-splines for a truck and trailer vehicle*, IEEE Transactions on Automation Science and Engineering, 11 (2013), pp. 187–203.

[47] D. Goeke and M. Schneider, *Routing a mixed fleet of electric and conventional vehicles*, European Journal of Operational Research, 245 (2015), pp. 81–99.

[48] A. Grislis, *Longer combination vehicles and road safety*, Transport, 25 (2010), pp. 336–343.

[49] S. Gros, M. Zanon, R. Quirynen, A. Bemporad, and M. Diehl, *From linear to nonlinear mpc: bridging the gap via the real-time iteration*, International Journal of Control, 93 (2020), pp. 62–80.

[50] L. Gurobi Optimization, *Gurobi optimizer reference manual*, 2020.

[51] B. Gutjahr, L. Gröll, and M. Werling, *Lateral vehicle trajectory optimization using constrained linear time-varying mpc*, IEEE Transactions on Intelligent Transportation Systems, 18 (2016), pp. 1586–1595.

[52] A. Hac, D. Fulk, and H. Chen, *Stability and control considerations of vehicle-trailer combination*, SAE International Journal of Passenger Cars-Mechanical Systems, 1 (2008), pp. 925–937.

[53] J. Hagman, S. Ritzén, J. J. Stier, and Y. Susilo, *Total cost of ownership and its potential implications for battery electric vehicle diffusion*, Research in Transportation Business & Management, 18 (2016), pp. 11–17.

[54] C. D. Harper, C. T. Hendrickson, and C. Samaras, *Cost and benefit estimates of partially-automated vehicle collision avoidance technologies*, Accident Analysis & Prevention, 95 (2016), pp. 104–115.

[55] Y. He, M. M. Islam, and T. D. Webster, *An integrated design method for articulated heavy vehicles with active trailer steering systems*, SAE International Journal of Passenger Cars-Mechanical Systems, 3 (2010), pp. 158–174.

[56] E. Hellström, J. Åslund, and L. Nielsen, *Design of an efficient algorithm for fuel-optimal look-ahead control*, Control Engineering Practice, 18 (2010), pp. 1318–1327.

[57] G. Hiermann, J. Puchinger, S. Ropke, and R. F. Hartl, *The electric fleet size and mix vehicle routing problem with time windows and recharging stations*, European Journal of Operational Research, 252 (2016), pp. 995–1018.

[58] A. Hoff, H. Andersson, M. Christiansen, G. Hasle, and A. Løkketangen, *Industrial aspects and literature survey: Fleet composition and routing*, Computers & Operations Research, 37 (2010), pp. 2041–2061.

[59] M. Hovgard, O. Jonsson, N. Murgovski, M. Sanfridson, and J. Fredriksson, *Cooperative energy management of electrified vehicles on hilly roads*, Control Engineering Practice, 73 (2018), pp. 66–78.

[60] X. Hu, L. Johannesson, N. Murgovski, and B. Egardt, *Longevity-conscious dimensioning and power management of the hybrid energy storage system in a fuel cell hybrid electric bus*, Applied Energy, 137 (2015), pp. 913–924.

[61] M. M. Islam, X. Ding, and Y. He, *A closed-loop dynamic simulation-based design method for articulated heavy vehicles with active trailer steering systems*, Vehicle system dynamics, 50 (2012), pp. 675–697.

[62] M. M. Islam, N. Fröjd, S. Kharrazi, and B. Jacobson, *How well a single-track linear model captures the lateral dynamics of long combination vehicles*, Vehicle system dynamics, 57 (2019), pp. 1874–1896.

[63] M. M. Islam, Y. He, S. Zhu, and Q. Wang, *A comparative study of multi-trailer articulated heavy-vehicle models*, Proceedings of the Institution of Mechanical Engineers, Part D: Journal of Automobile Engineering, 229 (2015), pp. 1200–1228.

[64] I. ISO14791, *Road vehicles-heavy commercial vehicle combinations and articulated buses-lateral stability test methods*, tech. rep., Tech. rep, 2002.

[65] B. Jacobson, *Vehicle dynamics compendium; edition 2019*, tech. rep., Chalmers University of Technology, 2019.

[66] L. Johannesson, M. Asbogard, and B. Egardt, *Assessing the potential of predictive control for hybrid vehicle powertrains using stochastic dynamic programming*, IEEE Transactions on Intelligent Transportation Systems, 8 (2007), pp. 71–83.

[67] L. Johannesson, N. Murgovski, E. Jonasson, J. Hellgren, and B. Egardt, *Predictive energy management of hybrid long-haul trucks*, Control Engineering Practice, 41 (2015), pp. 83–97.

[68] R. Johri and Z. Filipi, *Self-learning neural controller for hybrid power management using neuro-dynamic programming*, (2011).

[69] N. Kalra and S. M. Paddock, *Driving to safety: How many miles of driving would it take to demonstrate autonomous vehicle reliability?*, Transportation Research Part A: Policy and Practice, 94 (2016), pp. 182–193.

[70] M. S. Kati, *On Robust Steering Based Lateral Control of Longer and Heavier Commercial Vehicles*, Chalmers University of Technology, 2018.

[71] M. S. Kati, J. Fredriksson, L. Laine, and B. Jacobson, *Evaluation of dynamical behaviour of long heavy vehicles using performance based characterstics*, in FISITA 2014 World Automotive Congress-2-6 June 2014, Maastricht, The Netherlands, 2014.

[72] J. Kennedy and R. Eberhart, *Particle swarm optimization*, in Proceedings of ICNN'95-International Conference on Neural Networks, vol. 4, IEEE, 1995, pp. 1942–1948.

[73] H. K. Khalil and J. W. Grizzle, *Nonlinear systems*, vol. 3, Prentice hall Upper Saddle River, NJ, 1996.

[74] A. Khan, C. D. Harper, C. T. Hendrickson, and C. Samaras, *Net-societal and net-private benefits of some existing vehicle crash avoidance technologies*, Accident Analysis & Prevention, 125 (2019), pp. 207–216.

[75] S. Kharrazi, R. Karlsson, J. Sandin, and J. Aurell, *Performance based standards for high capacity transports in sweden, FIFFI project 2013-03881, report 1: Review of existing regulations and literature*, (2015).

[76] S. Kharrazi, M. Lidberg, and J. Fredriksson, *A generic controller for improving lateral performance of heavy vehicle combinations*, Proceedings of the Institution of Mechanical Engineers, Part D: Journal of Automobile Engineering, 227 (2013), pp. 619–642.

[77] S. Kharrazi, M. Lidberg, R. Roebuck, J. Fredriksson, and A. Odhams, *Implementation of active steering on longer combination vehicles for enhanced lateral performance*, Vehicle system dynamics, 50 (2012), pp. 1949–1970.

[78] S. W. Kirkpatrick, J. Simons, and T. Antoun, *Development and validation of high fidelity vehicle crash simulation models*, International journal of crashworthiness, 4 (1999), pp. 395–406.

[79] Ç. Koç, T. Bektaş, O. Jabali, and G. Laporte, *Thirty years of heterogeneous vehicle routing*, European Journal of Operational Research, 249 (2016), pp. 1–21.

[80] S. Kockum, R. Örtlund, A. Ekfjorden, and P. Wells, *Volvo trucks safety report*, tech. rep., 2017.

[81] H. Kopfer and B. Vornhusen, *Energy vehicle routing problem for differently sized and powered vehicles*, (2017).

[82] H. W. Kopfer, J. Schönberger, and H. Kopfer, *Reducing greenhouse gas emissions of a heterogeneous vehicle fleet*, Flexible Services and Manufacturing Journal, 26 (2014), pp. 221–248.

[83] P. Lebeau, C. Macharis, and J. Van Mierlo, *How to improve the total cost of ownership of electric vehicles: An analysis of the light commercial vehicle segment*, World Electric Vehicle Journal, 10 (2019), p. 90.

[84] P. Lebeau, C. Macharis, J. Van Mierlo, and K. Lebeau, *Electrifying light commercial vehicles for city logistics? A total cost of ownership analysis*, European Journal of Transport and Infrastructure Research, 15 (2015).

[85] D.-Y. Lee, V. M. Thomas, and M. A. Brown, *Electric urban delivery trucks: Energy use, greenhouse gas emissions, and cost-effectiveness*, Environmental science & technology, 47 (2013), pp. 8022–8030.

[86] J. D. Lemp, K. M. Kockelman, and A. Unnikrishnan, *Analysis of large truck crash severity using heteroskedastic ordered probit models*, Accident Analysis & Prevention, 43 (2011), pp. 370–380.

[87] M. W. Levin and S. D. Boyles, *Effects of autonomous vehicle ownership on trip, mode, and route choice*, Transportation Research Record, 2493 (2015), pp. 29–38.

[88] P. F. Lima, *Optimization-based motion planning and model predictive control for autonomous driving: With experimental evaluation on a heavy-duty construction truck*, PhD thesis, KTH Royal Institute of Technology, 2018.

[89] C.-I. Liu, H. Jula, K. Vukadinovic, and P. Ioannou, *Automated guided vehicle system for two container yard layouts*, Transportation Research Part C: Emerging Technologies, 12 (2004), pp. 349–368.

[90] O. Ljungqvist, N. Evestedt, M. Cirillo, D. Axehill, and O. Holmer, *Lattice-based motion planning for a general 2-trailer system*, in 2017 IEEE Intelligent Vehicles Symposium (IV), IEEE, 2017, pp. 819–824.

[91] Z. Lu, Z. Hu, H.-l. Yao, and J. Liu, *Field evaluation and analysis of road subgrade dynamic responses under heavy duty vehicle*, International Journal of Pavement Engineering, 19 (2018), pp. 1077–1086.

[92] M. Luijten, *Lateral dynamic behaviour of articulated commercial vehicles*, Eindhoven University of Technology, (2010).

[93] C. MacAdam and M. Hagan, *A simple differential brake control algorithm for attenuating rearward amplification in doubles and triples combination vehicles*, Vehicle System Dynamics, 37 (2002), pp. 234–245.

[94] A. A. Malikopoulos, *Supervisory power management control algorithms for hybrid electric vehicles: A survey*, IEEE Transactions on intelligent transportation systems, 15 (2014), pp. 1869–1885.

[95] M. Maurer, J. C. Gerdes, B. Lenz, H. Winner, et al., *Autonomous driving*, Berlin, Germany: Springer Berlin Heidelberg, 10 (2016), pp. 978–3.

[96] A. C. Mersky and C. Samaras, *Fuel economy testing of autonomous vehicles*, Transportation Research Part C: Emerging Technologies, 65 (2016), pp. 31–48.

[97] V. Monastyrsky and I. Golownykh, *Rapid computation of optimal control for vehicles*, Transportation Research Part B: Methodological, 27 (1993), pp. 219–227.

[98] A. Montoya, C. Guéret, J. E. Mendoza, and J. G. Villegas, *The electric vehicle routing problem with nonlinear charging function*, Transportation Research Part B: Methodological, 103 (2017), pp. 87–110.

[99] G. Morrison and D. Cebon, *Combined emergency braking and turning of articulated heavy vehicles*, Vehicle system dynamics, 55 (2017), pp. 725–749.

[100] N. Murgovski, B. Egardt, and M. Nilsson, *Cooperative energy management of automated vehicles*, Control Engineering Practice, 57 (2016), pp. 84–98.

[101] N. Nesterova, H. Quak, S. Balm, I. Roche-Ceraso, and T. Tretvik, *State of the art of the electric freight vehicles implementation in city logistics*, FREVUE Project Deliverable D, 1 (2013).

[102] P. Nilsson, L. Laine, B. Jacobson, and N. Van Duijkeren, *Driver model based automated driving of long vehicle combinations in emulated highway traffic*, in 2015 IEEE 18th International Conference on Intelligent Transportation Systems, IEEE, 2015, pp. 361–368.

[103] P. Nilsson, L. Laine, N. Van Duijkeren, and B. Jacobson, *Automated highway lane changes of long vehicle combinations: A specific comparison between driver model based control and non-linear model predictive control*, in 2015 International Symposium on Innovations in Intelligent SysTems and Applications (INISTA), IEEE, 2015, pp. 1–8.

[104] P. Nilsson and K. Tagesson, *Single-track models of an a-double heavy vehicle combination*, tech. rep., Chalmers University of Technology, 2014.

[105] J. Nocedal and S. Wright, *Numerical optimization*, Springer Science & Business Media, 2006.

[106] C. Nowakowski, S. E. Shladover, and H.-S. Tan, *Heavy vehicle automation: Human factors lessons learned*, Procedia Manufacturing, 3 (2015), pp. 2945–2952.

[107] H. Pacejka, *Tire and vehicle dynamics*, Elsevier, 2005.

[108] B. Paden, M. Čáp, S. Z. Yong, D. Yershov, and E. Frazzoli, *A survey of motion planning and control techniques for self-driving urban vehicles*, IEEE Transactions on intelligent vehicles, 1 (2016), pp. 33–55.

[109] G. Paganelli, G. Ercole, A. Brahma, Y. Guezennec, and G. Rizzoni, *General supervisory control policy for the energy optimization of charge-sustaining hybrid electric vehicles*, JSAE review, 22 (2001), pp. 511–518.

[110] G. Paganelli, T. M. Guerra, S. Delprat, J.-J. Santin, M. Delhom, and E. Combes, *Simulation and assessment of power control strategies for a parallel hybrid car*, Proceedings of the Institution of Mechanical Engineers, Part D: Journal of Automobile Engineering, 214 (2000), pp. 705–717.

[111] K. Palmer, J. E. Tate, Z. Wadud, and J. Nellthorp, *Total cost of ownership and market share for hybrid and electric vehicles in the UK, US and Japan*, Applied energy, 209 (2018), pp. 108–119.

[112] S. Pelletier, O. Jabali, and G. Laporte, *50th anniversary invited article—goods distribution with electric vehicles: review and research perspectives*, Transportation Science, 50 (2016), pp. 3–22.

[113] S. Pelletier, O. Jabali, G. Laporte, and M. Veneroni, *Battery degradation and behaviour for electric vehicles: Review and numerical analyses of several models*, Transportation Research Part B: Methodological, 103 (2017), pp. 158–187.

[114] P. Pettersson, *On Numerical Descriptions of Road Transport Missions*, Department of Mechanics and Maritime Sciences, Vehicle Engineering and Autonomous Systems, Chalmers University of Technology, 2017.

[115] P. Pettersson, S. Berglund, H. Ryberg, B. Jacobson, G. Karlsson, L. Brusved, and J. Bjernetun, *Comparison of dual and single clutch transmission based on global transport application mission profiles*, International Journal of Vehicle Design, 77 (2018), pp. 22–42.

[116] K. Rangavajhula and H.-S. J. Tsao, *Active trailer steering control of an articulated system with a tractor and three full trailers for tractor-track following*, International Journal of Heavy Vehicle Systems, 14 (2007), pp. 271–293.

[117] L. M. Rios and N. V. Sahinidis, *Derivative-free optimization: a review of algorithms and comparison of software implementations*, Journal of Global Optimization, 56 (2013), pp. 1247–1293.

[118] V. S. Rodrigues, M. Piecyk, R. Mason, and T. Boenders, *The longer and heavier vehicle debate: A review of empirical evidence from germany*, Transportation Research Part D: Transport and Environment, 40 (2015), pp. 114–131.

[119] R. Roebuck, A. Odhams, K. Tagesson, C. Cheng, and D. Cebon, *Implementation of trailer steering control on a multi-unit vehicle at high speeds*, Journal of Dynamic Systems, Measurement, and Control, 136 (2014).

[120] P. Rouchon, M. Fliess, J. Lévine, and P. Martin, *Flatness, motion planning and trailer systems*, in Proceedings of 32nd IEEE Conference on Decision and Control, IEEE, 1993, pp. 2700–2705.

[121] M. Sadeghi Kati, *Definitions of performance based characteristics for long heavy vehicle combinations*, tech. rep., 2013.

[122] SAE standard, *Taxonomy and definitions for terms related to on-road motor vehicle automated driving systems*, SAE Standard J, 3016 (2016), pp. 1–16.

[123] D. J. M. Sampson, *Active roll control of articulated heavy vehicles*, PhD thesis, University of Cambridge Cambridge, UK, 2000.

[124] O. Sassi, W. R. Cherif, and A. Oulamara, *Vehicle routing problem with mixed fleet of conventional and heterogenous electric vehicles and time dependent charging costs*, (2014).

[125] A. Schwarzkopf and R. Leipnik, *Control of highway vehicles for minimum fuel consumption over varying terrain*, Transportation Research, 11 (1977), pp. 279–286.

[126] L. Serrao, S. Onori, and G. Rizzoni, *A comparative analysis of energy management strategies for hybrid electric vehicles*, Journal of Dynamic Systems, Measurement, and Control, 133 (2011), pp. 0310121–0310129.

[127] A. A. Shabana, *Dynamics of multibody systems*, Cambridge university press, 2003.

[128] S. Shepherd, P. Bonsall, and G. Harrison, *Factors affecting future demand for electric vehicles: A model based study*, Transport Policy, 20 (2012), pp. 62–74.

[129] P. Sundström, B. Jacobson, and L. Laine, *Vectorized single-track model in modelica for articulated vehicles with arbitrary number of units and axles*, in Modelica conference 2014, Lund, Sweden, March 10-12, 2014, 2014.

[130] T. T. Taefi, J. Kreutzfeldt, T. Held, and A. Fink, *Strategies to increase the profitability of electric vehicles in urban freight transport*, in E-Mobility in Europe, Springer, 2015, pp. 367–388.

[131] ——, *Supporting the adoption of electric vehicles in urban road freight transport–a multi-criteria analysis of policy measures in germany*, Transportation Research Part A: Policy and Practice, 91 (2016), pp. 61–79.

[132] T. T. Taefi, J. Kreutzfeldt, T. Held, R. Konings, R. Kotter, S. Lilley, H. Baster, N. Green, M. S. Laugesen, S. Jacobsson, et al., *Comparative analysis of european examples of freight electric vehicles schemes—a systematic case study approach with examples from denmark, germany, the netherlands, sweden and the uk*, in Dynamics in Logistics, Springer, 2016, pp. 495–504.

[133] T. T. Taefi, S. Stütz, and A. Fink, *Assessing the cost-optimal mileage of medium-duty electric vehicles with a numeric simulation approach*, Transportation Research Part D: Transport and Environment, 56 (2017), pp. 271–285.

[134] M. Taiebat, A. L. Brown, H. R. Safford, S. Qu, and M. Xu, *A review on energy, environmental, and sustainability implications of connected and automated vehicles*, Environmental science & technology, 52 (2018), pp. 11449–11465.

[135] A. S. Trigell, M. Rothhämel, J. Pauwelussen, and K. Kural, *Advanced vehicle dynamics of heavy trucks with the perspective of road safety*, Vehicle system dynamics, 55 (2017), pp. 1572–1617.

[136] S. Tsugawa, S. Jeschke, and S. E. Shladover, *A review of truck platooning projects for energy savings*, IEEE Transactions on Intelligent Vehicles, 1 (2016), pp. 68–77.

[137] S. Uebel, N. Murgovski, C. Tempelhahn, and B. Bäker, *Optimal energy management and velocity control of hybrid electric vehicles*, IEEE Transactions on Vehicular Technology, 67 (2017), pp. 327–337.

[138] G. Ullrich, *Automated guided vehicle systems*, Springer, 2015.

[139] M. Van de Molengraft-Luijten, I. J. Besselink, R. Verschuren, and H. Nijmeijer, *Analysis of the lateral dynamic behaviour of articulated commercial vehicles*, Vehicle system dynamics, 50 (2012), pp. 169–189.

[140] N. van Duijkeren, T. Keviczky, P. Nilsson, and L. Laine, *Real-time nmpc for semi-automated highway driving of long heavy vehicle combinations*, IFAC-PapersOnLine, 48 (2015), pp. 39–46.

[141] Z. Wadud, *Fully automated vehicles: A cost of ownership analysis to inform early adoption*, Transportation Research Part A: Policy and Practice, 101 (2017), pp. 163–176.

[142] Z. Wadud, D. MacKenzie, and P. Leiby, *Help or hindrance? the travel, energy and carbon impacts of highly automated vehicles*, Transportation Research Part A: Policy and Practice, 86 (2016), pp. 1–18.

[143] M. Wahde, *Biologically inspired optimization methods: an introduction*, WIT press, 2008.

[144] J. Wang, P. Liu, J. Hicks-Garner, E. Sherman, S. Soukiazian, M. Verbrugge, H. Tataria, J. Musser, and P. Finamore, *Cycle-life model for graphite-lifepo4 cells*, Journal of Power Sources, 196 (2011), pp. 3942–3948.

[145] Q. Wang and Y. He, *A study on single lane-change manoeuvres for determining rearward amplification of multi-trailer articulated heavy vehicles with active trailer steering systems*, Vehicle System Dynamics, 54 (2016), pp. 102–123.

[146] World Health Organization, *Global status report on road safety: Summary*, Tech. Rep. WHO/NMH/NVI/18.20, 2018.

[147] G. Wu, A. Inderbitzin, and C. Bening, *Total cost of ownership of electric vehicles compared to conventional vehicles: A probabilistic analysis and projection across market segments*, Energy Policy, 80 (2015), pp. 196–214.

[148] Y. Zhang, A. Khajepour, and M. Ataei, *A universal and reconfigurable stability control methodology for articulated vehicles with any configurations*, IEEE transactions on vehicular technology, 69 (2020), pp. 3748–3759.

[149] M. Zhu, H. Chen, and G. Xiong, *A model predictive speed tracking control approach for autonomous ground vehicles*, Mechanical Systems and Signal Processing, 87 (2017), pp. 138–152.